THOMAS WAGNER

YOUNG UPLIFT IN THE NON-GLACIATED PARTS OF THE EASTERN ALPS

GEOMORPHOLOGICAL AND GEOCHRONOLOGICAL CONSTRAINTS

A dissertation submitted to the

Faculty of Natural Science
Karl-Franzens University of Graz
Austria

for the Degree of Doctor of Science

September 2010

“Only those who will risk going too far can possibly find out how far one can go.”
T.S. Eliot

PREAMBLE

The study of the growth of mountains and the evolution of their landforms is a subject at the heart of Earth sciences. However, only newly available geochronological methods allow to constrain the timing of formation of landforms in more detail. In particular the evolution of landforms in Pliocene to Pleistocene times is much debated, because of a worldwide increase in sedimentation rates observed at the same time. Climate changes and tectonic processes are possible candidates to explain this increase. The research effort presented in this thesis fills the gap of knowledge concerning the topographic evolution of the last few million years to today's face of a region along the eastern margin of the Alps: the Styrian Block. This block includes the Styrian Basin and its surrounding basement. New time constraints from various cave, stream and fault deposits are reported and are interpreted in terms of river incision rates, aggradation and re-excavation events. Uplift rates of the region are estimated. DEM data are used to identify the geomorphic disequilibrium of the whole Alps. The results support the notion that tectonically driven deformation and responding erosion is taking place to an increased level over the last 5-6 Ma. Climate changes are inferred to be of only subordinate importance.

OUTLINE OF THESIS

This thesis is divided into 4 chapters and 3 appendices.

Chapters 1 to 3 and appendix A are the principle contributions. All four parts of the thesis are published or under review at various international journals. Chapter 4 contains overall conclusions drawn from all these findings. Appendix B describes the sample preparation procedure applied for burial age dating. Finally, appendix C lists conference abstracts related to the thesis.

In **Chapter 1**, burial ages of cave sediments from the Central Styrian Karst are reported. Based on this record, minimum age constraints of various cave levels and maximum rates of river incision of the River Mur over the last ~5 Ma are inferred. Decreasing bedrock incision rates beginning ~2.5 Ma ago are explained by the fact of increasing sediment supply from the hinterland. Finally, this is put in an absolute vertical reference frame, indicating episodic uplift of the region. The chapter has already been published as:

- **Wagner.T, Fabel, D., Fiebig, M.,Häuselmann, Ph., Sahy, D., Xu, S., Stüwe, K.**, 2010. Young uplift in the non-glaciated parts of the Eastern Alps, Earth Planet. Sci. Lett. 295, 159-169, doi: 10.1016/j.epsl.2010.03.034.

In **Chapter 2**, evidence for west-east directed extensional tectonics within the Styrian Block in Late Neogene times is reported, including a first successful attempt to absolutely date fault activity by the terrestrial cosmogenic nuclides (TCN) burial age method. Basin inversion of the Styrian Basin is questioned hereby and uplift of the whole region is proposed to be related to the underthrusting of a Pannonian fragment by European and Adriatic plates. This chapter is currently under review:

- **Wagner, T., Fritz, H., Stüwe, K., Fabel, D.**, Pliocene to Pleistocene faulting at the transition between Alps and Pannonian Basin: Constraints from dating fault activity by the $^{26}Al/^{10}Be$ burial age method. Submitted to International Journal of Earth Sciences.

In **Chapter 3**, the existing understanding of landscape evolution of the Highland and Lowland of Graz is placed into an absolute time frame with absolute age constraints derived from TCN, optically stimulated luminescence (OSL) and U/Th dating methods. Finally, a relief evolution of the region from the beginning of extrusion and basin

formation (Early Miocene) to the present is proposed. A coherent block is uplifting since Pliocene times, thus allowing the preservation of planation surfaces at distinctive levels up to the present. Re-excavation of sediments stored at the Alpine margin may be a candidate for increased sediment supply of the region in Pleistocene times. This chapter is currently under review:

- **Wagner, T., Fritz, H., Stüwe, K., Nestroy, O., Rodnight, H., Benischke, R.**, Correlations of cave levels, stream terraces and planation surfaces along the River Mur – constraints on timing of landscape evolution along the eastern margin of the Alps. Submitted to Geomorphology.

Chapter 4 contains overall conclusions and outlook of this work.

Appendix A is a contribution where DEM data is used to infer the state of geomorphic disequilibrium of the whole Alps. Slopes of catchments of similar size are analyzed in relation to their elevation. Morphologically, the whole mountain belt seems to show a similar state of disequilibrium or prematurity. A simple uplift model is found to reproduce the observed behavior. Theoretically derived erosion rates are correlated with sediment budget data. Substantial topographic buildup is suggested to have begun just 5-6 Ma ago. This appendix has already been published as:

- **Hergarten, S., Wagner, T., Stüwe, K.**, 2010. Age and Prematurity of the Alps Derived from Topography, Earth Planet. Sci. Lett. 297, 453-460, doi:10.1016/j.epsl.2010.06.048

Appendix B describes the "cooking recipe" of the sample preparation for the burial age dating we (Diana Sahy and I) used in the cosmogenic nuclides laboratory in Vienna.

Appendix C lists abstracts of posters and talks that were presented in the course of this PhD at several national and international conferences and of a regional publication where I contributed to.

- **Wagner, T., Fritz, H., Stüwe, K., Fabel, D.**, 2010. Pliocene to Pleistocene faulting at the transition between Alps and Pannonian Basin: Constraints from dating fault activity by the $^{26}Al/^{10}Be$ burial age method. Journal of Alpine Geology 52, p.249, Pangeo 2010, Leoben, Austria.

- **Wagner.T, Fabel, D., Fiebig, M., Häuselmann, Ph., Sahy, D., Xu, S., Stüwe, K.**, 2010. Young uplift in the non-glaciated parts of the Eastern Alps. Geophysical Research Abstracts 12, EGU2010-9516, EGU General Assembly 2010, Vienna, Austria.

- **Hergarten, S., Stüwe, K., Wagner, T.**, 2010. Age and Prematurity of the Alps. Geophysical Research Abstracts 12, EGU2010-9409, EGU General Assembly 2010, Vienna, Austria.

- **Gasser, D., Gusterhuber, J., Krische, O., Puhr, B., Scheucher, L., Wagner, T., Stüwe, K.**, 2009. Geology of Styria: An overview. Mitteilungen des naturwissenschaftlichen Vereins Steiermark 139, 5-36.

- **Wagner, T., Hergarten, S., Stüwe, K.**, 2009. Slope-elevation relation of an orogen, a chance to decipher its stage of evolution? NAWI Graz Workshop, Session A2 – Scaling issues in earth sciences, 26. June 2009, Graz, Austria.

- **Plan, L., Döppes, D., Wagner, T.**, 2009. The significance of cave bears for passage morphology. 15th Int. Cong. of Speleology, Kerville, Texas, 16-26 July 2009, Proceedings p.116.

- **Sahy, D., Häuselmann, Ph., Grasemann, B., Kubic, P., Schenk, B., Stüwe, K., Wagner, T., Fiebig, M.**, 2009. Cave sediments as records of landscape evolution in the Eastern Alps. 15th Int. Cong. of Speleology, Kerville, Texas, 16-26 July 2009, Proceedings p.979.

- **Fiebig, M., Häuselmann, P., Stüwe, K., Sahy, D., Wagner, T., Schenk, B., Grasemann, B.**, 2009. Burial Age Dating in caves applied in current Austrian research projects. International symposium on Geology, Natural Resources and Hazards in Karst Regions (GEOKARST 2009). Hanoi, Vietnam, November 12-15, 2009.

- **Stüwe, K., Wagner, T., Wölfler, A., Legrain, N.**, 2009. Active tectonics at the Eastern end of the Alps: The Alps are certainly not “dead” at all. Geophysical Research Abstracts 11, EGU2009-9332, EGU General Assembly 2009, Vienna, Austria.

- **Wagner, T., Fabel, D., Stüwe, K., Fritz, H., Kurz, W.**, 2008. Incision rates based on burial age dating of cave sediments along the Mur river in Austria and their correlation to the nearby landscape formation. Journal of Alpine Geology 49, p.115, Pangeo 2008, Vienna, Austria.

- **Fiebig, M., Häuselmann, Ph., Stüwe, K., Audra, Ph., Fabel, D., Grasemann, B., Mihevc, A., Sahy, D., Wagner, T.**, 2008. Rates of valley incision in the European Alps approached by cosmogenic nuclides. 33rd IGC International Geological Congress Oslo 2008, Oslo, Norway, 6-14 Aug. 2008.

- **Wagner, T., Stüwe, K., Fritz, H., Kurz, W., Fabel, D., Häuselmann, Ph.**, 2008. River incision based on cave sediment analysis along the Eastern Alpine orogen – Pannonian Basin System transition zone. 16th International Karstological School “Classical Karst”, Karst sediments, Postojna, Slovenia, 2008.

- **Stüwe, K., Wagner, T.**, 2007. The western margin of the basin: highlights of young morphologies formed by basin inversion. Alpine – Carpathian – Pannonian Workshop, September 14-16, 2007, Proceedings p.26.

- **Wagner, T., Stüwe, K., Fritz, H., Kurz, W., Fabel, D.**, 2007. The Evolution of the Styrian Basin in the Neogene – Indications and First Conclusions. DRT 2007, 16th Deformation Mechanisms, Rheology and Tectonics Conference, September 2007, Milano, Italy.

- **Wagner, T., Stüwe, K., Fritz, H.**, 2007. An Elevation Correlated Map of the Neogene in the Styrian Basin. 2nd International Workshop on the "Neogene of Central and South-Eastern Europe", Joannea Geol. Paläont. 9, p.111 (2007), Kapfenstein, Austria.

- **Wagner, T., Stüwe, K., Fritz, H.**, 2007. Conspicuous features and their indications for the evolution in the Styrian Basin. Geophysical Research Abstracts 9, EGU2007-A-04573, EGU General Assembly 2007, Vienna, Austria.

SUMMARY

Constraining the genesis of cave levels, terraces and planation surfaces with the use of modern geochronological methods allows to confine the landscape evolution of mountain belts within the last ~5 million years. Especially to understand the influence of tectonic processes versus climatic changes to landscape evolution, age data has been gathered for this thesis. Cosmogenic isotopes measurements on cave sediments and sediment filling of faults, luminescence dating of terrace sediments and U/Th dating of speleothems provide important absolute ages of geological markers. With the help of these and including geomorphological and structural geologic observations, it could be deduced that a coherent block, the Styrian Block – consisting of the Styrian Basin and the surrounding basement located at the Alpine orogen - Pannonian Basin transition – has been uplifting around 600 m within the last ~5 Ma. An increase of sediment rates delivered from the hinterland of the Mur – deduced from a decrease in incision rates of the Mur River – is suggested to explain the periodic aggradation and re-excavation of sediments in the study area. The influence of climatic changes in Pliocene and Pleistocene times seems to be subordinate. The uplift of the Styrian Block and resulting erosion – primarily fluviatile – is most relevant for the forming of this landscape.

ZUSAMMENFASSUNG

Die zeitliche Eingrenzung der Genese von Höhlenniveaus, Terrassen und Verebnungsflächen mithilfe modernster geochronologischer Methoden ermöglicht es die Landschaftsentwicklung von Gebirgen in den letzten ~5 Millionen Jahre besser abzugrenzen. Speziell um den Einfluss von tektonischen Prozessen im Vergleich zu klimatischen Veränderungen auf die Landschaftsentwicklung besser zu verstehen, sind für diese Arbeit Altersdaten gesammelt worden. Messungen von kosmogenen Isotopen an Höhlensedimenten und Sedimentfüllungen von Störungen, Lumineszenz Datierungen von Terrassensedimenten und U/Th Datierungen an Speläothemen liefern wichtige Absolutalter geologischer Marker. Anhand dieser und anhand der Einbeziehung geomorphologischer und strukturgeologischer Beobachtungen konnte festgestellt werden, dass ein kohärenter Block, der Steirische Block – bestehend aus dem Steirischen Becken und dem umliegenden Grundgebirge gelegen an der Alpenorogen - Pannonisches Becken Übergangszone – sich in den letzten ~5 Ma um rund 600 m gehoben hat. Ein vermehrter Anstieg an Sedimentraten angeliefert aus dem Hinterland der Mur – abgeleitet von einem Rückgang an Einschneideraten der Mur – wird als mögliche Erklärung der beobachteten zyklischen Aufschüttungen und Wieder-Abtragung von Sedimenten im Untersuchungsgebiet interpretiert. Der Einfluß von Klimaveränderungen im Pliozän und Pleistozän scheint eher untergeordnet zu sein. Die Hebung des Steirischen Blocks und die resultierende Erosion – primär fluviatil – ist maßgeblich für die Formgestaltung dieser Landschaft.

CONTENTS

CHAPTER 1

YOUNG UPLIFT IN THE NON-GLACIATED PARTS OF THE EASTERN ALPS

Abstract We report the first incision rates derived from burial ages of cave sediments from the Mur river catchment at the eastern margin of the Eastern Alps. At the transition zone between the Alpine orogen and the Pannonian basin, this river passes through the Paleozoic of Graz – a region of karstifiable rocks called the Central Styrian Karst. This river dissects the study area in a north-south direction and has left behind an abundance of caves. These caves can be grouped into several distinct levels according to their elevation above the present fluvial base level. Age estimates of abandoned cave levels are constrained by dating fluvial sediments washed into caves during the waning stages of speleogenesis with the terrestrial cosmogenic nuclide method. These ages and the elevations of the cave levels relative to the current valley floor are used to infer a very complex history of 4 million years of water table position, influenced by the entrenchment and aggradation of the Mur river. We observe rather low rates of bedrock incision over the last 4 Ma (in the order of 0.1 mm/y) with an e-folding decrease in this trend to lower rates at younger times. We relate this incision history to a tectonic setting where an increase of drainage area of the Mur river due to stream piracy in Late Miocene to Pliocene times is linked to surface uplift. The later decrease in valley lowering rates is attributed to the rise of the base level related to aggradation of sediments within the valley. Sediment transport through the valley from the upstream section of the Mur river limited the erosional potential of the river to a transport limited state at the later stages of the incision history.

Keywords: burial age; cosmogenic nuclides; caves; river incision; landscape evolution

T. Wagner et al., Young uplift in the non-glaciated parts of the Eastern Alps, Earth Planet. Sci. Lett. 295, 159-169, doi: 10.1016/j.epsl.2010.03.034

1.1 Introduction

The young tectonic evolution of the Alps is a much debated topic in Earth science. Many studies investigate the uplift history and landscape evolution of the range over the last 10 Ma employing low temperature geochronological methods (Dunkl et al., 2005; Luth and Willingshofer, 2008; Vernon et al., 2008), geodetic uplift measurements (Kahle et al., 1997; Ruess and Höggerl, 2002), the interpretation of morphometric data (Frisch et al., 2001; Robl et al., 2008a; Székely et al., 2002) and new cosmogenic isotope methods to measure erosion rates (von Blanckenburg, 2005; Wittmann et al., 2007; Norton et al., 2010b).

Much of this debate focuses on the central Alps where it has been argued that the range is past its peak of tectonic activity and acts now merely in passive response to erosion (Champagnac et al., 2009; Schlunegger and Hinderer, 2001), despite its dramatic topography of up to 4000 m of relief. In contrast, the eastern margin of the Alps currently appears to experience a tectonic rejuvenation: Miocene fission track ages (e.g. Hejl, 1997) and post-Middle Miocene sediment cover (Dunkl and Frisch, 2002) suggest that much of the Neogene evolution of the eastern margin of the orogen was likely to be characterised by little relief and low elevation and that – therefore – today's topography is rather young. Morphological evidence for this is provided by paleosurfaces at higher elevations and steeply dissected gorges with an obvious break in slopes at about 1000 m a.s.l. (above sea level) in a landscape with up to 2000 m relief (Winkler-Hermaden, 1957).

This scenario – and the difference between the central and the eastern Alps – is consistent with our understanding of the plate scale tectonic processes: The rotation pole of the Adriatic plate is currently located near Torino south of the central Alps suggesting tectonic quiescence in the central Alps, but ongoing north-south convergence in the east (Champagnac et al., 2009; Fodor et al., 2005; Grenerczy et al., 2000, 2005). Moreover, general consensus holds that the inversion of the Pannonian basin commenced in response to the cessation of subduction underneath the Carpathian arc and ongoing north-south convergence became the dominant stress regime in the area since then (Bada et al., 2007; Horváth and Cloething, 1996; Ruszkiczay-Rüdiger, 2007). Onset of uplift in the Styrian Basin (being the western most lobe of the Pannonian Basin) around Pliocene to Quaternary times (Sachsenhofer et al., 1997) appears to be a reflection of this process. Moreover, mantle processes like slab break off or delamination may influence uplift rates (e.g. Genser et al., 2007).

Interestingly, specific data sets documenting this uplift are almost absent. In this paper we present cosmogenically derived burial ages of sediments from caves within the karstifiable rocks of the Paleozoic of Graz as the first evidence for a young incision history of the major drainage system that drains the Alps to the East: the Mur system.

We show that the incision of this system is slow but acts on a rejuvenating setting, providing an exciting illustration of the revitalization of a landscape forming process: a juvenile stage of relief adjustment to changes in rock uplift rates.

1.2 Topography of the eastern margin

The eastern margin of the Alps is the only part of the Eastern Alps that was never ice covered during the Quaternary (Fig. 1.1A; Van Husen, 1999). As such, glacial carving can be excluded as a land forming process and the region is uniquely suited to infer the pre-Quaternary uplift history from the incision history of its drainages.

In very general terms, the drainage system of the Eastern Alps evolved in relation to the eastward extrusion of the range (Frisch et al., 1998; Ratschbacher et al., 1991). Of the three major eastward draining rivers, the Enns-Salzach system in the north and the Drava system in the south follow major west-east striking strike slip systems. The third major drainage, the Mur, roots from the highest peaks of the eastern Alps at an elevation of 1898 m a.s.l. and drains much of the central region of the range eastwards into the Pannonian basin. In contrast to the others, the Mur does not follow any major fault system downstream of Bruck (Fig. 1.1A). Morphological analysis of these three major drainage systems shows that the Enns-Salzach and the Drava systems have knickpoints in their main channels that can be correlated with glacial features, while the Mur – outside the glaciated region – has an equilibrium channel profile (Robl et al., 2008a). However, a complicated set of stream terraces above the channel indicates that the river had a complicated aggradation and incision history (Winkler-Hermaden, 1955, 1957). Nevertheless, because of (i) the absence of fault control of the lower Mur; (ii) the fact that the Mur crosses the (Alpine) orogen-(Pannonian) basin transition near the city of Graz and (iii) the fortuitous fact that this transition zone is made up of karstified rocks, we focus here on dating the incision history of the Mur drainage system.

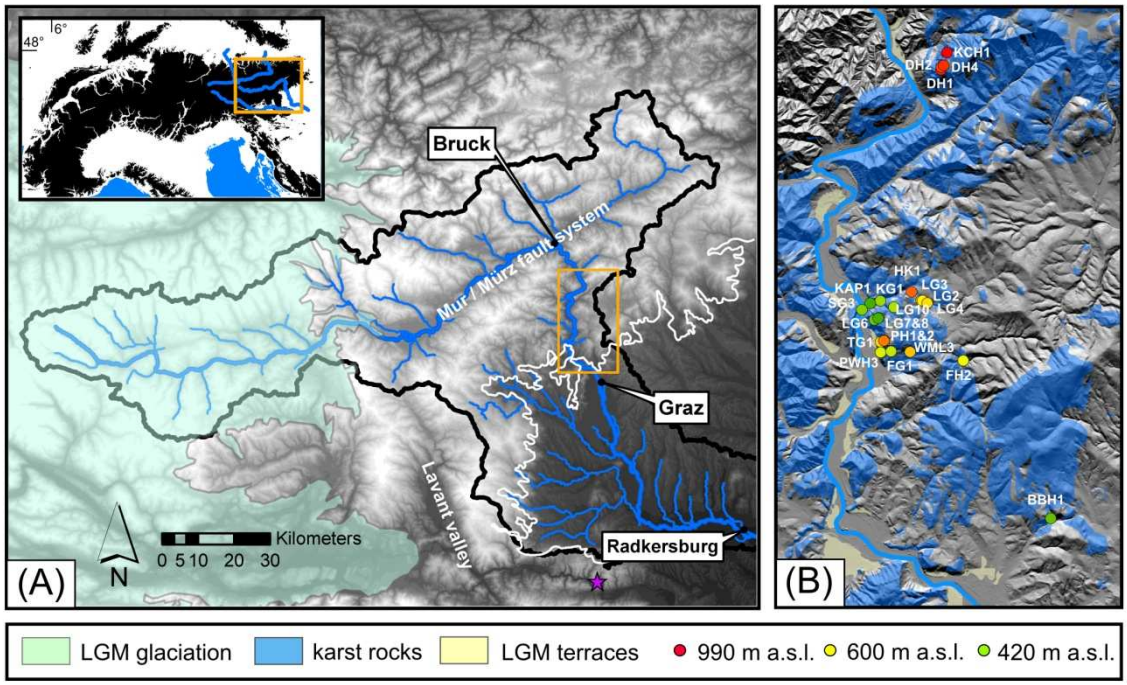

Fig. 1.1. Map showing the geographical position of the area under investigation. **(A)** The extend of the last glacial maximum in light blue, the perimeter of the Mur catchment as a black line, the orogen-basin transition as a white line and in blue the main river and larger tributaries displayed on top of the digital elevation model (white above 2000 m a.s.l., darkest shades about 200 m a.s.l.). The orange rectangle shows the area enlarged in 1B. The star indicates the site of an exposure age dated sample along the Drava river. The inset shows the whole Alps with an elevation above 600 m a.s.l. in black, indicating the area under investigation situated at the easternmost end of the Eastern Alps. Blue lines show the major rivers in the Eastern Alps. **(B)** Karstifiable rocks in blue and the last glacial terraces in yellow on top of a digital elevation model. Dots show the sample locations of the various cave sediments color coded according to their elevations above sea level (red = highest, green = lowest). Labeling of sample acronyms as used in Table 1.1.

1.2.1 Caves as a proxy for landscape evolution

The drainage basin of the Mur above Radkersburg is some 10000 km^2 in area and its main channel has a total length of 295 km from its spring down to the Austrian border. The so-called Central Styrian Karst, located at the orogen basin transition zone, belongs tectonically to the Paleozoic of Graz. Its most intensively karstified region consists of Upper Devonian limestones. As the Paleozoic of Graz is only some tens of kilometers across and only partly made up of limestones (Fig. 1.1B), many caves are recharged from siliceous rocks in the upland. Because of this and the fact that the topographic relief within and outside the Paleozoic of Graz is similar, local variations in incision and erosion rates are unlikely to be the consequence of differences in lithology. Caves are concentrated in two areas, the Hochlantsch area in the north and the Tanneben massif further south (Fig. 1.1B). Geologically, the Hochlantsch area is located in the upper whereas the Tanneben is in the lower nappe system of the Paleozoic of Graz (Fig. 1.1B). In the Hochlantsch area higher cave levels are preserved, whereas in the

Tanneben massif most of these have been eroded (Gasser et al., 2009). A total of some 500 caves that range from active caves on the current base level of the Mur to inactive caves up to about 800 m above the current valley floor are recorded in the Austrian cave registry. Caves are typically of phreatic origin with occasional vadose overprint (Fig. 1.3H). Sub-horizontal tubular passages are widespread and can be grouped into at least 5 distinguishable cave levels, or speleogenetic phases (Fig. 1.2). In the caves, we interpret these levels as indicators for the position of the former water table. They correlate well with other morphological features like terraces and planation surfaces across the region (Maurin and Benischke, 1992; Winkler-Hermaden, 1957). However, for this study we focus on caves alone because of (i) their abundance, (ii) because of the preservation of sediments within the caves and (iii) because surface markers are so far undated.

As erosion lowers the valley floor, the water table drops, leaving the caves as a record for the elevation of the paleo-water table (according to the concept of base level control of cave levels; Palmer, 1987). Many of the caves contain allochthonous sediments of fluvial origin made up of quartzose sand and coarse gravels derived from the crystalline hinterland and interpreted to be deposited during the waning stages of passage formation (Fig. 1.3). However, we will show later that they are likely to have been derived from sources within the close vicinity of the karstified region. As such they are ideally not influenced by further upstream sections of the main (Mur) river. The vertical distance between cave levels can be used to infer relative incision rates if the time of passage formation is known. Here we constrain the minimum age of passages by dating the time of emplacement of allochthonous quartzous fluvial sediments into the cave and interpret these ages as the time when valley incision progressed to abandon the passage level. Consequently, the calculated incision rates represent maximum values.

Field mapping demonstrates an asymmetrical distribution of caves and gravel accumulations along the Mur valley. An abundance of caves is observed on the eastern river side and scarcity on the western as sketched on Fig. 1.2. The Austrian cave registry lists 429 known caves on the eastern, but only 85 on the western river side. The five largest cave systems are all found on the eastern river side. A satisfying explanation for this is the focus of ongoing research and therefore of a speculative nature, but it is considered likely that it might be related to a westward shift of the Mur river (e.g. Maurin and Benischke, 1992). This observation illustrates the complexity of the study area.

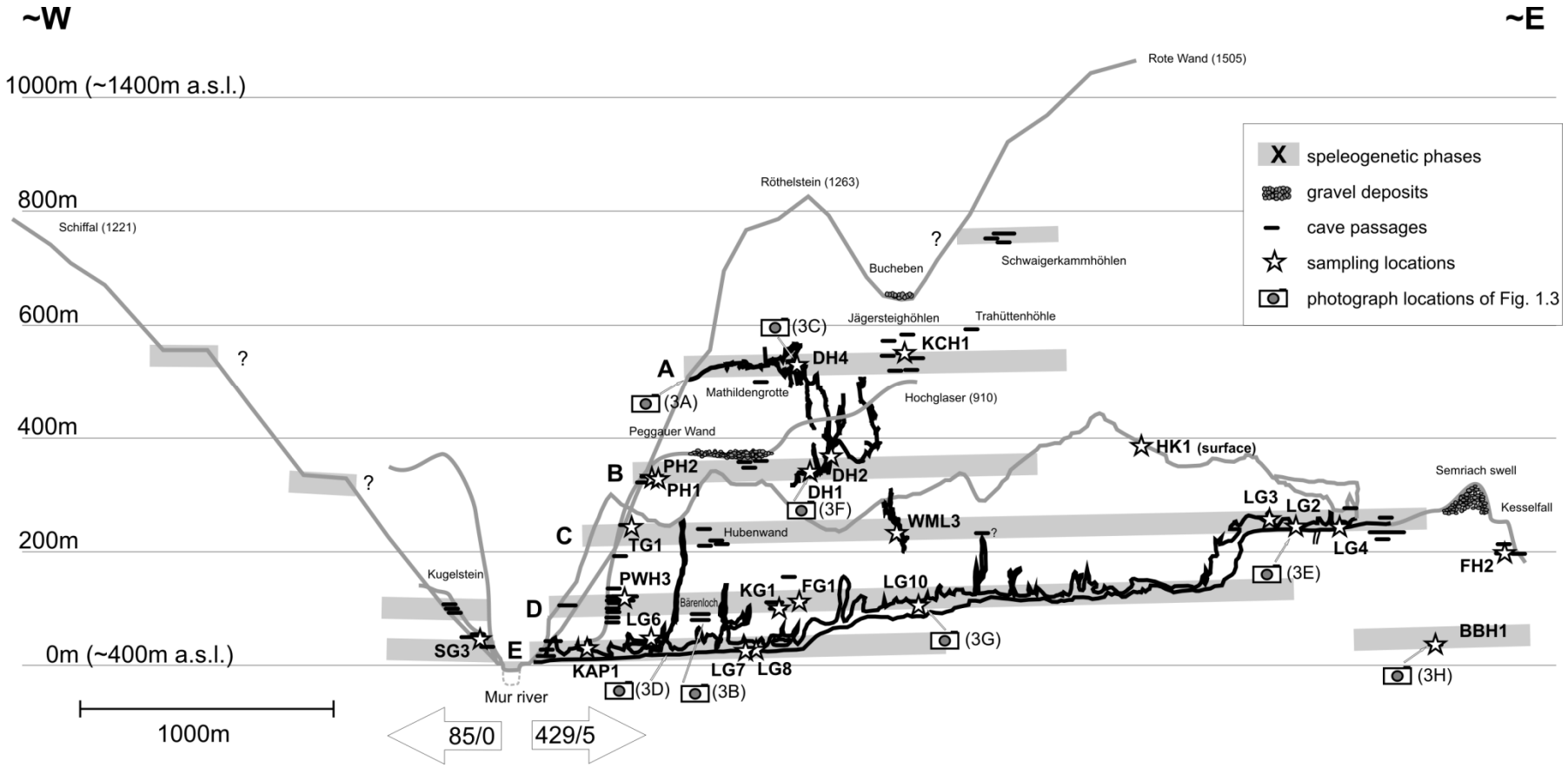

Fig. 1.2. Projected schematic view of cave systems of the Central Styrian Karst. Smaller caves illustrated by small black horizontal bars. Subhorizontal grey bars show speleogenetic phases A–E inferred from abundance of phreatic cave passages at these elevations. Stars indicate sampling locations of dated cave sediments. Camera symbols indicate the positions of the photographs shown in Fig. 1.3. Elevation in meters above the modern Mur river. Note that the whole region shows an asymmetrical distribution of dissolution caves and gravel deposits (see Section 1.2.1). Sample acronyms correspond to the following caves: Tanneben massif: FG=Ferdinandsgrotte, KAP=Kapellenhöhle, KG=Keesgang / Große Badlhöhle, LG=Lurgrotte, PH=Percohöhle, PWH=Peggauerwandhöhle, SG=Stufengrotte, TG=Tausgrotte, WML=Wildemannloch; Hochlantsch area: DH=Drachenhöhle, KCH=Kuschcanon; FH=Frauenhöhle, BBH=Blaubruchhöhle.

The main focus of our study are the Lurgrotte located in the Tanneben area and the Drachenhöhle (Fig. 1.3A) in the Hochlantsch area. These are two of the largest cave systems of the Styrian Karst, and both exhibit more than one level or speleogenetic phase. The Lurgrotte is the longest cave system in the Tanneben area (5975 m, 273 m vertical extent) and is developed along three subhorizontal levels (levels C–E, Fig. 1.2). Only the lower level is permanently active, but passages situated at higher elevations show obvious signs of reactivation, for example sinking streams during flood events (e.g. as shown by organic sedimentation within the cave). The whole cave system was filled with sediments and re-excavated several times, even in historical records. In the Hochlantsch area, the Drachenhöhle (length 4386 m, depth 250 m) shows two obvious speleogenetic phases developed along strike of bedding in the Hochlantsch limestones (Fig. 1.2). The upper level, here defined as level A, is situated at about 950 to 1000 m a.s.l., while the lower level of the Drachenhöhle can be correlated with the highest caves found in the Tanneben massif (level B) based on its elevation above streambed. Lower karstified levels, corresponding to levels C–E from the Tanneben massif, are less developed in the Hochlantsch region and did not contain sediments suitable for dating (Fig. 1.3B). Smaller caves from the Hochlantsch and Tanneben areas were correlated to distinct levels of the Drachenhöhle, and the Lurgrotte, respectively; based on similar elevation above the modern valley floor. In total, this speleogenetic record allows us to infer paleo-water table lowering over a vertical extent of more than 550 m.

A total of more than 120 caves have been investigated spanning a vertical range of 780 m. Finally, we selected 13 caves and dated 22 samples comprising siliceous rock pebbles (fine to very coarse gravels) using cosmogenic isotopes (for sample locations see Fig. 1.1B and Fig. 1.2). Careful subsurface field mapping was used to ascertain that the sampled sediments represent characteristic stages of passage formation. Additionally, one surface sample (HK1) was dated using cosmogenic isotopes to test for the presence of inherited burial signal in samples collected in the caves. Targeted U-Th dating of speleothems was used to support the burial ages with independent ages from stratigraphically related sediments (Table 1.2 and Fig. 1.3C, G).

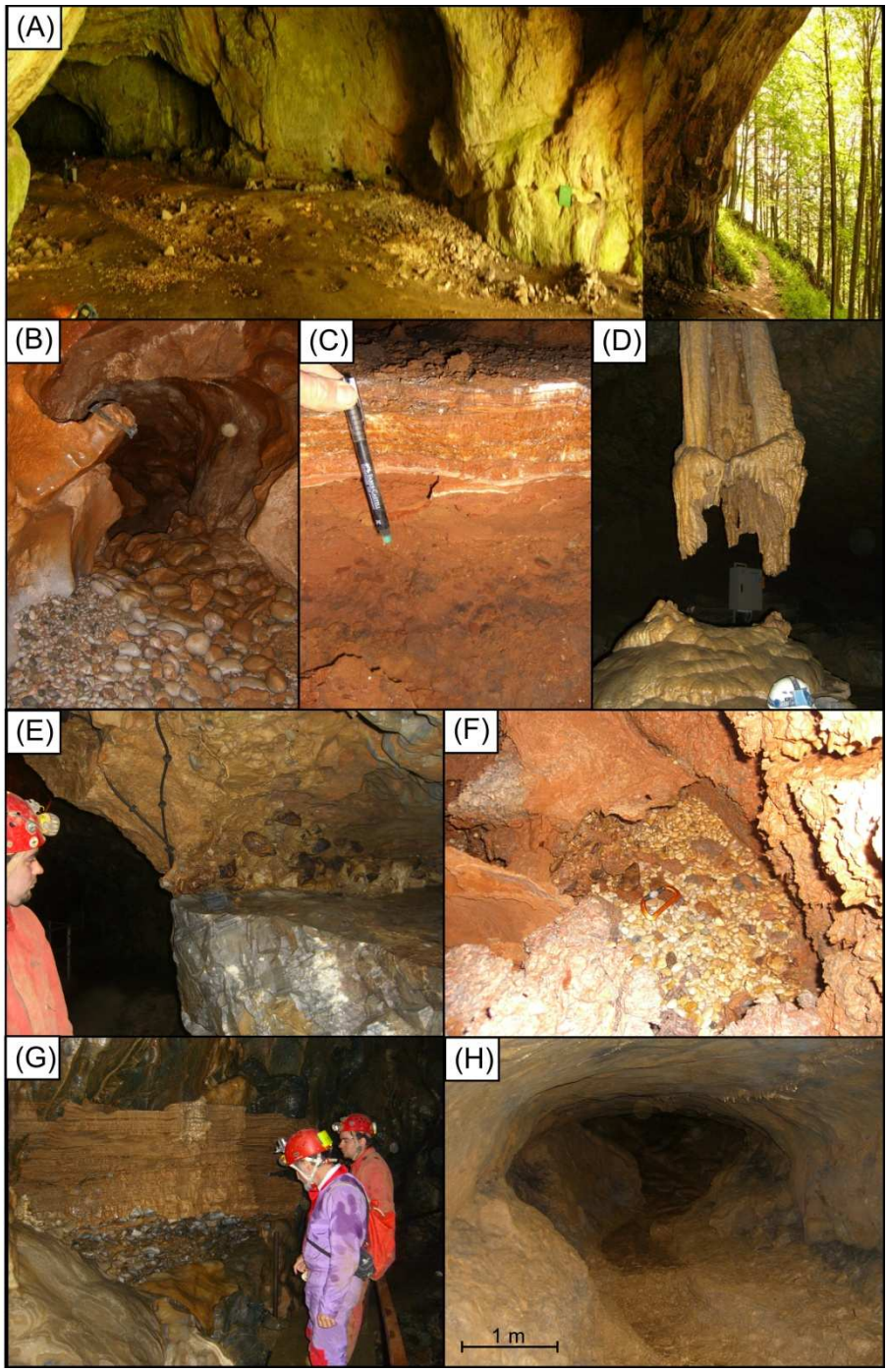

Fig. 1.3. Field impressions from the Central Styrian Karst: **A** Portal of the Drachenhöhle, Hochlantsch area. **B** Active passage of the Bärenloch, Hochlantsch area. Note that all the well rounded pebbles are carbonate rock only. **C** Sample location of sample DH4: Gravels as well as flowstone were dated (see Tables 1.1 and 1.2). **D** The so-called Prinz (prince) at level E of the Lurgrotte, an impressive stalagmite with gravel remainings at its base indicating former aggradation of this passage. **E** Sample location of sample LG2 in a wall notch at level C of the Lurgrotte. **F** Sample location of sample DH1 at the lower level B of the Drachenhöhle. **G** Sample location of sample LG10: Further entrenchment of the gallery has left behind remnants of an impressive calcite false floor with gravel remains still attached below indicating an aggradation event of level D in the Lurgrotte. **H** Phreatic passage in the Blaubruchhöhle showing the typical elliptic tube with beginning vadose overprint (key hole).

1.3 Burial ages

Deriving burial ages from cave sediments is a relatively new method (Granger et al., 2001) not yet successfully applied in the Eastern Alps (first attempts by Frisch et al., 2001). It involves the measurement of two isotopes (here ^{26}Al and ^{10}Be) that are produced by cosmic radiation in quartz near the surface prior to burial. ^{26}Al and ^{10}Be accumulate at a ratio of about 6.8:1 in quartz grains – a few atoms per gram of quartz per year. Quick and deep burial of such quartz-rich sediment in a cave (>20 m rock overburden) assures shielding from further cosmic rays. After burial the ^{26}Al and ^{10}Be concentrations in the sample are only affected by their relative decay resulting in a decrease in the $^{26}Al/^{10}Be$ ratio in the samples. Measured $^{26}Al/^{10}Be$ in the samples can be used to derive a burial age (Gosse and Phillips, 2001; Granger and Muzikar, 2001). The current upper limit for measurement of the ^{26}Al and ^{10}Be isotope pair is around 5 my. A prerequisite of the burial dating technique is that samples have been exposed long enough to cosmic rays and accumulated sufficient cosmogenic nuclides prior to burial. Unfortunately this cannot be determined a priori in the field.

In the laboratory, about 100 g of quartz was extracted and purified from bulk samples by magnetic and density separation and selective chemical dissolution. Quartz was dissolved in a 5:1 solution of concentrated HF and HNO_3 and spiked with about 0.74 mg ^{9}Be. Al and Be were separated and purified by ion chromatography and selective precipitation. Precipitates were oxidized and mixed with metal powder for accelerator mass spectrometry (AMS). $^{10}Be/^{9}Be$ and $^{26}Al/^{27}Al$ nuclide ratios in the sample and procedural blanks were measured at the SUERC AMS facility in Glasgow. The procedural blanks yielded $^{10}Be/^{9}Be$ ratios $<3.6 \times 10^{-15}$ and $^{26}Al/^{27}Al$ ratios of $<2.5 \times 10^{-15}$, representing <6% of total ^{10}Be atoms and <10% of total ^{26}Al atoms in the samples. Only sample TG1 had low measured ratios of $11.5\pm0.9 \times 10^{-15}$ and $5.4\pm1.8 \times 10^{-15}$ respectively and the procedural blanks represent <22% and <46% of the ^{10}Be and ^{26}Al atoms respectively. Stable aluminium concentrations were determined by ICP-OES. The stated errors are 1σ calculated from AMS and ICP-OES uncertainties. Aside from obtaining burial age data, the isotope concentrations can also be used to infer paleo-erosion rates of the source area prior to burial of the clasts. This is accomplished by backward modeling the quantity of nuclides present prior to the burial coupled with local production rate estimates. Cosmogenic nuclide production rates were assumed to be constant and were estimated for a mean source altitude of 1000 m a.s.l. and a latitude of 47.2°.While we cannot exclude variations in the elevation of the source area over the last few millions of years, we consider our estimate of 1000 m to be realistic. The pre-burial $^{26}Al/^{10}Be$ ratio (~6.8:1) is basically not influenced by production rate and thus elevation (Nishiizumi et al., 1989; Stock et al., 2005b) and therefore burial ages remain unaffected by altitude changes in the source area. However, our assumption increases the uncertainty of our pre-burial erosion rates, as these are based on measured isotope concentrations and elevation dependant production rates.

Figure 1.4A shows our results in a logarithmic two isotope plot. The curved lines are burial ages in million years; the steep straight lines are radioactive decay trajectories plotted for pre-burial erosion rates (m/my) increasing from right to left. It can be seen that the measured burial ages range from practically zero to 5 Ma, spanning the whole range of the burial age dating method (Fig. 1.4A). Some samples experienced only minor burial: the Lurgrotte samples LG7 and LG4 and the surface sample HK1. The Lurgrotte samples LG4 and LG7 were taken from flood deposits close to the current active streams in the cave at level E and C which explains their young age. Sample HK1 was collected at the surface on top of the Tanneben massif at 780 m a.s.l. and has a finite burial age of 0.25 ± 0.08 Ma indicating that other samples may also have experienced a minor but complex burial history prior to their deposition in the caves. The fact that the dating method yielded young ages at sites where subsurface mapping indicated the possibility of late emplacement of the sediments increases the overall confidence level of the dataset. Complementary to this, all the U-Th ages of stratigraphically related speleothems are significantly younger than the burial ages of subjacent gravels (Tables 1.1 and 1.2).

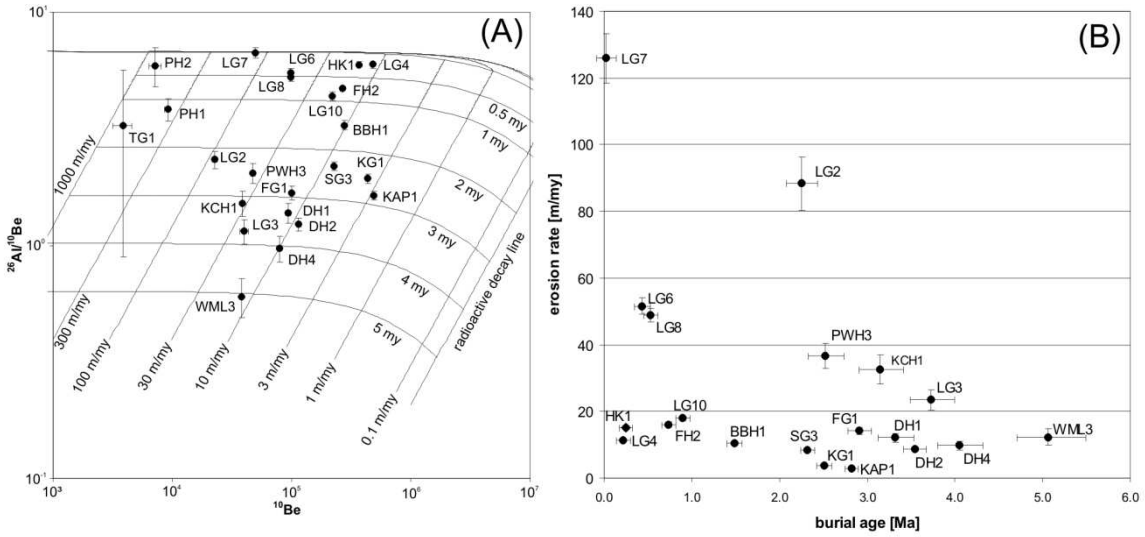

Fig. 1.4. Burial age data graphically displayed. **(A)** Two isotope plot showing the samples burial ages and pre-burial erosion rates, assuming local production rates as shown in Table 1.1. **(B)** Burial age versus pre-burial erosion rates, suggesting rather constant erosion rates in the source areas of the cave sediments of about 20 m/my.TG1, PH1 and PH2 are outside the plotted range (see Section 1.3).

Sample	A.C.R. No.	Height*** (m)	^{26}Al* (10^4 at/g)	^{10}Be* (10^4 at/g)	^{26}Al/^{10}Be	Burial age** (Ma)	Erosion rate# (m/my)
LG7	2836/1	25 ± 5	33.37 ± 1.33	4.98 ± 0.19	6.70 ± 0.37	0.02 ± 0.12	125.95 ± 7.41
KAP1	2836/19	25 ± 5	80.54 ± 2.44	49.19 ± 1.53	1.64 ± 0.07	2.82 ± 0.09	2.77 ± 0.13
LG8	2836/1	26.5 ± 5	51.81 ± 1.43	9.87 ± 0.26	5.25 ± 0.20	0.53 ± 0.08	48.86 ± 2.00
BBH1	2832/3	34 ± 5	90.79 ± 2.84	27.70 ± 0.90	3.28 ± 0.15	1.48 ± 0.09	10.47 ± 0.51
LG6^S	2836/1	45 ± 5	54.07 ± 0.96	9.83 ± 0.39	5.50 ± 0.24	0.43 ± 0.09	51.60 ± 2.40
SG3	2784/6	47 ± 5	49.65 ± 1.08	22.66 ± 0.81	2.19 ± 0.09	2.32 ± 0.09	8.30 ± 0.38
LG10^S	2836/1	91 ± 5	95.77 ± 1.97	21.94 ± 0.79	4.36 ± 0.18	0.90 ± 0.09	18.01 ± 0.81
KG1	2836/17	100 ± 5	84.67 ± 2.57	43.71 ± 1.56	1.94 ± 0.09	2.51 ± 0.09	3.75 ± 0.19
FG1	2836/44	107 ± 5	16.77 ± 0.96	9.98 ± 0.35	1.68 ± 0.11	2.91 ± 0.14	14.17 ± 1.03
PWH3	2836/38	117 ± 5	9.71 ± 0.88	4.76 ± 0.19	2.04 ± 0.20	2.52 ± 0.22	36.66 ± 3.93
FH2	2832/15	205 ± 5	125.32 ± 2.47	26.61 ± 0.95	4.71 ± 0.19	0.74 ± 0.09	16.11 ± 0.71
WML3	2836/27	225 ± 5	2.30 ± 0.42	3.81 ± 0.16	0.60 ± 0.11	5.06 ± 0.43	12.33 ± 2.51
LG2	2836/1	243 ± 5	5.30 ± 0.35	2.28 ± 0.12	2.33 ± 0.20	2.25 ± 0.19	88.38 ± 8.03
LG4	2836/1	245 ± 5	288.97 ± 5.64	48.36 ± 1.57	5.98 ± 0.23	0.22 ± 0.08	11.46 ± 0.47
TG1	2836/82	245 ± 5	1.27 ± 0.89	0.39 ± 0.07	3.27 ± 2.38	1.54 ± 2.74	750.01 ± 600.60
LG3	2836/1	260 ± 5	4.59 ± 0.42	4.00 ± 0.31	1.15 ± 0.14	3.73 ± 0.27	23.44 ± 3.06
PH1	2836/164	325 ± 5	3.53 ± 0.29	0.92 ± 0.06	3.83 ± 0.41	1.20 ± 0.24	372.93 ± 43.45
PH2	2836/164	331 ± 5	4.26 ± 0.64	0.72 ± 0.08	5.91 ± 1.11	0.29 ± 0.44	759.55 ± 154.23
DH1	2839/1	350 ± 5	12.99 ± 1.12	9.41 ± 0.48	1.38 ± 0.14	3.31 ± 0.22	12.17 ± 1.32
DH2	2839/1	370 ± 5	14.15 ± 0.72	11.50 ± 0.46	1.23 ± 0.08	3.54 ± 0.14	8.79 ± 0.62
HK1	-	385 ± 5	216.87 ± 3.33	36.55 ± 1.18	5.93 ± 0.21	0.25 ± 0.08	15.04 ± 0.58
DH4^S	2839/1	528 ± 5	7.74 ± 0.94	7.97 ± 0.29	0.97 ± 0.12	4.05 ± 0.28	9.83 ± 1.36
KCH1	2839/37	550 ± 5	5.88 ± 0.68	3.88 ± 0.17	1.51 ± 0.19	3.15 ± 0.27	32.60 ± 4.34

Table 1.1. Cosmogenic nuclide concentrations and sediment burial ages from caves in the Central Styrian Karst.

* ^{26}Al/^{27}Al and ^{10}Be/^{9}Be measured by accelerator mass spectrometry at the SUERC AMS facility relative to Z92-0222 with ^{26}Al/^{27}Al taken as 4.11 x 10^{-11} and NIST SRM 4325 with ^{10}Be/^{9}Be taken as 3.06 x 10^{-11}. ~0.74 mg ^{9}Be added as carrier to ~100 g quartz samples. Quartz [Al] measured by ICP-OES (PerkinElmer, Optima 5300 DV) and assigned 3% uncertainty.

** Burial ages and erosion rates determined by iterative solution of Eqs. (14) and (15) in Granger and Muzikar (2001), assuming local production rates of $P_{n\&\mu,26}$ = 74.1 at g^{-1} yr^{-1} and $P_{n\&\mu,10}$ = 10.9 at g^{-1} yr^{-1}, based on the CRONUS Earth online calculator (Version 2.2). Reported uncertainties represent 1σ measurement uncertainty. For comparing the burial ages this is sufficient, but when comparing them with other burial ages, total uncertainties including systematic uncertainties in production rates, ^{26}Al/^{10}Be production ratio and radioactive decay constants would have to be taken into account.

*** Height of the sample sites is given in meters above the current fluvial base level of the Mur river.

Modeled pre-burial erosion rates of the source area of the cave sediments prior to burial assuming local production rates of $P_{n\&\mu,26}$ = 74.1 at g^{-1} yr^{-1} and $P_{n\&\mu,10}$ = 10.9 at g^{-1} yr^{-1}, based on the CRONUS Earth online calculator (Version 2.2). For discussion see Section 1.3 – Burial ages.

S Burial ages are supported by speleothem U-series ages. The age estimates of stratigraphically related speleothems are considerably younger then the burial ages of the gravels, which is consistent with the conclusions of Stock et al. (2005a).

Sample	Lab no.	U (ngg^{-1})	[^{230}Th/^{238}U]	[^{234}U/^{238}U]	[^{232}Th/^{238}U]	[^{230}Th/^{232}Th]	Age (ka)	[^{234}U/^{238}U]$_i$
LG6-FSB	UMA02795 Jul-2009	104	1.081(5)	1.688(5)	0.02254(24)	1.9	99.6 ± 2.1	1.913(7)
LG10-FSB	UMA02796 Jul-2009	80	1.285(7)	1.736(4)	0.29751(169)	2.1	99.9 ± 32.3	1.977(88)
DH4-FSB	UMA02793 Jul-2009	72	1.113(10)	1.084(4)	0.22907(162)	1.4	559 (+inf/-110)	1.427(+0.53/-inf)

Table 1.2. U-Th age estimates of stratigraphically related speleothems from caves in the Central Styrian Karst. Sample preparation and measurements done by John Hellstrom, University of Melbourne. Activity ratios were determined with a Nu Plasma MC-ICP-MS following the procedure of Hellstrom (2003). Age is corrected for initial ^{230}Th using Eq. (1) of Hellstrom (2006) and an initial [^{230}Th/^{232}Th] of 1.5 ± 1.5 (uncertainties are fully propagated). 95% confidence intervals of the last digits of each value are given within round brackets.

Some samples show relatively high pre-burial erosion rates above 300 m/my (PH1, PH2 and TG1; Fig. 1.4). Interestingly, all these samples come from caves located in a prominent gulley of the Tanneben massif, where field work indicates that late deposition of sediments into caves is possible. Moreover, the high pre-burial erosion rates indicate possibly strong erosion events around the time of sediment deposition in the cave. This implies that the burial ages of these samples may not necessarily reflect a meaningful age of passage formation. Most of the other samples give pre-burial erosion rates around 20 m/my (Fig. 1.4B). These rather consistent and low pre-burial erosion rates over the whole time span support the fact that strong changes in erosion rates in the system either by tectonics or by climate are unlikely in the local catchments. Among these samples, there is a corresponding correlation of burial age and elevation with a noticeable clustering of data around 2.5 Ma.

1.3.1 Interpretation of the data in terms of incision

Plotting the burial age data from Fig. 1.4 against sample elevation above the current Mur level provides insight into the landscape evolution of the region (Fig. 1.5). In the ideal case such a presentation of the data should reflect the abandoning of formerly phreatic passages and lowering of the paleo-water table, which can ultimately be used to infer the rate of valley entrenchment (Audra et al., 2006). The surface sample HK1 and the samples LG4 and LG7 (documented above to belong to recent deposits/events) are not shown on Fig. 1.5. The oldest burial age for each level is used as it corresponds to the minimum age of passage formation if re-mobilization from higher levels can be excluded (Häuselmann and Granger, 2005). Figure 1.5 shows that the study area has a more complex history. First of all it must be noted that our data stem not from a single cave system, but from an abundance of smaller cave systems and remnants thereof. Because of this and because of the complex aggradation and incision history of the region all obtained ages must be discussed individually before any trends can be interpreted.

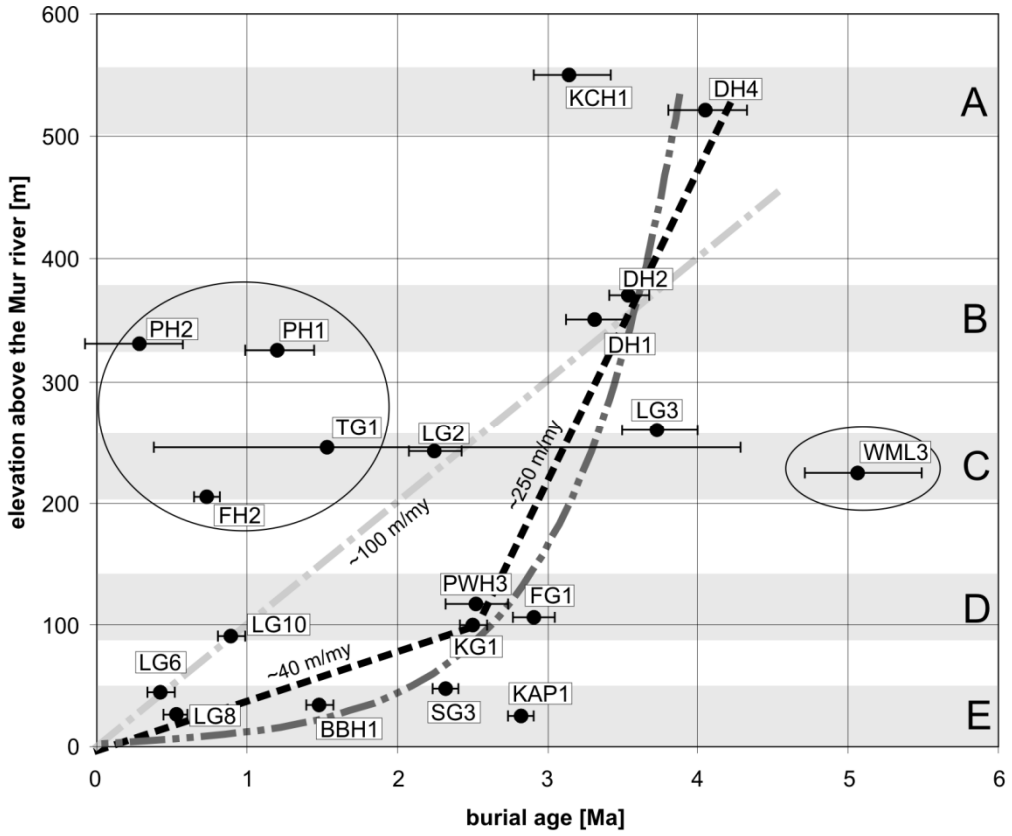

Fig. 1.5. Plot of burial age versus elevation above the Mur river. The data reveals the complex history of water table lowering related to valley entrenchment and aggradation. The speleogenetic levels are labeled as on Fig. 1.2. Trends are shown by dashed lines, an e-folding function is fitted through DH4, DH2, DH1, LG3, PWH3, FG1, KG1, SG3, BBH1; LG8, LG6 and the zero-point: elevation above Mur [m] = 1.38 $e^{1.58 * \text{burial age [Ma]}}$ with a coefficient of determination $R^2 = 0.58$. Encircled samples are considered to not represent the age of the elevations they are situated in (see Section 1.3).

The group of samples with low ages and high elevations on Fig. 1.5 has been discussed above: Except for FH2 they are all samples with high pre-burial erosion rates (Fig. 1.4) and are explained by later emplacement of the gravels. Sample FH2 comes from a cave in an independent limestone area that was influenced by another speleogenetic base level. Field observations show that this base level only incised 60 m (in the dated 0.75 Ma) since the cave was abandoned. In Fig. 1.5 it appears higher, because the vertical axis shows elevation above the Mur. If it were plotted only 60 m above the Mur, its age is consistent with others at that elevation above their respective trunk streams. The oldest burial age, sample WML3, comes from a shaft cave on the Tanneben massif, where there is evidence for complex multiphase formation. The sample was collected above massive terra rossa deposits interpreted by Maurin and Benischke (1992) as evidence for a Quaternary warm period in the region. This would indicate reversed stratigraphy and demands the exclusion of this data point from the incision rate estimation. However its burial age of 5.06 ± 0.43 Ma indicates the existence of older (and higher) cave levels in the Tanneben area that are no longer preserved. Finally,

KCH1 was collected in a canyon which was part of a larger cave system of phreatic origin, preserved today as an assembly of cave remnants in the Hochlantsch area, and related to the upper level of the Drachenhöhle (level A). This is the highest known occurrence of suitable cave sediments in the study area, so a sample was collected even though fieldwork indicated that later emplacement is possible.

The remaining data are all from caves where the stratigraphic relations between different cave sediments and the relationship between clastic sediments and passage morphology have given us confidence that there is no internal re-deposition from higher levels. The data are bracketed by the age of DH4 (Fig. 1.3C) from the upper level of the Drachenhöhle (4.05 ± 0.28 Ma at 968 m a.s.l., level A; sampled from a gravel bed known to be the stratigraphically oldest deposit within the passage; Schadler, 1931) and the current base level of the Mur River (at 440 m a.s.l. in the Hochlantsch region). This burial age suggests the onset of karstification to be earlier than 4 Ma, most likely already in the Miocene and permits using the remaining data set to compute a broad trend. A least square fit of the remaining data results in incision rates of ~90 m/my, whereas the incision rate inferred only from DH4 and the current base level is ~130 m/my; adding up to an average incision rate in the range of 100 m/my.

To determine deviations from this trend individual samples are discussed in more detail below. We begin with the samples from level B since level A is adequately discussed in the previous section. Based on the elevation correlation between the two study regions, the samples DH1 and DH2 from the lower level of the Drachenhöhle in the Hochlantsch area have their corresponding samples PH1 and PH2 in the Tanneben massif. Within the Drachenhöhle shafts ascend from the lower towards the upper level, but only one connecting passage is known. Remobilization of samples DH1 (Fig. 1.3F) and DH2 from the upper level is therefore unlikely. The ~3.4 Ma of burial of these two samples indicates an incision rate of 270 m/my from level A to level B. The interpretation of the LG2 and LG3 ages is somewhat challenging, but they are the only meaningful samples from level C. Sample LG2 is from a wall notch (Fig. 1.3E) and LG3 from gravel cemented to the ceiling during an episode of in-filling. Both samples come from the upper level of the Lurgrotte not far from each other despite their obvious difference in age. LG2 (2.25 ± 0.19 Ma) is interpreted as being emplaced after the formation of the passage, whereas LG3 (3.73 ± 0.27 Ma) might indicate relocation from higher up; restricting the real age of passage formation to somewhere in between. Samples KG1, FG1 and PWH3 from level D consistently show burial ages between 2.5 and 2.9 Ma, and are well distributed all over the Tanneben massif. Field evidence and the consistent burial ages designate this level D to be a turning point: relatively rapid incision rates occurred prior to ~2.5 Ma at ~250 m/my and then decreased considerably to ~40 m/my afterwards. LG10 (also from level D) was located below a one meter thick calcite false floor which is conserved as small remnants in the now further entrenched passage throughout level D in the Lurgrotte (Fig. 1.3G). This indicates a local aggradation event

post-dating the original passage formation. SG3 is the only sample from the western side of the Mur valley and is located between levels D and E (Fig. 1.2). The cave from which sample SG3 was collected is one of 24 caves located in the center of one of the Mur rivers meanders and is related to an underground meander cutoff. The burial age is only somewhat younger than the samples from level D and the height difference of 60 m makes a continuing incision rate of 200 m/my down to this elevation plausible. Sample BBH1 comes from the only accessible horizontal phreatic cave (Fig. 1.3H) of the Schöckl area located south of the Tanneben massif (Fig. 1.1). Considering its position in the vicinity to the current base level it has a rather old burial age of 1.48 ± 0.09 Ma. Potential re-deposition from higher levels could not be verified. Nevertheless the age fits well to the slow trend of the last 2-2.5 Ma. Finally, the active level E is most prominently developed in the active parts of the Lurgrotte cave system. Indeed, there is multiple evidence for young emplacement: (i) LG6 and LG8 have a consistent age of about 0.45 Ma despite their difference in elevation of 20 m (LG6 from an inactive sub-level). (ii) There are fine sediments interpreted to be the latest deposits of a damming event in close proximity to sample LG6. We suggest that such damming may have occurred by blocking the cave outlet by sediment aggradation in the valley. (iii) Stalactites on this level often have gravels embedded in their tip (Fig. 1.3D). All this is evidence for incomplete passage fill related to such damming events. The burial ages might correlate to the Marine Isotope Stage (MIS) 12 and to related gravel aggradation (in classical Alpine terminology “Mindel”) in the Mur valley. An abandoned small cave in the Tanneben massif, the Kapellenhöhle, is the cave closest to the actual Mur river. From there sample KAP1 was successfully analyzed. Allochthonous consolidated gravels were recovered from the ceiling which consists of local collapse material and prevents further exploration. This suggests that the unexpectedly high burial age of 2.82 ± 0.09 Ma of this deposit indicates re-mobilization from higher levels via conduits that are unknown and not, as we initially suspected, from a rather recent flood deposit, related to the event observed in the Lurgrotte just some hundreds of meters downstream.

In summary, we infer incision rates of the river Mur in the order of 100 m/my in the region 25 km upstream of the Alpine orogen – Pannonian basin transition at Graz during the last 4-5 my. Alternating phases of stability and pulses of incision successively created and abandoned cave levels. More detailed analysis of the data suggests that this incision was initially more rapid (~250 m/my) and slowed considerably (to about 40 m/my) towards the present.

1.4 Discussion

Our determined mean incision rates are an order of magnitude lower than those from glacial valleys in the Swiss Alps obtained by the same method. However, they are in

good agreement with rates prior to the influence of glacial carving (Häuselmann et al., 2007b). Pre-burial erosion rates (around 20 m/my) show the same constancy over the evaluated time interval as data from Mammoth caves, Kentucky (Granger et al., 2001). That area is tectonically quite different, but of similar glacial setting as the region investigated here: It is also situated in a non-glaciated region in a marginal position to former ice-sheets. Even though glaciation is responsible for increased incision rates in the Mammoth Cave area, there is evidence of unchanged upland erosion rates throughout the investigated period of 3.5 my. Pre-burial erosion rates are slightly lower compared to our data from the orogen margin, which is interpreted to relate to the area's location in the interior low plateaus of the United States. Incision rates from burial ages of cave sediments in the Sierra Nevada mountains of California revealed similar rates of incision with the indication of decreasing rates towards present (Stock et al., 2004, 2005a) as is observed here. Possible scenarios capable of reducing rates of valley lowering are discussed below in the light of the geological setting of the study area, and are subsequently linked into an absolute vertical reference frame.

1.4.1 Reduced incision during glaciation?

The decrease in incision rates since about 2.5 my is in contrast with increased erosion rates during this period as observed elsewhere in both the Alps and globally. Sediment budget data from the Eastern Alps (Kuhlemann et al., 2002, 2007) show an increase in rates at about the same time as the incision rate in the Mur valley decreased. In the glaciated regions of the Alps higher incision rates due to ice carving during glacial periods are well documented (e.g. Schlunegger and Hinderer, 2003) for part of the low-incision interval determined from our data. Caves of deeper levels may have formed during the interglacials, but the valley deepening itself occurred during glacial carving (Häuselmann et al., 2007b). Molnar (2004) observed a worldwide increase in sedimentation rates around 2-4 Ma which is attributed to increased erosion rates due to climate oscillations.

We suggest that increased sediment discharge rates in most of the Alps in the last few million years provides a possible explanation for our observations of decreased incision rates in the non-glaciated part of the Alps. Sediments transported from the headwaters within that time period accumulated in the Mur valley and may have protected the bedrock from further incision. During such times, the river system is in a transport limited state – in contrast to the detachment limited state during bedrock incision stages (Whipple, 2004; Wobus et al., 2006). Only after the sediments have been eroded again, bedrock incision can continue. As such, there would be an oscillating scenario of valley aggradation and entrenchment in the Mur valley resulting in a decreased mean incision rate during the second half of our inferred evolution. Today, preserved last-glacial gravels prevent further bedrock incision in the Mur valley and are currently being excavated. A similar scenario is observed along the Drava river crossing the Pohorje

dome. That region is similar as it was also not glaciated and fed by glaciated headwaters (as the source for sediment supply). There is also evidence for recent / ongoing uplift (Sölva et al., 2005). Moreover the Mur and the Drava share the same base level and merge some 80 km downstream of Radkersburg. As there are no limestones and consequently no caves could form, an exposure age of 14.75 ± 1.7 ka deduced from a quartz vein (D. Fabel, unpublished data) just above the current river level implies that there is currently no bedrock incision. If this can be assumed to be representative for the entire 2.5 my, it is feasible that bedrock incision is reduced in times of a transport limited state of a river system.

In view of this interpretation, it is important to note that there are other explanations for rivers being in a transport limited state (other than too much sediment from upstream sections). These include (i) too much sediment supply from the hillslopes by landslide or rockfall events during pulses of stronger incision, and (ii) decrease in stream power by decreasing catchment size or by decreasing river gradients (channel slopes). Because of the long duration of the decreased incision rate period, the first of these two alternatives is excluded. However, decreasing the stream power by changing the base level is conceivable for the Mur incision history: Uplift of the inverting Styrian Basin (Ebner and Sachsenhofer, 1995; Sachsenhofer et al., 1997) downstream of the study area may have lifted the local base level leading to a change from a detachment to a transport limited state. Also, the fact that the modeled pre-burial erosion rates are low (about 20% of the inferred average incision rate) indicates that the sampled gravels stem from source areas of continuous and slow erosion rates (Fig. 1.4B). Therefore, we suggest that the cave sediments cannot come from the glaciated region (where erosion rates are undoubtedly higher) and stem from local sources.

1.4.2 Uplift or incision?

In order to infer aspects of the landscape evolution of the Alps, the incision history documented above needs to be placed into an absolute vertical reference frame. Two end member scenarios are possible: (a) no recent tectonic uplift occurred and the Mur dissected a topography of some 2000 m elevation with an over-steepened channel gradient at the orogen-basin transition near Graz, where it plummeted into the basin. (b) The Mur is an antecedent river at more or less constant elevation since 5 Ma with the incision history reflecting the surface uplift of the surrounding topography. Based on reasons outlined below, we suggest a scenario closer to the latter of these two possibilities.

The topographic history of the Styrian basin is reasonably well known (detailed review by Ebner and Sachsenhofer, 1995). The youngest marine sediments in the basin are shallow-water limestones of Upper Badenian age (~13 Ma), currently found at an altitude of ~400 m a.s.l. analogous to ~100 m above the present river bed some tens of

kilometers downstream of the region considered here. Thereafter marine conditions ended and brackish to limnic conditions prevail in much of the basin. Important to note is a considerable hiatus in sediment record more pronounced in the Western than in the Eastern Styrian basin, where Upper Badenian to Upper Pliocene sediments are truncated (Piller et al., 2004). This fact is interpreted to be the consequence of erosion due to uplift of the region (e.g. Ebner and Sachsenhofer, 1995; Sachsenhofer et al., 1997). This uplift is likely to be spatially broad, as gravel spreads do not show any substantial tilt or elevation differences between terraces of different age (Winkler-Hermaden, 1957). Exhumation in the surrounding Koralpe, Gleinalpe and Wechsel mountains is moderate or small, as apatite fission track ages preserve a much older stage of the exhumation history around 40-50 Ma (Hejl, 1997). Peneplains would not be preserved if erosion / exhumation would be high.

From these combined observations it is likely that the base level at the orogen-basin transition was around sea level up to about 8-5 Ma and then rose to its present elevation of some 350 m since then (presuming no sudden reversal / subsidence in the meantime), neglecting eustatic sea level changes. As the channel profile of the Mur shows no obvious knick point at the orogen-basin transition (Robl et al., 2008a) and seismic activity is absent, an uplifting realm coupling basin and orogen is likely. Thus we suggest that most of our documented relative incision history reflects surface uplift of the study area.

This interpretation is supported by the capture history of the Mur river. Dunkl et al. (2005) suggested, based on apatite fission track age-provenance data, that it is only since the Mid-Miocene or later that today's course of the Mur river developed. Prior to this time, the river draining the upstream regions followed the Mur / Mürz fault system in an easterly direction and drained either through the Mürz valley into the Vienna basin and / or through the Lavant valley to the south (Dunkl et al., 2005; Fig. 1.1). In such a scenario, the Paleo-Mur near Graz would only have been a stream draining local areas. During a slight difference in surface uplift of the orogen relative to the basin, this stream would steepen and migrate headwards. This headward migration needs to cut only a distance of about 10 km of crystalline bedrock and a negligible vertical distance (Frisch et al., 1998) to reach Bruck. Thus, this headwards migrating river would eventually reach the Mur-Mürz fault system thereby capturing drainages from there and substantially increasing its catchment, causing the onset of rapid incision in the lower reaches of the system. This headward migration has been facilitated by the fact that the Noric Depression (the pull-apart basins along the Mur-Mürz fault) was once a consistent elongated basin with high sediment thickness (Frisch et al., 1998), which has been eroded since then. This is revealed by vitrinite reflectance data of coals from the basin fillings. It could be shown that paleo-sediment cover was substantial, especially in the basin of Leoben-Bruck (Sachsenhofer, 1989). This is exactly where the capture

event happened. In addition the former more likely outlet of the Mur through the Lavant valley was uplift in post-Middle Badenian times (Strauss et al., 2001).

The incision of about 500 m of bedrock within the last 4 Ma is consistent with the uplift history of the Styrian Basin a few kilometers downstream of the studied region. Based on vitrinite reflectance data and subsidence analysis, around 300-500 m of sediments have been eroded from the basin in the last ~5 Ma (Sachsenhofer et al., 1997, 2001). The increase in drainage area sometime after the Mid-Miocene due to stream capture resulted in a disequilibrium of incision rates of the trunk stream and its tributaries. As this might have happened not long before the investigated time, it could at least partly be reflected in the higher incision rates at the beginning of our investigated time span. That there was no general increase or decrease in local erosion rates over the investigated time span (concluded from the pre-burial erosion rate estimates of our data) suggests that there is no dramatic change in uplift rates in the source area of the cave sediments and no obvious climate change effect. The slow incision rates observed within the last ~2.5 Ma are closer to erosional steady state (geomorphologic decay) where values of incision rates and local erosion rates would be balanced. In other words, the two trends prior and after ~2.5 Ma both reflect rates of geomorphic disequilibrium. These considerations suggest an intermediate scenario where increased erosional power due to enlargement of its catchment causes the river to dissect a slowly uplifting area. This increased stream power leads to effective entrenchment in the study area during the first ~1.5 my of the investigated time period. Thereafter, while adjusting to the new equilibrium state, the main river switches to a transport limited state due to decreasing river gradients but unchanged or even increasing sediment load. An increase in sediment load might be explained by overproduction of coarse sediment in the headwater regions related to glacial carving.

As the difference between incision rates before and after ~2.5 Ma is large, another possible scenario that would fit an e-folding function (as plotted in Fig. 1.5) would be a short-lived uplift pulse somewhere between 5 and 4 Ma, which slowed down thereafter. As there is strong evidence for the above discussed stream piracy event, a superposition of an uplift pulse and increase in drainage area is hard to separate. However, what argues against an uplift pulse is the fact that sediment budget of the Eastern Alps is not decreasing towards the present, but still increasing especially around 2 Ma were we see a decrease in incision rates (e.g. Kuhlemann, 2007).

Direct assessment of absolute surface uplift rates is not straight forward in this setting and we suspect uplift rates between the two incision trends, most likely around the mean rate of ~100 m/my. This implies a more gradual still ongoing – although not stable – uplift of the region. As this is the first data set of its kind it needs to be confirmed with additional investigations able to produce absolute rates of landscape evolution in time along the margin of the Eastern Alps.

Relating relative incision of the Mur river to surface uplift makes it necessary to touch upon the possible mechanisms that are responsible for this surface uplift. It seems reasonable to suggest the inversion of the Pannonian basin as the cause (Bada et al., 2007; Horváth and Cloething, 1996; Ruszkiczay-Rüdiger, 2007). In fact the actual renewal of dominance of north-south convergence is important (Fodor et al., 2005; Bus et al. 2009). Recent findings of vertical steps in the Moho in the region related to a possible Pannonain fragment which is underthrusted by the European as well as the Adriatic plate (Brückl et al., 2007; Behm et al, 2007) arises the interest of possible mechanisms related to deeper seated processes. Slab break off or delamination have also been used to explain uplifting realms (e.g. Genser et al., 2007). Climate change alone has recently become attractive to explain increased uplift. Cederbom et al., (2004) suggested postorogenic mass reduction and isostatic rebound of the Swiss Alps and the neighboring foreland basin related to an increase in atmospheric moisture. The geomorphic setting in the study area allows us to exclude an important erosion-driven component to uplift, as pre-burial erosion rates of this study and fission track data (e.g. Hejl, 1997) contradicts such a setting.

1.5 Conclusion

In summary, we conclude the following points from the first successful burial age dating of cave sediments in the Eastern Alps, Austria:

In the transition zone between Alpine orogen and Pannonin basin near Graz, the river Mur incised some 500 m in the last 4 my recording a very complex incision history resulting in a mean incision rate of about ~125 m/my. The karstification most likely started in late Miocene times (>4-5 my).

Closer analysis of the data indicates higher incision rates (~250 m/my) prior to ~2.5 Ma followed by a considerable decrease in rates (~40 m/my) up to the present. The higher rates prior to ~2.5 Ma are related to surface uplift and an increase in catchment size as the result of stream piracy. The decrease in incision rate after ~2.5 Ma can be related to a shift from detachment limited to transport limited channel erosion of the main (Mur) river due to decreasing stream gradient and ample sediment supply from upstream sections. A primarily climatic trigger for incision rate changes over time is unlikely because of constant pre-burial erosion rates over the whole time period. This fact also constrains changes of uplift of the local source area to be low.

When put into a vertical reference frame, the relative incision rates allow us to infer rates of surface uplift in the order of 100 m/my. A detailed trend is not derivable, as stream piracy and later aggradation due to overproduction of coarse sediment in the

headwater regions complicate the interpretation of the relative incision rates; although we exclude a short-lived uplift pulse. However, our data document the rejuvenation of a landscape that resided at low elevations during most of the Miocene over the last ~4 my.

The cause of the uplift remains unsolved, but strong influence of the inversion of the Pannonian basin and the general change in the stress regime resulting in renewed north-south compression is likely.

Acknowledgements The authors thank the numerous cavers for sharing their knowledge and for discussions about the area. Special thanks to R. Benischke, H. Grillhofer, H. Kusch and S. Oswald, as well as the local caving clubs: Höhlenbären and the Landesverein für Höhlenkunde in der Steiermark. Without all of them such a study would have been impossible. L. Plan, M. Filipponi and C. Spötl are thanked for thought-provoking discussions and comments on this paper. Comments from Ari Matmon and one anonymous reviewer helped to improve the manuscript. We express our gratitude to John Hellstrom, University of Melbourne, for U-Th dating of the speleothems. Many thanks to Wilfried Körner for providing the ICP-OES data. Sincere thanks are given to E. Tillmanns and H. Effenberger (Institute of Mineralogy and Crystallography, Univ. Vienna) for their support of our laboratory work and to the Center of Earth Sciences for supporting our work in the frame of the Earth Science Cooperation between the University of Vienna and the University of Natural Resources and Applied Life Sciences, Vienna. We greatly acknowledge the work of the SUERC AMS group in Glasgow, Scotland. The project was funded by the “Kooperationsprojekt Erdwissenschaften NAWI Graz (§ 141)” and the ESF project I-152.

CHAPTER 2

PLIOCENE TO PLEISTOCENE FAULTING AT THE TRANSITION BETWEEN ALPS AND PANNONIAN BASIN: CONSTRAINTS FROM DATING FAULT ACTIVITY BY THE ^{26}AL/^{10}BE BURIAL AGE METHOD

Abstract Late Neogene west-east directed extensional tectonics accommodated by high-angle normal faults is observed in the Styrian Block at the Alpine Orogen – Pannonian Basin transition zone. This contradicts suggestions in the literature that the tectonic setting in the last ~5 Ma was compressional. This is based on arguments upon (i) stress field data (ii) surface uplift and (iii) overall plate configurations that favor inversion of the Pannonian Basin and Adria push from the south. In order to elaborate on this contradiction, we report here on the post-Miocene fault pattern and the first dating of fault activity using the cosmogenic nuclide method applied so far for sediment burial dating within caves. We used the nuclide pair ^{26}Al and ^{10}Be to measure the time of entrapment of quartz-rich pebbles within a tension gash, obtaining a burial age of 1.56 ± 1.11 Ma. This age gives evidence for young faulting / tectonic activity within the area. Reorganization of plate configuration coupled with eastward decreasing plate motion of the Pannonian fragment at the waning stage of extrusion tectonics might account for these field observations.

Keywords: *Neogene fault pattern; ^{26}Al/^{10}Be; fault dating; burial age dating; Eastern Alps; Pannonian fragment*

Submitted to International Journal of Earth Sciences

2.1 Introduction

For the geodynamic interpretation of the Alpine-Carpathian-Pannonian realm, the Pliocene to Pleistocene tectonic evolution at the transition between the Eastern Alps and the Pannonian Basin poses a series of open questions: (1) What is the significance of the fault pattern that evolved during latest orogenic evolution? The general Lower- to Middle Miocene fault pattern accommodated much of the Eastern Alpine eastward extrusion and is fairly well known (e.g., Ratschbacher et al., 1989). However, some of these major faults are found to be still active at kinematics typical for Middle Miocene times (Bus et al., 2009; Grenerczy and Kenyeres, 2006; Reinecker and Lenhardt, 1999), although it has been suggested that the stress regime at the orogen-basin transition changed substantially during the Miocene (Peresson and Decker, 1997). Thus, the significance of the post-Miocene faulting is still in question. (2) Why are there apparently no structures related to basin inversion at the Alpine - Pannonian transition as found elsewhere in the central Pannonian Basin (Fodor et al., 2005)? So far such structures have not been identified, which raises questions upon the mechanism of uplift in the Styrian Basin. General consensus holds that roll back and retreat of the Carpathian Slab steered extensional tectonics in the Miocene (e.g., Robl et al., 2008c; Royden, 1983), but ceased around Late Miocene (Cloetingh and Lankreijer, 2001; Mason et al., 1998). This resulted in inversion of the Pannonian Basin (Horváth and Cloetingh, 1996). The observed surface uplift at the western termination of the Pannonian Basin, i.e., the Styrian Basin is commonly associated with this process (Ebner and Sachsenhofer, 1995). (3) What is the interpretation of ~10 km vertical steps of the Moho at the transition between Eastern Alps and the Pannonian Basin as revealed by seismic experiments? Behm et al. (2007) and Brückl et al. (2007, 2010) identified a triple junction between European, Adriatic and Pannonian / Tisza plates west of the SE corner of the study area. Hence, the question arises whether the simple picture of Miocene extension by extrusion between Adriatic and European plates and renewed Pliocene compression induced by cease of the Carpathian slab pull has to be modified.

In this paper we present an analysis of brittle faults in the transition zone between the Alpine Orogen and the Pannonian Basin with the aim to place constraints on the post-Miocene tectonic evolution in this region. Our data are pinned in absolute time with a geochronological age for the timing of activity of a brittle fault. We adopt the concept of burial age dating by cosmogenic nuclides (Granger and Muzikar, 2001) applied to quartz rich sediments entrapped within voids opened by faults. This approach is usually applied to cave sediments and used to infer a minimum age estimate of cave void evolution (Granger et al., 2001; Chapter 1). Here we use it to date a sediment filled fault zone.

2.2 Geological Setting

The study area comprises the transition zone between the Alpine orogen and the Pannonian Basin in which two distinct morphological and geological domains are distinguished. Hilly lowlands of the western most lobe of the Pannonian Basin (here referred to as Styrian Basin; ~300 m a.s.l.) are comprised of Neogene sediments deposited on heterogeneous basement units that define southern (Pohorje Mts.; ~1100 m a.s.l.), western (Koralpe Mts.; ~1700 m

a.s.l.) and northern (Highland of Graz ("Grazer Bergland"), Wechsel Mts.; ~1400 m a.s.l.) mountainous domains. The Styrian Basin is considered an extensional structure on top of the Miocene eastward extruding Eastern Alpine crustal wedge (Ebner and Sachsenhofer, 1995). The basin geometry is characterized by eastward tilted blocks dividing the basin into major ~ N-S trending swells separating individual sub-basins. Subsidence analysis and basin modeling (Ebner and Sachsenhofer, 1995; Sachsenhofer et al., 1997) reveals onset of W-E stretching in the Ottnangian/Karpatian associated with delivery of clastic sediments and accompanied by acidic volcanism. Immature sediments include partly coarse pebbles delivered from local source, probably associated with formation of escarpment faults. Full marine environment developed in the Badenian followed by reduced marine conditions in the Sarmatian (Ebner and Sachsenhofer, 1995; Gross et al., 2007). Compared to the early phase of basin formation a reduced W-E stretching has been proposed for Badenian to Sarmatian times (Sachsenhofer et al., 1997). Enhanced hinterland erosion initiated in Pannonian times with delivery of typically quartz-rich sediments derived from adjacent metamorphic sequences and deposited in fluvial to lacustrine environments. The termination of subsidence during the Pannonian and a Quaternary uplift phase has been explained by major changes in the regional stress field (Sachsenhofer et al., 1997). Since the latest Miocene, the Styrian Basin has been uplifted to its present elevation some 300 m above sea level. Pliocene surface uplift is also supported by data on river incision and formation of the recent drainage system of the Mur River south of Bruck (Dunkl et al., 2005; Chapter 1) (Fig. 2.1). Quaternary peri-glacial terraces occur throughout the Styrian Basin. However, age relations between individual terraces have been largely estimated by correlating their elevation and their absolute ages remain unknown (Winkler-Hermaden, 1955, 1957).

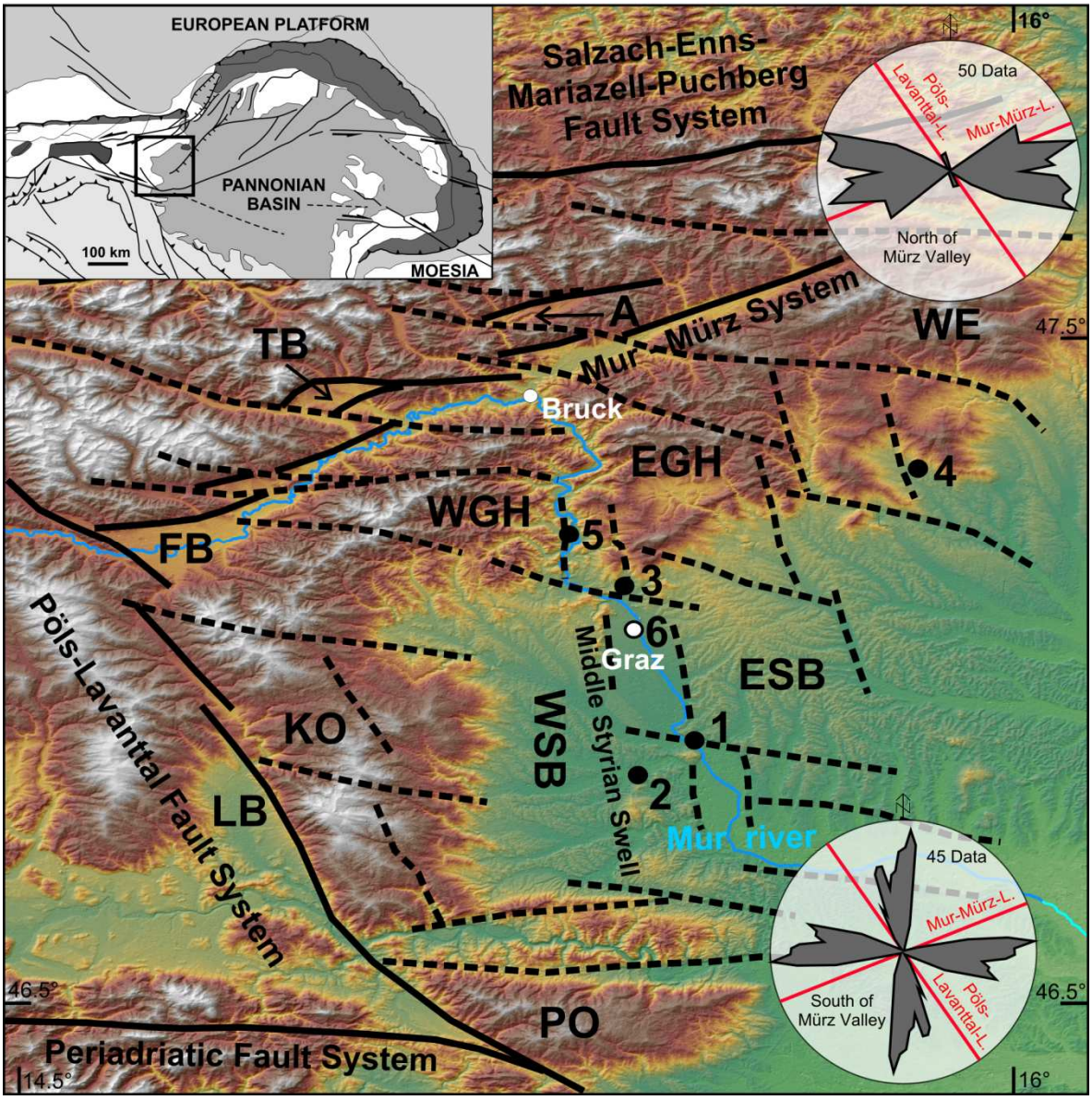

Fig. 2.1. Digital elevation model (SRTM3 V4) from the study area including major Miocene fault zones (continuous black lines) and timely unconfined lineaments, probably younger faults and tension structures (stippled lines). Sample locations given by dots with numbers (1 - 6). Mur River is shown as a blue line and the towns of Graz and Bruck as white dots. Rose diagrams show lineament orientations separated for domains north and south of the Mur-Mürz System. The orientations of the Pöls-Lavanttal and the Mur-Mürz Fault Systems are displayed as red lines in the rose diagrams. WSB= Western Styrian Basin; ESB = Eastern Styrian Basin; LB = Lavant Basin; FB = Fohnsdorf Basin; TB = Trofaiach Basin; A = Aflenz Basin; WGH = Western Graz Highland; EGH = Eastern Graz Highland; PO = Pohorje; KO = Koralpe. See insert for location of the study area within the Alpine – Carpathian – Pannonian system.

Basement units adjacent to the Styrian Basin experienced their last metamorphic imprint around 90 Ma (e.g. Thöni, 2006). Subsequent cooling below ~60-120°C and inferred exhumation terminated between 50 and 15 Ma as evidenced by fission track ages (Hejl, 1997; Neubauer et al., 1995; Fodor et al., 2008). The well known faults related to Miocene extrusion (e.g., Decker and Peresson, 1996; Ratschbacher et al., 1989) include the Salzach-Enns-Mariazell-Puchberg, Mur-Mürz, Pöls-Lavanttal and Periadriatic Fault Systems (Fig. 2.1). All of them are decorated by Early to Middle Miocene pull-apart type basins defining onset of

faulting. It is worth noticing that all of the basins also exhibit post-sedimentary faulting throughout the Neogene (e.g. Pischinger et al., 2008; Strauss et al., 2001). Besides these faults numerous lineaments are visible on DEM images that may be traced crossing basement units and basin sediments and might define faults or tension gashes of unknown age (Fig. 2.1).

Fission track cooling ages display remarkable differences within distinct basins and crustal blocks surrounding the Styrian Basin (Dunkl et al., 2005). The southern Pohorje Mts. cooled below 60-120°C (apatite partial annealing zone) at ~18-15 Ma (Fodor et al., 2008). These ages are in contrast to cooling ages > 40 Ma known from the Austroalpine units at Wechsel Mts. (Dunkl and Frisch, 2002) (Fig. 2.1) whereas no data exist from the Paleozoic rocks north of Graz (Highland of Graz). A complex cooling history is recorded from the Koralpe Mts. to the west of the Styrian Basin. The vast majority of cooling ages >40 Ma indicate an early Paleogene phase of exhumation without any response to time equivalent sedimentation in any of the adjacent basins (Lavanttal Basin, Styrian Basin). Final exhumation of the Koralpe block below the apatite fission track retention temperature was achieved by Pliocene faulting (~5 Ma) (Wölfler et al., 2010). This is taken as a hint for low topography during initial exhumation and evolution of significant topography during Pliocene to Pleistocene. Young faulting and/or regional uplift and mountain dissection must be considered significant in shaping morphology of the Alpine - Pannonian transition.

2.3 Delineation of the Styrian Block

Using DEM data of various resolution (~90 m: SRTM3, ~30 m: GDEM30 and ~10 m: 10x10 m DEM from GIS Styria), a visual lineament analysis is performed and cross checked with field data (Fig. 2.1). Different sets of lineaments are found north and south of the Mur-Mürz Fault System , part of the well-know major Miocene fault pattern. To the north of the Mur-Mürz Fault System mainly ENE and ESE orientations were found, to the south, ~N-S and ~W-E to WNW-ESE systems. Interestingly, the N-S lineaments are predominantly found to the south and almost absent north of the Mur-Mürz Fault System (Fig.2.1).

Survey of the seismic activity and earthquake focal mechanism (Fig. 2.2) allows visualizing active deformation and possibly kinematics along faults. Data display high seismic activity along Middle Miocene faults, especially along the Mur-Mürz and Periadriatic Fault Systems that likely represent still active sinistral and dextral fault zones, respectively. By contrast, the Styrian Basin and its surrounding basement are seismically inactive, except the SW corner of the basin and few earthquake epicenters that loosely define NW trending lineaments. One of those aligns with a pronounced escarpment at Wildon (site 1, Fig. 2.1) and another with the fault bundle next to Zitoll (site 5, Fig. 2.1) that may be traced westwards to the Fohnsdorf Basin (Fig. 2.1).

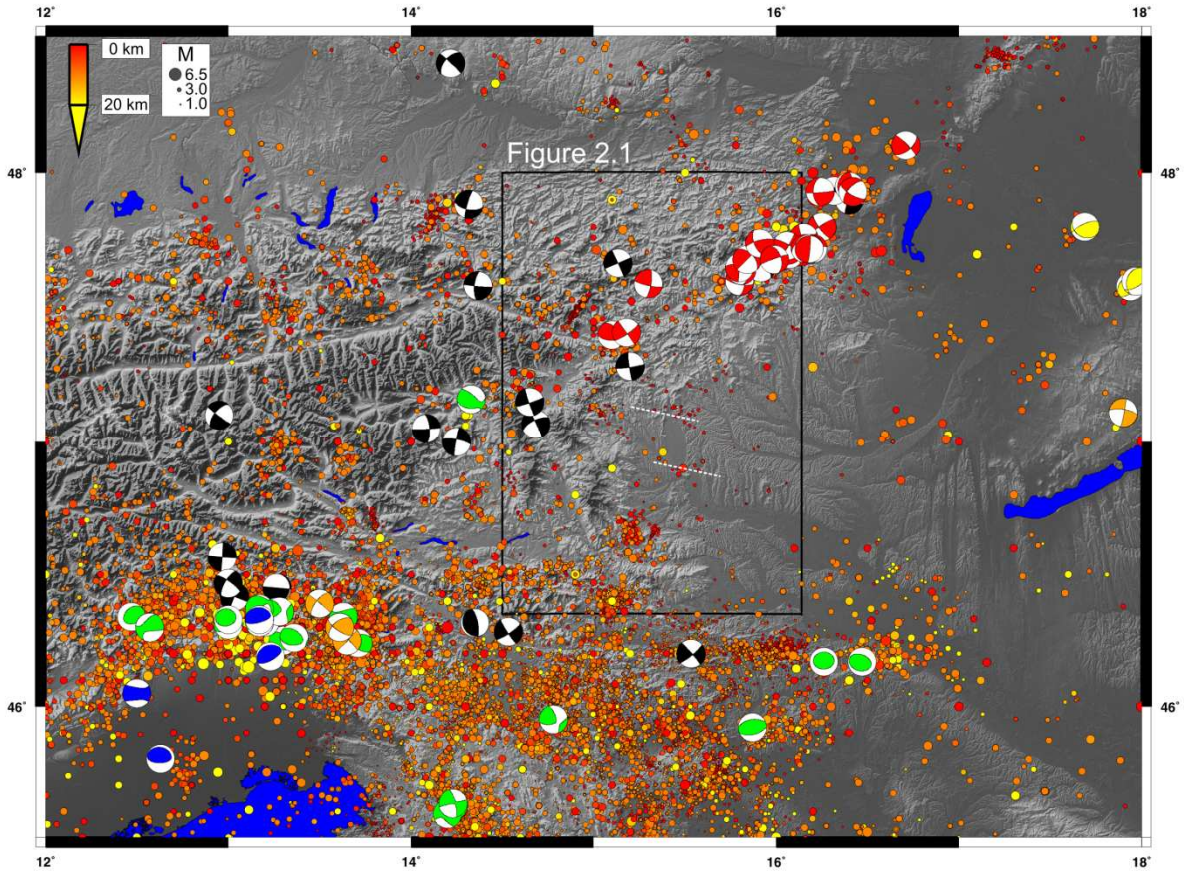

Fig. 2.2. Earthquake data of the Alpine – Pannonian transition. Seismic activity is displayed by dots showing all recorded earthquakes (all magnitudes) within the last 45 years (1964 to the present; color coded according to their depth and scaled according to their magnitude; see labeling); from IRIS database [http://www.iris.edu/data/event], accessed February 2010. Beach balls display focal mechanism data from various literature and web-sources (accessed February 2010): in black Reinecker and Lenhardt (1999); in red and yellow Bus et al. (2009); in green RCMT Catalog [http://www.bo.ingv.it/RCMT]; in blue Global CMT Catalog [http://www.globalcmt.org]; in orange USGS Earthquake database [http://neic.usgs.gov/neis/epic/epic_rect.html]. Note the scarcity of earthquake activity in the central study area (Fig. 2.1). Dashed white lines indicate alignment of earthquake epicenters along observed faults.

View on the larger scale shows that the domain to the south of the study area is characterized by intense Pliocene to Pleistocene tectonics and high seismic activity. Pliocene fold and thrust belts to the south (i.e., Save Fold Belt) and north (i.e., Haloze Fold Belt within the Mura-Zala Basin) of the Periadriatic Lineament suggest a strong N-S to NNW-SSE component of shortening, partly partitioned into dextral slip along the Periadriadic Lineament (Marton et al., 2002).

Based on a series of observations we argue that the Styrian Basin and its immediate surrounding basement behaved as a coherent unit, here termed “Styrian Block”, during its post Middle Miocene evolution. The line of arguments includes: (i) Scarcity of seismic activity that contrasts pronounced activity along the Mur-Mürz, the Pöls-Lavanttal and the Periadriatic Fault System. These fault systems are considered to define the margins of the Styrian Block. (ii) Existence of differently orientated fault pattern north and south of the Mur-Mürz Valley. (iii) Coincidence of lineament orientations of the Styrian Basin with the

immediate surrounding basement units, especially with those derived from the Highland of Graz.

The distinction of different coherent units along the Alpine-Pannonian transition is in concordance with estimates on plate velocities and strain rates derived from GPS data (Bus et al., 2009) and recent data on plate configurations (Brückl et al., 2010). According to their data the West Pannonian region may be defined as Pannonian fragment that is currently under west-east extension and bordered by shear domains, the above mentioned Mur-Mürz and Periadriatic Fault Zones.

2.4 Fault analysis in the Styrian Block

Within the Styrian Block, two important sets of lineaments are observed that occur in both, the region of the Styrian Basin and in the surrounding basement. Most prominent is a set of ESE trending lineaments that cut through Middle Miocene sediments of intramontane basins (e.g. Aflenz-, Trofaiach-, Fohnsdorf Basins) as well as through sediments of the Styrian Basin (Fig. 2.1). One of those initiates in the Fohnsdorf Basin for which a general post Middle Badenian N-S compression has been proposed (Strauss et al., 2001). Interestingly these faults correspond also with deflection points in the course of the Mur River (and other East Styrian rivers) that define a “staircase pattern” with N-S and WNW-ESE trending river segments. A conspicuous deflection aligns with the ESE trending escarpment of a post Middle Miocene fault at Wildon (site 1, Fig. 2.1) along which offset of Pleistocene terraces as well as minor earthquake activity (Fig. 2.2) is recorded.

The other prominent orientation is a set of N-S lineaments. They trend parallel to the Middle Styrian Swell (Fig. 2.1) that separates West- and East Styrian Basins with distinctly different sedimentary record. In the Western Styrian Basin sediments from Otnangian/Karpathian to the Badenian are recorded. In the Eastern Styrian Basin sedimentation continued up to Pannonian times (Gross et al., 2007). This lineament was already defined as Quaternary normal fault by Fodor et al. (2005) and is also evident in the pre-Tertiary basement maps (Kröll, 1988). In the Highland of Graz N-S trending lineaments align with the course of the Mur Valley and separate the Highland of Graz into a western and eastern segment with different geological and morphological evolution: Accumulation of Pliocene pebbles in today elevated regions (up to 1000 m a.s.l.) is exclusively found within the Eastern Graz Highland (EGH: Fig.2.1) and caves are observed almost exclusively in the East as well, although proper lithologies are also present in the Western Graz Highland (WGH: Fig. 2.1) (Chapter 1). The Middle Styrian Swell and its northern elongation along the Mur River towards Bruck seem to represent a major N-S trending lineament. Differential exhumation with higher uplift and/or erosion of western (including the Koralpe) relative to the eastern domains might explain the different erosional settings west and east of it.

In order to constrain these two sets of structural orientations, a series of sites were investigated in detail. In total six sites ranging from basement outcrops to Pleistocene

sediment deposits are discussed in the following (site locations are displayed in Fig. 2.1). Within basin sediments displacement on faults is deduced from offset of lithological markers.

Site 1 is located near the town of Wildon along the Middle Styrian Swell, where Badenian (up to ~13 Ma) shallow marine sediments (Leitha Limestone) are exposed forming a WNW-ESE trending escarpment. North trending tension gashes are frequent, faults and slickenside striations are extremely rare (Figs. 2.3a, 2.4a). The escarpment aligns with a pronounced lineament visible on DEM image (Fig. 2.1) along which low magnitude earthquakes are observed (Fig. 2.2). Badenian sediments are covered by terraces of assumed Pleistocene age (pre-Riß) that are vertically displaced by a maximum of about 100 meters along this lineament (SW side up) suggesting young fault activity. Site 2 is located in the Hengsbergtunnel, a tunnel in the Styrian Basin that was constructed for a railway project. The exposed rock types are Badenian ("Florianer Schichten") and Pleistocene sediments. Abundant normal faults cutting through Badenian and also Pleistocene sediments display NW-SE extension (Figs. 2.3b, 2.4b). Site 3 in the Pailgraben north of Graz is located within Sarmatian pelites overlain by probably Early Pannonian gravels. In addition, gravel-filled tension gashes are found in the nearby basement rocks. This site just north of the orogen-basin transition shows mainly eastward dipping extensional faults (Figs. 2.3c, 2.4c). Site 4 at Pöllau is the easternmost studied outcrop. Here, high angle west- and east-dipping extensional faults (Figs. 2.3d, 2.4d) developed within fluvial sediments of supposed Pleistocene age. The last two sites are located within Devonian carbonates that belong to the Paleozoic rocks of Graz where fault patterns may have developed throughout the Variscan and Alpine orogenic cycles. In order to obtain only data from "young faults" we have chosen tension gashes filled with assumed Pliocene to Pleistocene sediments and related faults for analyses. Filled tension gashes pass frequently into shear-extension and Riedl shears that exhibit fine grained, grey to reddish fault gauges. Those faults were considered. Site 5 at Zitoll is located along one of the major N-S lineaments that are visible on the DEM (Fig. 2.1): Locally, faults occupy W-E and N(NW)-S(SE) trends (Fig. 2.3e). Low magnitude earthquakes occurred along the W-E trending lineament, the N-S faults parallel a fault along to the west bank of the Mur valley (Fritz 1991). Finally, site 6 is located in the underground of the Graz Castle Hill ("Grazer Schloßberg"): The man-made tunnels (build as bomb shelters during World War 2) of ~6 kilometers total length allowed subsurface access to a large fault system. A quasi 3D investigation was possible due to the fact that individual faults could be mapped in various galleries (Figs. 2.3f, 2.4e, f). Many gravel filled faults are accessible. Such faults are also frequently found within Paleozoic rocks surrounding Graz. Gravel filled tension gashes trend NW, faults trend N-S and WNW-ESE respectively. Here too, slickensides on fault planes are extremely rare but the excellent outcrop situation allows constraining the kinematic on some sets of faults. The fault zone where burial ages were obtained (see below) contains well rounded silicious pebbles with shear and tension structures that pass laterally into the fault core and damage zone (Fig. 2.4e, f). The geometric relations between those structures suggest major high angle normal faulting with down step of eastern blocks coevally or later to entrapment of pebbles. Interpretation of kinematics is confirmed in thin sections that display kataclastic carbonate showing a system of fluid infiltrated reddish faults and associated Riedl shear and tension gashes forming extensional bridges between shears (Fig. 2.5a). Although normal faults predominate, a subordinate component of strike-slip resolved in rare sinistral

and dextral faults along N-S and WNW-ESE trending steep faults, respectively (Fig. 2.3f). Clasts entrapped within tension gashes include mainly polycrystalline quartz, rock fragments and white mica, all of which suggesting a metamorphic source area (Fig. 2.5b).

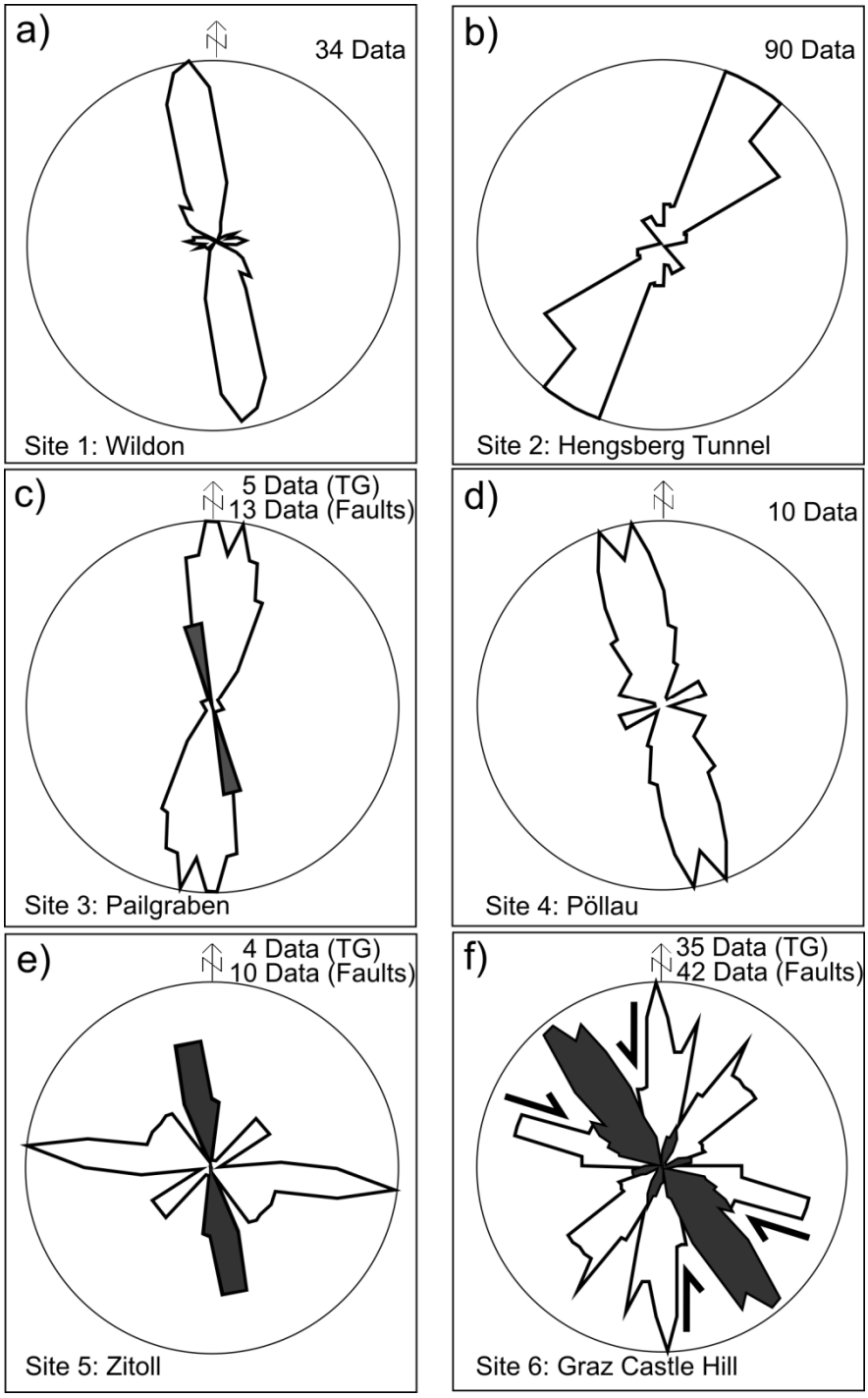

Fig. 2.3. Rose diagrams of tension gashes and steep normal faults cutting through Badenian (site 1, 2; Weissenegg formation, Florianer beds), upper Sarmatian (site 3) and Pliocene (site 4) sediments of the Styrian Basin (a-d). Faults (white) and pebble-filled tension gashes (TG; grey) from carbonate rocks of the Graz Paleozoic (site 3, 5, 6; c, e, f). Minor strike-slip component is indicated for faults at site 6. For locations see Fig. 2.1.

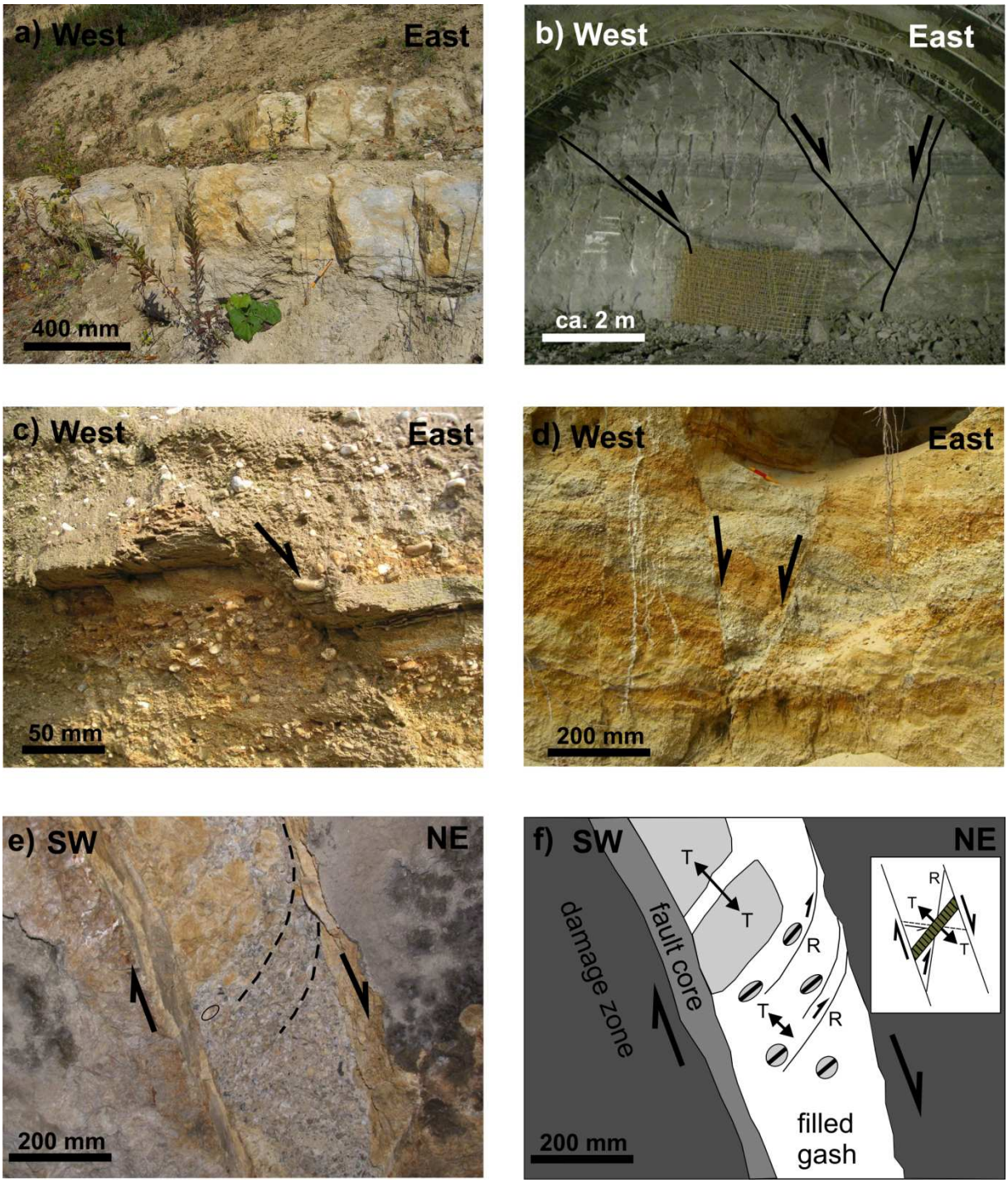

Fig. 2.4. Field examples for tension gashes in Badenian limestone at Wildon (a; site 1); normal faults within Badenian sediments at Hengsberg tunnel (b; site 2), upper Sarmatian sediments at Pailgraben (c; site 3) and within Pleistocene sediments near Pöllau (d; site 4). Pebble-filled tension gash in the Graz castle hill (e, f; site 6). Burial time of pebbles within fault shown in e has been dated by the $^{26}Al/^{10}Be$ burial age technique. (f) Schematic line drawing of e showing the system of tension gashes and Riedl shear defining normal faulting (kinematic frame given in insert). Pebbles entrapped with the faults contain tension gashes (black bars, double arrows define local extension). This is taken as an argument for syn- to post entrapment deformation.

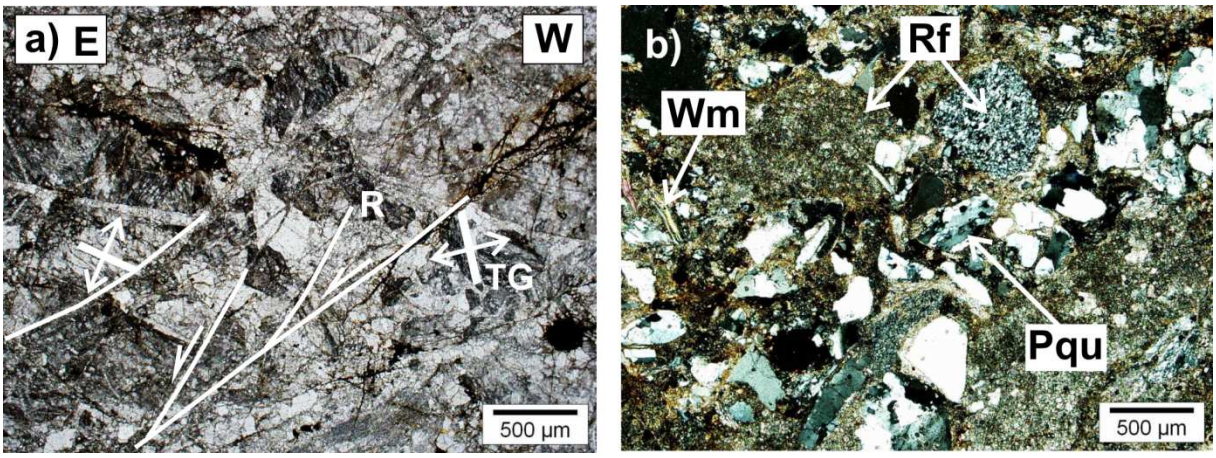

Fig. 2.5. Thin sections from kataclastic carbonates at Graz castle hill showing complete disintegration by systems of shear and tension gashes (a; site 6). Section derived from damage zone next to pebble filled tension gashes. Fine grained reddish material derived most probably from infiltration of oxidizing fluids along young faults. TG – tension gash; R – Riedel shear (b) Thin section showing fine grained clastic material (micro-pebbles) from dated fault. Pqu – polycrystalline quartz; Wm – white mica; Rf – rock fragments.

The fault orientations described above may be interpreted in terms of a W-E extensional stress regime at the time of faulting. Principal stress orientations (Fig. 2.6) are derived from a subset of all data for which the displacement direction on faults could be constrained on the basis of slickenside striations and shear sense criteria. The data show, despite the wide dispersion of investigations sites, fairly homogeneous (N)W-(S)E tension throughout the Styrian Basin and surrounding basement. (Paleo)-stress orientation derived from the right dihedra method gives well defined W-E horizontal σ3 and less well defined vertically to N-S horizontally oriented σ1 (Fig. 2.6). Existence of widespread normal faults favors vertical σ1 orientation. Conversely, a N-S horizontal σ1 orientation would point to a component of strike-slip compatible with those rarely found at site 6 (Fig. 2.3f). In order to place constraints on the timing of faulting in the Styrian Block, in particular on the timing of the N-S oriented systems that do not occur outside the Styrian Block, we present absolute age information below.

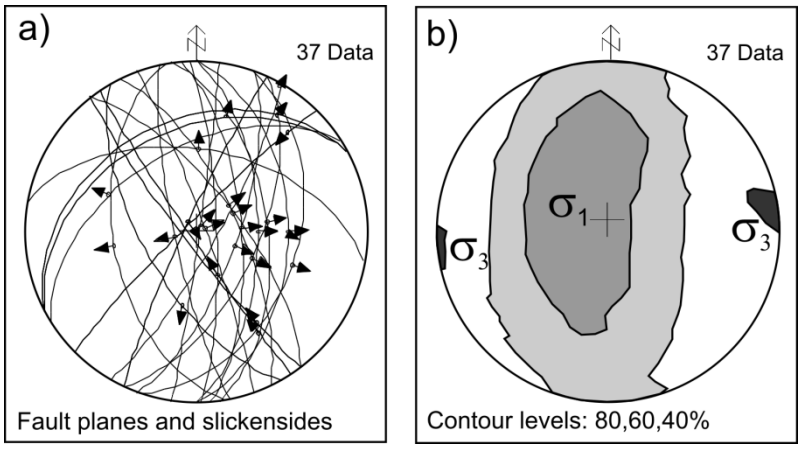

Fig. 2.6. Compilation of data from faults with slickenside striations and usable shear sense indicators. (a) Fault planes and slickenside striations and (b) stress orientations derived by the right dihedral technique from data shown in a.

2.5 Timing of fault activity

The analysis of successively evolving fault systems is a standard technique to resolve changes of stress regimes over time and the motion of crustal blocks within tectonically active belts. However, this task is frequently hampered by the fact that the absolute dating of brittle faults is not trivial. The study of faults displacing rocks / sediments with known age is probably the most common way to deduce minimum age of fault activity and to establish relative time relations of faulting. Direct fault dating by geochronology / thermochronology is a challenging task but may be successful when new minerals are formed (e.g., fault gauge dating: Eide et al., 1997; Kralik et al., 1987; van der Pluijm et al., 2001, 2006) or modified during the faulting process (e.g., apatite annealing through faulting: Wölfler et al., 2010; Yamada et al., 2007). In the sections above it has been shown that most of the structures are post Badenian or Sarmatian (younger than about 12 my) and that some observed extensional structures contain supposed Pannonian gravels or cut Pleistocene sediments. However, it is important to note that neither the Pannonian gravels, nor any of the Pleistocene sediments in the Styrian Basin are dated in absolute time. As such, it remains unclear if these faults are younger or older than the supposed change in the stress regime in the Styrian Basin some 5-7 my ago that is often made responsibly for the inversion and uplift of the basin.

In the following we therefore present some results on the absolute ages of these faults. A sample from the Graz Castle Hill (site 6, Fig. 2.1; Fig. 2.4e) has been dated to set limits on age of faulting. In our approach we adopt the radionuclide burial age dating method of allochthonous quartz rich cave sediments (Häuselmann, 2007; Häuselmann and Granger, 2005; Granger et al., 2001), here applied on sediments entrapped in faults, a possibility of fault dating not yet exploited. This sample adds to a series of burial age data from cave sediments taken nearby with the aim to retrace river incision and rock uplift (Chapter 1); data that certainly provide useful information when combined with young faulting activity.

2.5.1 The burial age method and its result

Burial age dating is based on the fact that cosmogenic nuclides accumulate in rocks as long as they are near the surface. The two different isotopes, ^{26}Al and ^{10}Be, have different production rates and thus their isotopic concentration increases with a constant ratio of 6.8:1. If such sediment that has accumulated enough cosmogenic isotopes during hillslope erosion and transport is then quickly carried into a cave, or like in this case deep enough into a fault (>20 m), then the radioactive decay starts shielded from any further cosmic rays. The decay constants of these two isotopes are different by a ratio of about two. As a consequence this ratio decreases with time of burial. This allows computing the time the sediment has spent subsurface (Gosse and Phillips, 2001; Granger and Muzikar, 2001). Age estimation of the gravel fill translates into time of fault activity only if arguments for syn-tectonic entrapment of sediments (gravels) are provided. In our case we consider this assumption justified because faults and gravel fill experienced deformation at identical kinematics.

After sampling the fault filling (sample SBS1, Fig. 2.4e), about 100 g of quartz was extracted and purified from bulk samples by magnetic and density separation and selective chemical dissolution. Quartz was dissolved in a 5:1 solution of concentrated HF and HNO_3 and spiked with about 0.74 mg ^{9}Be. Al and Be were separated and purified by ion chromatography and selective precipitation. Precipitates were oxidized and mixed with metal powder for accelerator mass spectrometry (AMS). $^{10}Be/^{9}Be$ and $^{26}Al/^{27}Al$ nuclide ratios in the sample and procedural blanks were measured at the SUERC AMS facility in Glasgow relative to Z92-0222 with $^{26}Al/^{27}Al$ taken as 4.11×10^{-11} and NIST SRM 4325 with $^{10}Be/^{9}Be$ taken as 3.06×10^{-11}. The procedural blanks yielded $^{10}Be/^{9}Be$ ratios $<3.8 \times 10^{-15}$ and $^{26}Al/^{27}Al$ ratios $<1.8 \times 10^{-15}$. SBS1 had low measured ratios of $15.7 \pm 0.9 \times 10^{-15}$ and $11.7 \pm 3.4 \times 10^{-15}$ respectively and the procedural blanks represent <24% and <16% of the ^{10}Be and ^{26}Al atoms respectively. Stable aluminium concentrations were determined by ICP-OES (PerkinElmer, Optima 5300 DV) and assigned 3% uncertainty. Burial ages and pre-burial erosion rates were determined by iterative solution of Eq. (14) and (15) in Granger and Muzikar (2001), assuming averaged local production rates of $P_{n\&\mu,26} = 74.1$ at g^{-1} yr^{-1} and $P_{n\&\mu,10} = 10.9$ at g^{-1} yr^{-1}, based on the CRONUS Earth online calculator (Version 2.2). The stated errors are 1σ calculated from AMS and ICP-OES uncertainties. These measurements yielded an $^{26}Al/^{10}Be$ ratio of 3.25 ± 1.33 for sample SBS1 (^{26}Al content of $1.83 \pm 0.71 \times 10^{4}$ at/g, ^{10}Be content of $0.56 \pm 0.08 \times 10^{4}$ at/g) and finally a burial age of 1.56 ± 1.11 Ma. The rather high uncertainty arises from low isotope ratios already close to the measured blanks. Nevertheless the burial age is considered valuable.

An age of 1.56 ± 1.11 Ma for the sediment entrapment suggests late Pliocene to Pleistocene fault activity, a time constraint that is hardly obtained otherwise. Because other faults and tension gashes from the Styrian Basin display the same kinematics and orientation we argue that these structures developed also during, or were at least reactivated at that period of time. Fig. 2.7 shows a two isotope plot where graphically the burial age (in Ma) of the fault filling is displayed. In addition to this samples (SBS1), others derived from cave sediments within the Highland of Graz just a view kilometers upstream of the Mur River are shown (Chapter 1). These data suggest that late uplift of the Highland of Graz and associated river incision closely coincides with development of the fault pattern. This further emphasizes relief-rejuvenation of this region within Pliocene to Pleistocene times.

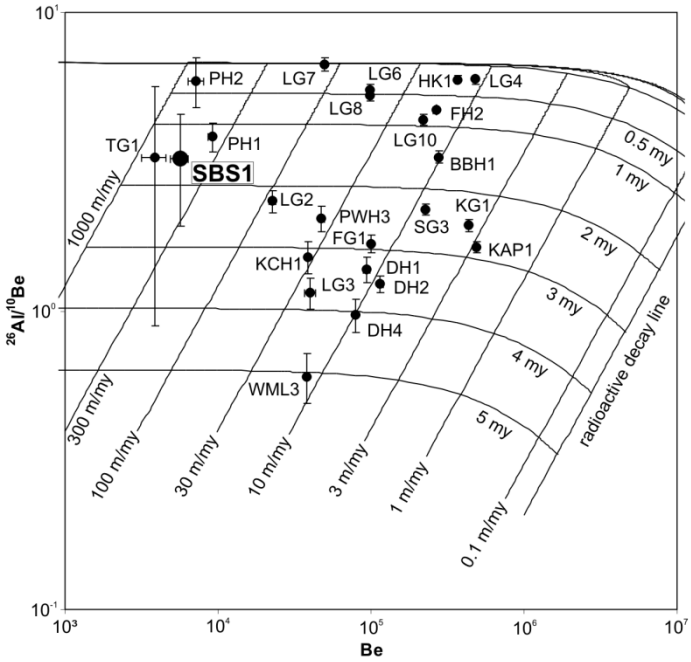

Fig. 2.7. A logarithmic two isotope plot showing the graphical representation of burial age data. SBS1 is derived from the pebble fill of a tension gash in the Graz castle hill. The others represent data from cave samples (Chapter 1). The curved lines are burial ages in million years; the steep straight lines are radioactive decay trajectories plotted for pre-burial erosion rates (m/my) increasing from left to right.

2.6 Discussion

Eastward extrusion assisted by the retreating Carpathian slab certainly shaped the Eastern Alps and the eastward adjacent Pannonian Basin from 22 Ma onwards (e.g., Robl et al., 2008c). However, it has been argued that subduction roll back in the Carpathian arc ceased around the Late Miocene (Cloetingh and Lankreijer, 2001; Mason et al., 1998) and that the Pannonian Basin is under W-E compression since. Structures related to basin inversion including reverse faults with northwest displacement have been documented from the Hungarian part of the Pannonian Basin (Fodor et al., 2005). By contrast, the structures described here are all high angle normal faults indicating W-E tension, occasionally accompanied with minor strike-slip components. The overall strain related to this extension is considered low as suggested by the infrequency of prominent faults and the fact that the high angle faults usually accumulate minor strain unless they are linked with listric detachments. General W-E tension is compatible with the present day stress and strain fields derived from GPS data and modeling on plate tectonic scale (Bada et al., 2007; Bus et al., 2009; Grenerczy and Kenyeres, 2006; Reinecker and Lenhardt, 1999) but inconsistent with the supposed basin inversion since the Late Miocene. Thus, our data open the question about the mechanism of well known uplift within the Styrian Basin (e.g. Sachsenhofer et al., 1997) and exhumation of surrounding basement (Wölfler et al., 2010) in post-Miocene times.

Here we argue that the western Pannonian Basin (especially the Styrian Basin) experienced uplift caused by underthrusting of the surrounding European and Adriatic plates (Fig. 2.8;

Brückl et al., 2010). The Styrian Block is part of the western Pannonian fragment where an extensional regime is documented (Brückl et al., 2010). Thus uplift initiated by underthrusting may have caused gravitationally driven W-E extension in Pliocene to Pleistocene times lasting up to the present. The rate of extension diminishes with the decreasing uplift towards the east until it is balanced by W-E shortening against the backstop of the eastern European platform (Carpathinan arc). Transition from extensional to shortening (basin inversion) structures occurs at the locus where influence of both triggers (extension by underthrusting and shortening by Carpathian backstop) is balanced, which is considered close to Budapest.

The interpretation presented above is consistent with a series of geophysical data. GPS data (Bus et al., 2009) show north to northeastward motion of the Adriatic plate and the southern Pannonian fragment relative to Europe with diminishing velocities towards East (Fig. 2.8). North to the Styrian Block motion turns eastward again with eastward diminishing plate velocities within the eastward moving Pannonian unit. This releases the strong strike slip component, with northeastward diminishing displacement along the Mur-Mürz Fault Zone. Stress trajectories (Fodor et al., 2005) align well with directions of plate motions and swing from north to east and back north when crossing the Mur-Mürz Fault Zone. These data suggest strong N-S shortening, especially south of the Styrian Block that releases strike-slip along a northern, rigid European Plate. Based on seismic experiments Brückl et al. (2010) suggested that the spur of this European plate is located close to the Mur-Mürz Fault Zone and that the European Plate underthrusts the Pannonian fragment. To the south the Pannonian fragment is underthrusted by the Adriatic Plate with its eastern spur close to the Mölltal-Idria Fault System and a transition from a thickened Dinaric crust to a thinned Pannonian crust (black dashed line in Fig. 2.8) close to the Pöls-Lavanttal Fault System.

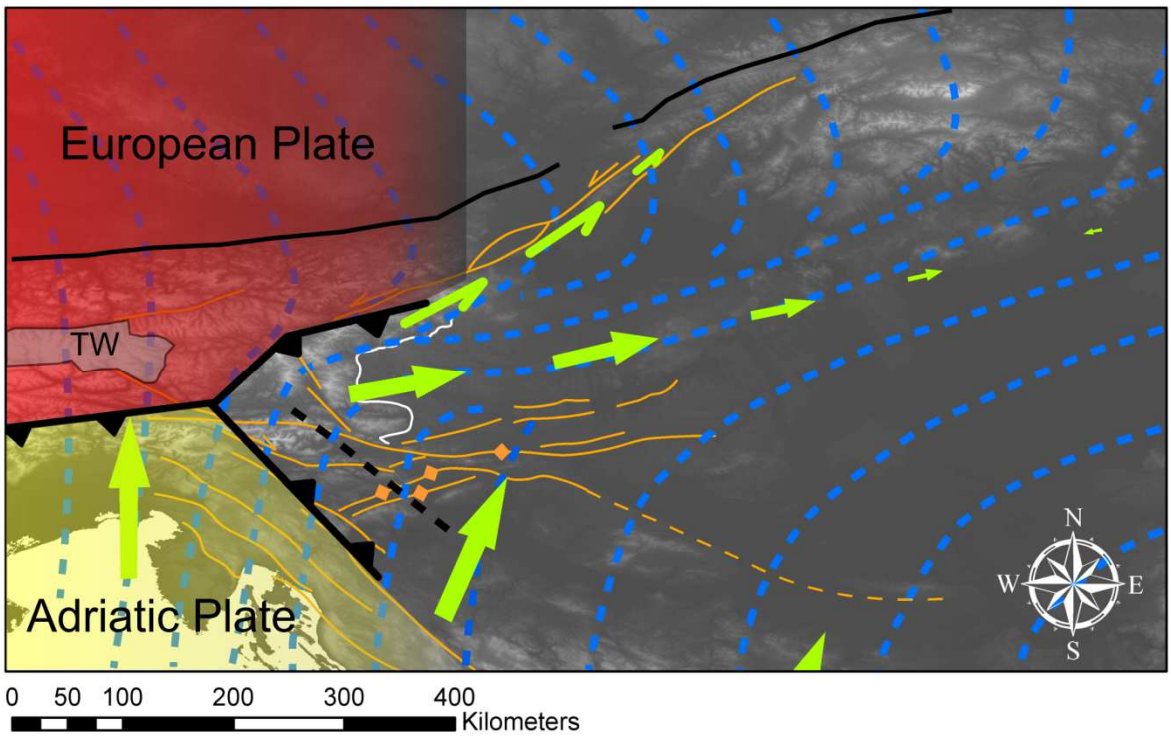

Fig. 2.8. Compilation of GPS velocities (green arrows; Bus et al., 2009); smoothed maximum horizontal stress orientation (dashed blue lines; Fodor et al., 2005); vertical steps in Moho depths (black lines with arrows indicating underthrusting; Behm et al., 2007; Brückl et al., 2010) and a transition zone of thicker and thinner crustal portions within the Pannonian fragment (Brückl et al., 2010) displayed as dashed black line. Reddish colored area indicates European plate and yellowish the Adriatic plate. The orogen-basin transition zone is indicated by the white line. The study area is situated on top of a postulated Pannonian fragment that is underthrusted by European and Adriatic plates (black arrows). Orange lines represent major fault zones and fold belts (fold axes indicated by diamonds); TW = Tauern Window.

2.7 Conclusions

Lineament analysis in the transition between Alpine orogen and Pannonian Basin shows that a kinematically coherent and seismically inactive block can be defined in this region. This block – here called the "Styrian Block" – is delineated by the Mur-Mürz Fault System in the north, the Pöls-Lavanttal Fault System in the west and the Periadriatic Fault System in the south and includes both the eastern most part of the Alps and the westernmost part of the Pannonian Basin. Fault analysis shows that the young stress field within this block appears to be extensional in W-E direction. A burial age (1.56 ± 1.11 Ma) of quartzous sediments trapped into a tension gash allows to constrain the timing of this extension to be later than the supposed basin inversion often made responsible for the current uplift of the region. Here we interpret the post-Miocene fault pattern as result of north-south convergence between European and Adriatic plates and displacement partitioning along margins of coherent crustal fragments. The investigated Styrian Block is part of the Pannonian fragment. Strike-slip displacement resolved along margins of this coherent block, especially along the northern Mur-Mürz Fault System. Here the European plate acts as a rigid backstop along which N-S plate motion trajectories are deflected into eastward flow, thereby releasing strike slip

displacement. The Styrian Block is continuously extending since Early to Middle Miocene and it experiences uplift since about the Miocene-Pliocene boundary. We explain this by two interfering processes: (1) The weak Pannonian fragment is underthrusted from north and southwest by European and Adriatic plates and (2) decreasing extension rates towards east. While the Pannonian Basin (excluding the Styrian Basin) experiences W-E convergence since the cease of Carpathian subduction, the Styrian Block is still extending eastwards. This scenario reflects a multiplate interference system and highlights the complex interplay of plate motion and its consequences to topography and landforming processes.

Acknowledgements Silvia Steiner, Gudrun Pack and Martin Übeleis are thanked for their help in gathering structural data. We greatly acknowledge the work of the SUERC AMS group in Glasgow, Scotland. We would like to express our heartfelt gratitude to Diana Sahy, Philipp Häuselmann, Markus Fiebig and the numerous others involved in the lab work in Vienna. This research was funded by the "Kooperationsprojekt Erdwissenschaften NAWI Graz (§ 141)" and the ESF project I-152.

CHAPTER 3

CORRELATIONS OF CAVE LEVELS, STREAM TERRACES AND PLANATION SURFACES ALONG THE RIVER MUR – CONSTRAINTS ON TIMING OF LANDSCAPE EVOLUTION ALONG THE EASTERN MARGIN OF THE ALPS

Abstract The study of stream terraces and planation surfaces is of major interest in the understanding of landscape evolution; in particular their correlations to environmental changes in the Pliocene to Pleistocene have been of growing interest in recent years. The transition zone of the Eastern Alps to the Pannonian Basin provides significant information for this research aim. Direct dating of buried sediments via terrestrial cosmogenic nuclides and optically stimulated luminescence yield a set of age constraints that allow combination of these data with geomorphological and morphostratigraphical evidence into a temporal evolution of land formation over the Pliocene to Pleistocene. Here we report on recently available absolute age constraints of the Styrian Block (Styrian Basin and its surrounding basement) and discuss this information in the light of tectonic and climatic imprints in the various landforms. The viability of subterranean archives, cave systems and their preserved deposits, for landform reconstruction are revealed. The region was ice-free during the whole Pleistocene and as such, direct influence of glacial carving on the land forming can be excluded. Minimum age constraints of cave levels from burial ages of cave sediments covering the last ~4 Ma are used to place age constraints on surface features by parallelizing cave levels with planation surfaces. Further, aggradations in the Mur valley are correlated with dated events of the plugging of caves. A first absolute dating of sediment burial via OSL of the top section of the type locality of the Helfbrunn terrace implies an Early Würm (Marine Isotope Stage 5) development (80.5 ± 3.7 to 68.7 ± 4 ka). Due to a suggested continuous sedimentation process of the whole terrace sequence, it's origin as a penultimate gravel deposit (in classical Alpine terminology Riss) is therefore questioned. U-series speleothem ages from caves nearby indicate formation during Marine Isotope Stages 5c and 5a; at about the same time as deposition of the terrace. This supports the idea of temperate climatic conditions at time of deposition. The complementary use of TCN, OSL and U/Th absolute age data allow the placing of absolute age estimates on Pliocene to Pleistocene landforms. Tectonic activity is interpreted to be the main driving force for the formation and evolution of these landforms. Climate change is suggested to be of minor importance. Obvious hiatuses of Miocene to Pleistocene sediments are related to ongoing erosion and re-excavation of an uplifting and rejuvenating landscape. This shows the complex

interaction of these (feedback) mechanisms sculpting the landscape and further highlight the value of cave deposits in understanding landscape evolution.

Keywords: *cave level; planation surface; stream terrace; cosmogenic nuclide; luminescence; sediment burial*

Submitted to Geomorphology

3.1 Introduction

The landscape evolution of the Alps over Late Neogene times is a subject of topical interest (e.g. Frisch et al., 2001; Dunkl et al., 2005; Kuhlemann, 2007; Champagnac et al., 2009; Willet, 2010). The transition zone between the Alpine orogen and the Pannonian Basin around the town of Graz, Austria is a key site which provides significant information regarding the evolution of landforms over this time period as it has never been glaciated and glacial carving can thus be excluded as a landforming process (Fig. 3.1a, Van Husen, 2000). The Mur River is the main drainage dissecting this region (Fig. 3.1a). It drains the Eastern Alps from the eastern edge of the Tauern Window into the Pannonian Basin, crossing the orogen-basin transition zone near the city of Graz. The landscapes of the Styrian Basin and the Highland of Graz south and north of this transition zone, respectively, comprise numerous planation surfaces and stream terraces which can be grouped into several distinct levels that cover a vertical spread of almost 1 km. Due to the presence of karstifiable rocks in the Highland of Graz, also phreatic cave levels developed (e.g. Maurin and Benischke, 1992). If multiple levels are preserved above the current stream bed and age estimates of these landforms are available, the landscape evolution can ideally be reconstructed.

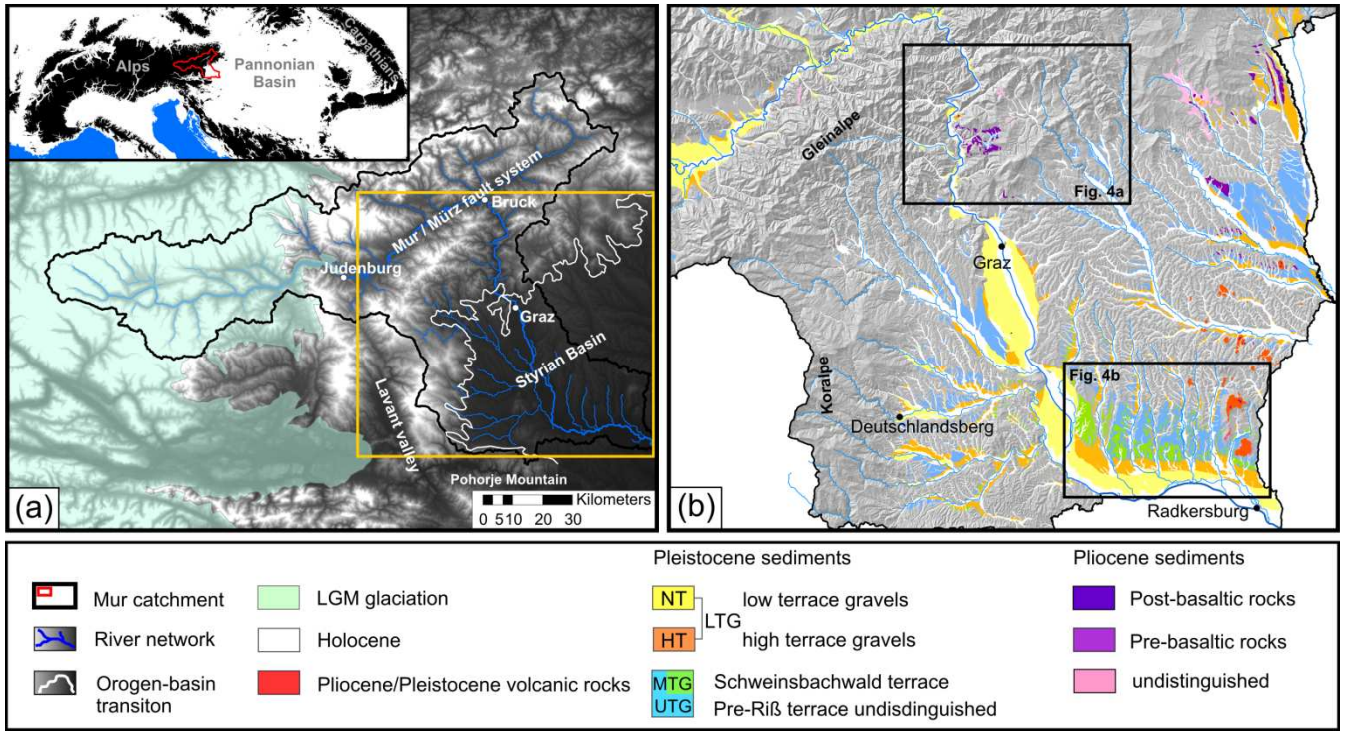

Fig. 3.1. The area under investigation. (a) The current catchment area of the Mur River, the river course itself and of its tributaries and the extent of the last glacial maximum (LGM) on top of a DEM. The white line indicates the transition from the basement to the basin. Inset shows the Alpine - Carpathian - Pannonian realm (black above 600 m, white below) and the Mur catchment within the Austrian border in red color. Extend of (b) indicated by the orange box. (b) Pliocene, Pleistocene and Holocene sediment distribution (sediment covered planation surfaces and stream terraces) and Pliocene/Pleistocene volcanic rocks. Pleistocene sediments are subdivided into the low terrace gravels (“Niederterrasse” or Würm terrace), the high terrace gravels (“Hochterrasse”, which might be further split in a Riss (penultimate) glacial terrace and the Helfbrunn interglacial terrace) and terraces that are pre-Riss (older than the previous ones). In the latter, the so-called Schweinsbachwald terrace is distinguished as the youngest subunit in the lowland, especially in the Grabenland, where this is morphologically feasible (and likely related to the lateral (southward) shift of the Mur River in the area). Further upstream such a differentiation was not possible anymore as absolute age constraints are not available. The same holds for the few Pliocene sediments in the region. Only pre- and post-basaltic gravels are distinguished where possible and the rest of the sediments could not be further distinguished. The detailed study areas shown in Fig. 3.4a (the Central Styrian Karst in the Highland) and Fig. 3.4b (the Grabenland region in the Lowland) are indicated by black rectangles.

In this paper we discuss the landscape evolution of this region on the basis of absolute and relative chronology of these levels and a correlation of these levels between north and south of the orogen-basin transition zone. A relative chronology of these levels has previously been established, based on the elevation of these geomorphic markers above and along the stream (e.g. Winkler-Hermaden, 1955), and a correlation of these markers with tectonic activity and / or climatic changes back in time has been attempted (e.g. Winkler-Hermaden, 1957). However, absolute ages of these landforms remain poorly constrained by scarce cross-correlations with dated volcanic rocks (Balogh et al., 1994) and some paleontological evidence (e.g. Mottl, 1949). The main objective of this work is to use new geochronological data to constrain the timing of these geomorphic markers. State of the art geochronological methods are applied to cover the time frame of the last about 5 Ma: The terrestrial cosmogenic nuclide (TCN) method and optically stimulated luminescence (OSL) were used to determine sediment burial ages (this and Chapter 1). U/Th age estimates of speleothem growth complete this data set (this work and Spötl et al., 2007). The absolute age constraints are discusses in the light of tectonic and climatic influences on erosive processes and landform evolution, thus, allowing to shed some light on the morphological evolution of the Styrian Block and ultimately on the eastern margin of the Alps in general.

3.2 The study area – the Styrian Block and the River Mur

The Styrian Block is a crustal fragment interpreted in Chapter 2 as a block that behaves coherently during the last few million years. It consists of the Styrian Basin and the surrounding basement. The block is delimited by the Mur-Mürz fault zone in the North, the Lavanttal fault zone in the West, the Pohorje Mountain in the South and the Pannonian Basin (excluding the Styrian Basin) to the East. It comprises three major tectonic units that have distinct landforms and different geological histories: (i) The Austroalpine crystalline basement south of the Mur-Mürz fault zone and east of the Lavanttal fault zone; (ii) The Graz Paleozoic forming the Highland of Graz in the orogen basin transition zone near Graz and (iii) the Styrian Basin, being the westernmost lobe of the Pannonian Basin. These three parts of the Styrian Block all have their characteristic features: The *crystalline basement* comprises mountainous landscape of high grade metamorphic rocks with elevations more than 2000 m a.s.l. with rounded and flat summits and deeply incised valleys characteristic for a non-glaciated landscape. It forms a presumably slowly exhuming region as fission track ages in the range of 35-50 Ma are preserved (Neubauer et al., 1995; Hejl, 1997; Dunkl and Frisch, 2002). These data suggest a small amount of Neogene denudation. However, Hejl (1997) could show that increased exhumation within the last 5-10 Ma is likely. The Koralpe is an area of relics of Miocene relief; although breaks along the hillslopes of headward migrating tributaries of the Mur River with high stream power point toward geomorphic disequilibrium (Winkler-Hermaden, 1957; Robl et al., 2008a). The *Graz*

Paleozoic contains a strongly karstified region of Paleozoic carbonates and schists called the Central Styrian Karst. Peaks reach up to 1700 m a.s.l.. No low temperature thermochronological data are available within the Graz Paleozoic. Finally, the *Styrian Basin* forms an undulating lowland (henceforth termed the Lowland of Graz) comprising Neogene sediments with elevations between 200 and 600 m a.s.l.. Despite the topographic and morphological differences between the three different regions of the block, the Styrian Block appears to behave as a single tectonic unit postdate to the Miocene (Chapter 2)

The most important tectonic event related to the onset of the Miocene to present morphological evolution of the region is the formation of the Pannonian Basin east of the Alps (e.g. Dunkl et al., 2005). Major subsidence in the early to mid Miocene related to the onset of lateral extrusion (Ratschbacher et al., 1989) initiated the formation of the Styrian Basin. This coincides with the development of the W-E directed drainage system typical for the Eastern Alps and related pull-apart basins along the major strike-slip zones, e.g. the Mur-Mürz fault system (Ebner and Sachsenhofer, 1995). In the Styrian Basin a fully marine sedimentary pile developed between ~18-11 Ma punctuated by volcanic activity around 15 Ma. According to Ebner and Sachsenhofer (1995) the basin is supposed to have inverted since ~5-6 Ma causing the end of its aquatic evolution and the beginning of its uplift history. A second phase of volcanic activity happened around the Plio-/Pleistocene boundary. The onset of surface uplift in the hinterland is much less well constrained, but minor changes in the dewatering courses of major rivers have been correlated to events as late as the glaciations in the Quaternary (Robl et al., 2008a). The onset of general relief increase is inferred to have commenced around the Miocene/Pliocene boundary (Dunkl et al., 2005). Based on thermochronological data it is also known that a good 1000 m of sediment has been eroded somewhere in the Middle to Late Neogene (Dunkl and Frisch, 2002). Based on vitrinite reflectance data and subsidence analysis in the Styrian Basin (Sachsenhofer et al., 1997), some 300-500 m have been removed within the last ~5 Ma. This time period coincides with the increase in eroded sediment volume of Kuhlemann (2007). Even a more general spatially broad uplift within the last 5-6 Ma of the Alps is recently discussed (Appendix A). This is also about the time when the inversion of the Pannonian Basin further east launched (Horváth and Cloetingh, 1996; Bada et al, 2007). Ongoing lateral extrusion is indicated by GPS measurements (Bus et al., 2009) and strike-slip displacement along the major fault zones during the last glaciations of the region (Plan et al., 2010).

The course of the Mur River south of Bruck is of special interest within the Styrian Block as it is believed to be a rather young (post Middle Miocene). Today it forms a rather narrow valley down to Graz and then proceeds its course through the Styrian Basin. Although minor faults do follow the river course (Maurin, 1953), the Mur does not flow along any of the major faults in the region. Its formation has been related to

headward migration and river catchment of the Mur-Mürz drainage area (Dunkl et al., 2005; Chapter 1). However, the channel profile indicates morphological equilibrium and rather low values of stream power, contrary to some of its tributaries (Robl et al., 2008a). Along its course, a series of planation surfaces, terraces and caves are developed up to many hundreds of meters above the current base level. The river also divides the landscape into a region with a peculiar but unexplained west-east asymmetry. In the mountainous region (known) caves and gravel deposits are predominantly preserved on the eastern river side of the Mur and almost absent on the western. In the Styrian Basin this asymmetry is also apparent. Besides partial Pleistocene sediment cover, the youngest sediments in the western basin part are of Badenian age whereas on the eastern part they are as young as Pannonian with the occasional Pliocene pre- and postbasaltic gravels preserved around volcanic rocks. This hiatus in the west of more than 10 Ma becomes obvious in the geologic sketch map of Figure 2 in Gross et al. (2007) and in the Austrian stratigraphic table of Piller et al. (2004). This asymmetry is still a matter of debate and no satisfying explanation is yet provided, although there is a general consensus that lots of sediment must have been eroded up to the present.

3.3 Morphological observations and their correlation

Along the course of the River Mur various geomorphic markers like stream terraces, planation surfaces, denudation planes, and cave levels are preserved and will be used below to place constraints on the timing of landscape evolution (Table 3.1). The systematic investigation of these landforms by Winkler-Hermaden (1955, 1957) and later work based on his groundwork (e.g. Flügel, 1960; Untersweg, 1979; Gollner and Zier, 1985; Maurin and Benischke, 1992) provided a relative chronology of individual levels along studied profiles and the correlations to each other in the Styrian Block and beyond. Elevation differences of terraces and planation surfaces and different weathering intensities were main distinctive features to distinguish the various levels from each other. As oldest levels, Winkler-Hermaden (1957) classified the Kor and the Wolscheneck levels based on possible plain relics that can be found along crests of various elevations above 1300 m a.s.l.. These levels will not be discussed here in more detail, as they find no counterparts in the Styrian Basin, they are badly developed (or preserved), their age constraints are rather ambiguous and signs of phreatic cave formation is missing (Untersweg, 1979).

Level names	Aliases and /or subdivisions	Proposed age (W-H, 1955)	Features & peculiarities	elevation above Mur River [m]
Kor level	-	Upper Sarmatian	possible plain relics along crests	1200-1500
Wolscheneck level	-	Lower Pannonian	possible plain relics along crests	900-1000
Hubenhalt level (**HUB**)	Glashüttner level	Middle Pannonian	first level indicating phreatic cave formation	700-800
Trahütten level (**TN**)	"1000 m - landscape"	Latest Pannonian	pre-basaltic gravels	500-600
Hochstraden level (**HN**)	Kalkleiten-Möstl (V.Hilber, 1912); Gebirgsrandflur (Untersweg, 1979)	uppermost Pliocene	pronounced plain system; Pediment; post-basaltic gravels	325-450
Stadelberg / Zahrerberg level (**SB/ZB**)	-	Pliocene /Pleistocene	last pre-glacial denudation plain(s)	180-300
"Obere Terassengruppe", Upper Terrace Group (**UTG**)	-	Early Pleistocene, Calabrian to Günz	early Pleistocene outflow level	80-120
"Mittlere Terassengruppe", Middle Terrace Group (**MTG**)	Rosenberg terrase	Günz/Mindel to Mindel/Riss IG	decarbonatisation, related to a warmer climate	60-100
	Schweinsbachwald or Kaiserwald terrace			40-60
"Untere Terassengruppe", Lower Terrace Group (**LTG**)	"Hochterasse", high terrace gravels (**HT**)	Riss to Würm glacial	missing loamy cover sequence	35-40
	Helfbrunn terrace		thick loamy cover sequence above "rotten" pebbles of crystalline rocks	25-40
	"Niederterrasse" (**NT**); low terrace gravels		extended thick gravel deposit; 40 m deep trough below upper edge of Würm terrace	5-20
Alluvium	Mur floodplain	Holocene	incised / nested in Würm terrace	0-10

Table 3.1. Condensed overview of levels preserved in the study area. Compiled in consideration of previous work by Winkler-Hermaden (1955, 1957), Untersweg (1979), Gollner and Zier (1985) and Maurin and Benischke (1992). Naming and proposed ages of these levels are listed according to various authors. Special features and peculiarities of the individual levels are highlighted. Approximate elevations of the levels for the study region are given in m above the present Mur River.

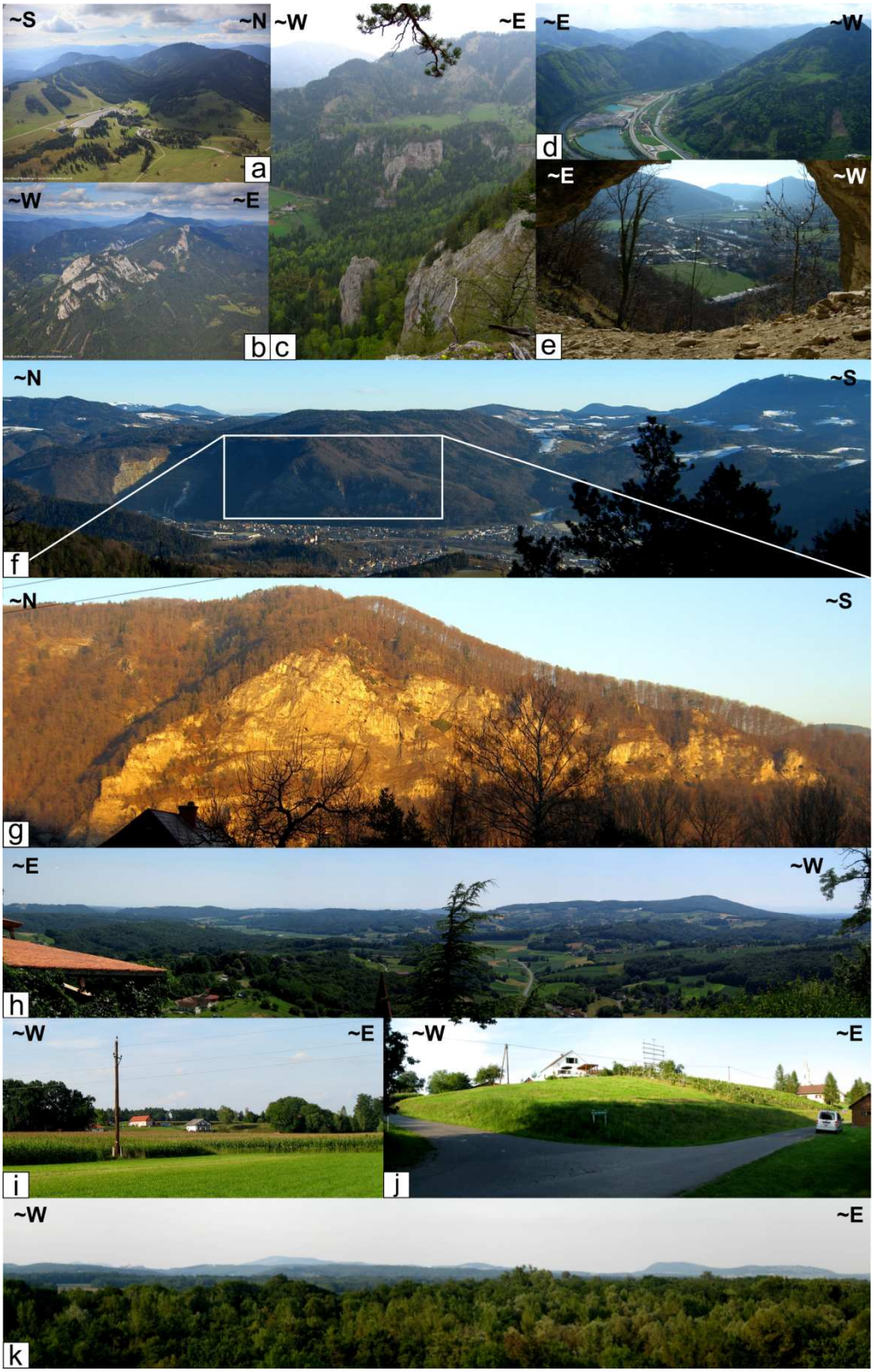

Fig. 3.2. Field impressions of the study area: (a) Aerial photograph of the Teichalm planation (~1200 m a.s.l.), correlated to the Hubenhalt level. View towards WSW. Downstream of the lake, the Mixnitzbach creek crosses the Bärenschützklamm gorge. (b) Aerial photograph from the Hochlantsch region. View from SSW. The Röthelstein (1263 m a.s.l.) in the foreground, the Bucheben saddle (1081 m a.s.l.) and then the Rote Wand (1505 m a.s.l.). The summit in the background is the Hochlantsch (1720 m a.s.l.).

Aerial photographs (a) and (b) by courtesy of Ruedi Homberger. (c) View from the Bucheben saddle towards north. Two planations are separated by a steep rockwall. The upper planation surface is correlated to the HL (here ~850 m a.s.l.) and the lower to the SB/ZB level (~700 m a.s.l.). (d) Planation surfaces along the Schiffal (~750 m a.s.l.) correlate to the SB/ZB level, seen from the Röthelstein close to the entrance of the Drachenhöhle (DH). Note the gravel pits and a swimming pont along the Mur River. (e) View from a cave of the Peggauerwand rockwall at 511 m a.s.l. down into the Mur valley towards south. Based on burial ages of cave sediments this cave level of about 100 m above the current base level of the Mur developed ~2.5 Ma ago. (f) View from the west towards the Tanneben massif. The plateau right above the rock wall and the quarry becomes obvious. This planation belongs to the HL. The peak in the upper right of the picture is the Schöckl (1445 m a.s.l.) and the town visible in front of the Tanneben massif is Peggau (410 m a.s.l.). The town is located in the Mur valley, which forms the current base level. (g) Detailed photograph of the Peggauerwand rockwall. The obvious perched caves indicate former water tables and groundwater elevations, thereby illustrating relative valley lowering over the last million years. (h) View from Kapfenstein towards south. The plateau-like rise (~550 m a.s.l.) in the right of the picture is the Stradnerkogel. The planation surface is correlated to the HL. Further to the east planation surfaces of the Zaraberg and the Stadelberg are noticeable (~400 m a.s.l.). They belong to the subsequent SB/ZB level. (i) and (j) Terrace riser (anthropogenic changes are likely) of the Helfbrunn terrace, seen from the low terrace gravels. The investigated loam pit is situated some 100 m to the North. (k) View from Gosdorf “Murturm” towards the north. Terraces and planation surfaces are visible, although the forested floodplain makes it difficult to clearly see terrace risers. Note the grassland in the lower left of the picture, which belongs to the Helfbrunn terrace. In the background the volcanic cones of Stradnerkogel (left) and Klöch (right) with their pronounced denudation plains are noticeable.

3.3.1 Levels in the Styrian Block

Distinctive levels of the study area can be placed into two groups. The more elevated levels appear to be denudation plains, whereas levels at lower elevations are usually terraces. Below, we will touch on each of these levels beginning from the highest: (i) The uppermost eminent level is the so-called Hubenhalt level (HUB) (Fig. 3.3). This level is presumably the oldest of all surfaces in the Styrian Block and occurs exclusively in the Highland. It is of supposed Middle Pannonian age (Winkler-Hermaden, 1957) and can be found as a pronounced planation surface east of the Hochlantsch summit: the Teichalm (Figs. 3.2a, 3.3a). Various smaller planation surfaces can be grouped into this level. The HUB is named after the Hubenhalt, a small planation preserved at a crest just east of Nechnitz (Fig. 3.3a). (ii) The next lower (and younger) planation surface, possibly representing a dry valley, belongs to the Trahütten level (TN). The TN is pronounced around elevations of about 1000 m a.s.l. in the Highland and the crystalline basement and supposed to be of Latest Pannonian age (Winkler-Hermaden, 1957). This level is named after a planation surface on the eastern side of the Koralpe just west of Deutschlandsberg. This level is distinct due to its speleogenetic occurrences in the Central Styrian Karst, but not preserved in the Styrian Basin. In the Koralpe region, planations correlate well in elevation with planations in the Highland of Graz (Winkler-Hermaden, 1957) and further support the idea of a spatially broad evolution of planation surfaces along erosional base levels of that particular time over the whole Styrian Block regardless of lithology. This becomes even more evident for the subjacent level. (iii)

The Hochstraden level (HN) is the highest level that can be observed in the Highland as well as in the Lowland, due to the preservation of denudation plains at about 550 m a.s.l. on top of a volcanic cone in the basin, the so-called Stradnerkogel (Fig. 3.3b). This level is of supposed uppermost Pliocene age (Winkler-Hermaden, 1957). On top of this denudation plain so-called post-basaltic gravels are preserved in the vicinity of a locality named Hochstraden. An alias for this level is Kalkleiten-Möstl (Hilber, 1912). Kalkleiten is a locality in the north of Graz (Fig. 3.3a). It is an obvious planation surface termed the “balcony of Graz”, because of its panoramic view over Graz. This system of planation surfaces was called “Gebirgsrandflur” by Untersweg (1979) and it is highlighted as a level of continuous and widespread extent observed on various lithologies and across prominent faults. Thus, this level can definitely be defined as one that emphasizes a consistent and uniform vertical uplift since its formation up to the present. (iv) The double plain of Stadelberg/Zahrerberg (SB/ZB) is named after planations on the Stadelberg (~4 km east of St.Anna a. Aigen in Burgenland) and the Zaraberg (west of Klöch; previously named Zahrerberg) (Fig. 3.3b). This level is considered to be the last pre-glacial denudation plain developed around the Plio-/Pleistocene boundary and is found some 180 m to 300 m above the present base level, i.e. the Mur River. An exceptional view of the HN and the SB/ZB denudation plains is provided from the Kapfenstein castle on top of a volcanic cone (Fig. 3.2h).

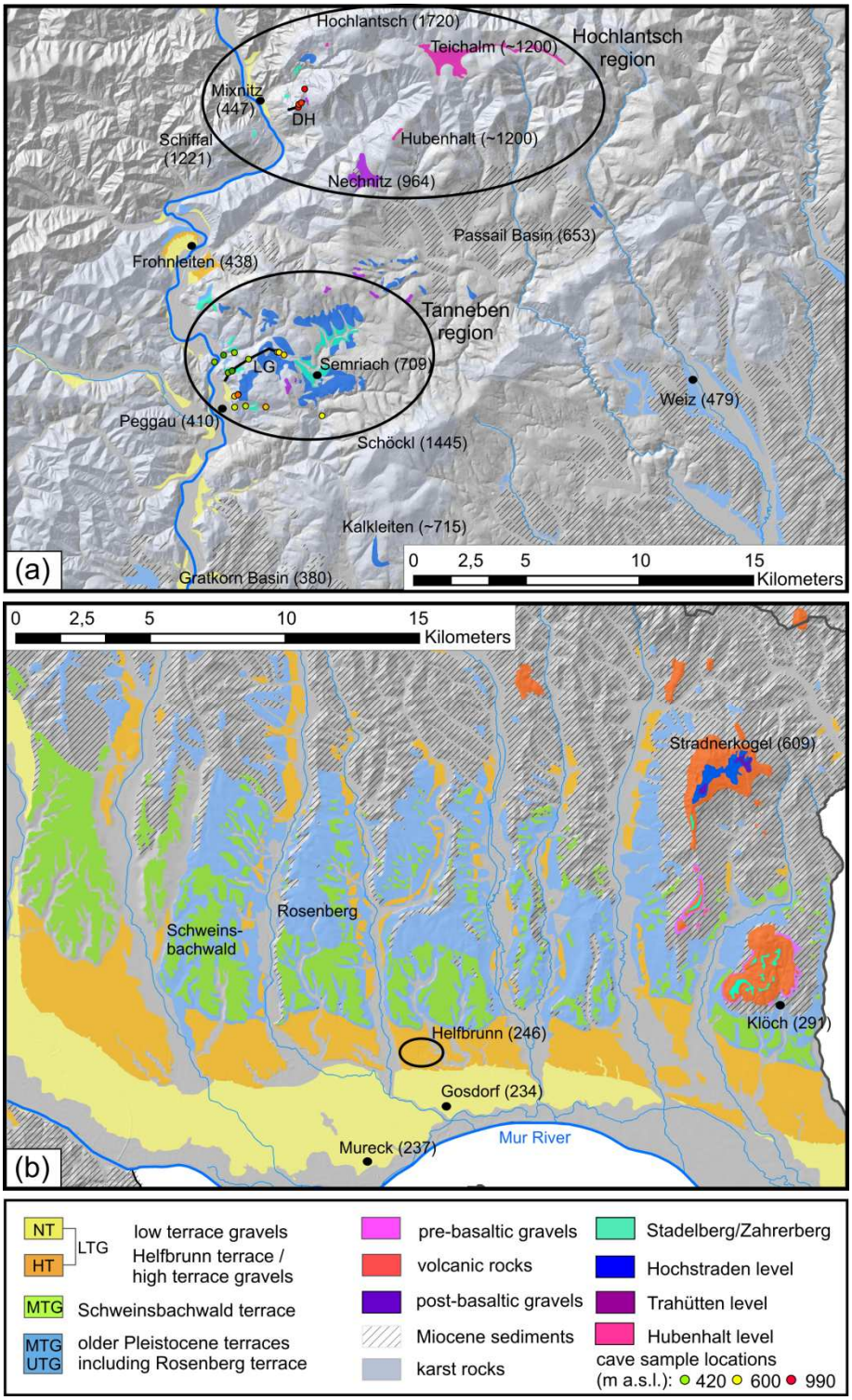

Fig. 3.3. More detailed level overview of the Highland (a) and the Lowland (b). (a) The Highland of Graz with the focus on the Hochlantsch region with the HUB (Teichalm), the TL (Bucheben); the HL (Burgstall top) and the SB/ZB (Burgstall base) and the Tanneben region with levels preserved related to the TL and lower levels. (b) The Grabenland as the main focus of the Lowland of Graz shows an obvious valley asymmetry and the various levels ranging from the denudation planes of the HL and the SB/ZB to the terrace levels of the UTG, MTG and LTG. Pre- and post-basaltic gravels related to volcanic rocks are also displayed. The loam pit where the samples for OSL dating were taken is indicated by a black circle. All numbers in parentheses are elevations in m a.s.l..

The terrace levels that developed at lower elevations, from about 120 m above, down to the current base level of the Mur River, are obvious gravel terraces with - in the majority of cases - thick loam deposits developed on top. In general these terraces are correlated to glaciations record in the headwaters of the Mur River (e.g. Piller et al., 2004). Only the lowermost terrace which is related to the Würm glaciations is a pure gravel deposit preserved along the Mur River. An upper terrace group (UTG) is distinguished from a middle terrace group (MTG) and a lower terrace group (LTG). The morphological distinction is easily possible in the lowland where obvious terraces are developed, but this is more difficult in the Highland, as older terraces are obscured by younger sedimentation and erosion. (v) The UTG is suggested to represent an early Pleistocene outflow level and is placed somewhere in the Calabrian to Günz by Winkler-Hermaden (1955). (vi) The MTG includes terraces in the range of 40-100 m above the local base level. In the lowland, in particular in the Grabenland, the Schweinsbachwald terrace and a more elevated Rosenberg terrace are distinguished based on the different amount of denudation and dissection of the loamy cover section of these terraces. Further upstream along the Mur, the MTG and the UTG are not distinguished, because this is not possible anymore in the more narrow valleys. For simplicity, these terraces are related to be of pre-Riss age and termed older Pleistocene terraces of questionable age. However, it is noticed that all these terraces are characterized by a top sequence of loam. (vii) The LTG is subdivided into the "Hochterrasse" (HT, high terrace gravels) and the "Niederterrasse" (NT, low terrace gravels). The HT is suggested to be of Riss glacial or Riss-Würm interglacial origin. Based on the fact that the HT relics in the Lowland show an obvious loam sequence developed on top of the gravels and the HT relics in the Highland miss this cover sequence, a further subdivision into a glacial and an interglacial terrace was suggested by Winkler-Hermaden (1955). The NT is an obvious pure gravel terraces of glacial origin related to the last glacial maximum (Van Husen, 1997) and is exclusively found along the Mur River and tributaries in the Koralpe region where local glaciers were established (Fig. 3.4c).

The various levels and planation surfaces listed above are concentrated in three key areas that will be discussed in some detail below. Two of them, the *Tanneben region* and the *Hochlantsch region,* are located within the Highland of Graz and belong to the Central Styrian Karst. There, an abundance of caves and some remnants of planation surfaces are studied in more detail. These are the regions of speleologic interest investigated in Chapter 1. The third region of interest is located in the Styrian Basin some kilometers downstream of Graz*: the Grabenland*. There, levels range from nicely preserved glacial and/or interglacial terraces to denudation planes at higher elevations on volcanic rocks.

3.3.2 The Highland of Graz – in the Graz Paleozoic

The Highland of Graz is part of the Paleozoic of Graz and consists of Paleozoic limestones, metavolcanics and schists. They comprise the Central Styrian Karst, an area of conspicuous landforms as old as the Miocene (Winkler-Hermaden, 1957). It includes two regions of particular interest to our study: the Hochlantsch region and the Tanneben region (Fig. 3.3a). Various generations of planation surfaces, cave levels and dry valleys are apparent and can be discerned on the basis of their altitudinal distribution (Winkler-Hermaden, 1955; Untersweg, 1979). Multi-stage entrenchment becomes obvious by these relics. The occasional dry valley (e.g. Nechnitz) indicates abandoned river courses oriented towards the south (e.g. Winkler-Hermaden, 1957) and later redirection towards the west.

The Hochlantsch area at the northern edge of the Graz Paleozoic includes the higher and possibly older levels recognized in the Highland of Graz. Various levels of karstification and caves formed besides numerous planation surfaces (Fig. 3.2a-d). The largest cave system of the Hochlantsch region is the kilometer long Drachenhöhle system, some 600 m above the current river. Cave systems show obvious stages of decay at elevations above ~1000 m a.s.l. as only remnants of previously interconnected systems are preserved. The most significant planation surface is a peneplain called Teichalm at about 1200 m elevation, which is suggested to be of Middle Pannonian age and has been ascribed to the HUB level (Winkler-Hermaden, 1957). The small lake of this peneplain drains through the Bärenschützklamm, a deeply dissected limestone gorge in a western direction towards the Mur River (Fig. 3.2a). The channel profile of this creek (Mixnitzbach) shows an obvious knickpoint and stream power is the highest in the Mur catchment (Robl et al., 2008a) where the Mixnitzbach crosses a gorge (Bärenschützklamm). The dry valley of Nechnitz (964 m a.s.l.), where some of the highest Neogene fluvial deposits are preserved, is correlated to the TN and is suggested to indicate a former southward dewatering trend (e.g. Winkler-Hermaden, 1957). The occurrence of Upper Cretaceous Bärenschütz conglomerate at various elevations ranging from 600 to 1300 m a.s.l. is related to Neogene block tectonics along an obvious NE-SW trending fault zone crossing the Mixnitzbach (Gollner and Zier, 1985). However, a continuous plain relic on top of the younger (Neogene) Burgstall Breccia (Fig. 3.2c) is correlated with the HN and indicates no vertical displacement since the time of its evolution.

In the Tanneben region highest elevations are around 1100 m and the region thus preserves only levels at and below the TL. Relics of higher landforms are only preserved in isolated remnants of the Schöckl limestones in the eastern part of the Semriach Basin. The Tanneben massif is also an area of great speleological significance, which is manifested by an abundance of some 300 caves relating to cave levels at and below the HL including one of the largest cave systems of the region: the

~5 kilometer long Lurgrotte system. An old burial age of ~5 Ma from a cave which indicates remobilization from an older, higher and nowadays eroded cave level indicates the presence of older levels in former times (Chapter 1). However, the preserved lower levels are more prominent in this region compared to the Hochlantsch area further north. The HL typified by the planation surface above the Peggauer Wand in the Tanneben massif (Fig. 3.2f) preserved widespread fluvial gravel spreads (e.g. Ertlhube) and are evidence of a low-gradient Paleo-Mur River prior to its incision into the present valley slightly further west. Later, the incision of the Mur River seems to be more vertically and not much lateral incision is observed in the Highland of Graz.

The Lurgrotte cave system has autogenic but also allogenic recharge from the Semriach Basin, a small intramontane Neogene depression. Impressively, the hooklike course (90° bent) of the Lurbach creek upstream of Semriach shows the deviating from its former SW oriented drainage course (e.g. Maurin and Benischke, 1992). The Rötschgraben which drained the hinterland of the Tanneben massif prior to these changes in the hydrological setting (e.g. Untersweg, 1979) shows a prominent knickpoint, the so-called Kesselfall. The former dewatering of the Lurbach to the south into the Rötschbach is related to a swell at the southwestern side of the Semriach basin comprised of gravels of unconstrained age (Pannonian or younger). This swell is found at elevations corresponding to the HL, indicating the time of the Lurbach stream capture event and its subsequent subterraneous course (e.g. Maurin and Benischke, 1992). Also the paleo-Mur has likely shifted westwards, as a dry valley on the southern side of the Tanneben massif indicates (e.g. Maurin and Benischke, 1992). This points toward a stronger hydraulic gradient perpendicular to the incising Mur valley and thereby influenced its tributaries. In this fluviokarst area the lowering of the erosion base, the Mur River, beheaded and diverted tributaries. Some of them disappear into ponors like the Lurbach into the Lurgrotte cave system (the main ponor), due to subterraneous corrosion and erosion. Due to its karst underground some planation surfaces are preserved along the Mur valley which allows correlating speleogenetic levels and surface forms. The Peggauer Wand (Fig. 3.2e-g) is a beautiful example where cave streams emerge as springs along the base of a valley wall. More elevated abandoned cave passages form speleogenetic levels and indicate paleo-base levels, representing former valley bottom elevations. The Lurgrotte is the longest passable cave system in the Tanneben region (~5 km in length). The system shows three phreatic levels (e.g. Maurin and Benischke, 1992). The lowest permanently active level shows obvious signs of backflooding that can be related to aggradation of sediments within the valley itself and consequently plugging and a temporary increase in the local base level (Chapter 1). Occurrences of last glacial gravels and syphons ascending to the current outlet of the cave system indicate possible deeper karstification and consequently deeper valley incision prior to the LGM; but only in the order of a few meters to a maximum of 40 m. This is based on drillings near the town of Peggau penetrating the gravel deposits down

to the bedrock (Weber, 1969). In fact, this shows that the Mur River has not yet re-excavated last glacial sediments within the Holocene.

In general, speleogenetic levels encountered in the Central Styrian Karst are linked to surface levels. These were described in Chapter 1 and termed cave level A to E. We will relate this nomenclature to the traditional level names described above. Cave level A can be correlated to or parallelized with the Trahütten level (TL); cave level B to the Hochstraden Level (HL), C is related to the Stadelberg/Zahrerberg level (SB/ZB) and marks the lowest pre-glacial denudation plane, and D represents the Upper Terrace group (UTG). Level E covers the Middle Terrace Group (MTG) and the Lower Terrace Group (LTG). The LTG in turn combines the high terrace gravels (HT) and the low terrace gravels (NT). The larger extent of level E identified in Chapter 1 is the consequence of various sublevels closely spaced and/or even overlapping. This led to the fact that these (sub-) levels are not distinguishable as individual speleogenetic levels. This is attributed to the episodic incision, aggradation and re-excavation of the Mur valley in that period of time. However, individual terraces are distinguished in the Styrian Basin, the Lowland of Graz, and allow a separation of these younger individual stages of landscape evolution.

3.3.3 The Lowland of Graz – the Styrian Basin

In the Lowland of Graz, the so called Grabenland region (Figs. 3.1b, 3.3b) is of particular interest. The Grabenland is a southward draining region of a series of parallel tributaries to the Mur River in the central Styrian Basin (Fig. 3.1b). It is between 200 m and 600 m above sea level. Highest elevations are typically those of the volcanoes of the region. The Grabenland features a series of terrace levels and planation surfaces on the Plio/Pleistocene volcanoes that can be used to place timing constraints on their formation. Importantly, the Grabenland is also the type locality of the high terrace gravels (HT). The so-called Helfbrunn terrace is the terrace right above the NT. As the latter is the terrace related to the last glacial maximum the next higher one, the Helfbrunn terrace is generally believed to relate to the penultimate glaciation (Riss) or to the Riss-Würm interglacial. The Helfbrunn terrace shows a much higher disintegration of the individual clasts compared to the low terrace gravels. This was the main argument to propose an older age (Riss glacial) of this terrace (Fink, 1961). Mottl (1949) reported *Ursus spelaeus* in fluviatile cave sediments in a Kugelstein cave 40 m above the Helfbrunn terrace level, which occurred in the Mindel-Riss interglacial. As this cave belongs already to another older level, a Würm-Riss interglacial has been suggested by Winkler-Hermaden (1955), who favored an interglacial origin of the terrace. The gravels of the Helfbrunn terrace are covered by an up to 8 m thick dust loam of rather questionable origin. However, this loamy section is not a classic loess deposit, as it is free of carbonate, especially free of carbonate cement that is normally

responsible for its stability along roadcuts. There are at least two other obvious terraces at higher elevations: the Schweinsbachwald and the Rosenberg terrace (Fig. 3.3b) which are similar in composition to the Helfbrunn terrace with a thick loamy top section. The fact that the Helfbrunn terrace is still accessible due to an outcrop in a former loam pit, enabled sampling along a profile from the top of the deposit down to the beginning of the gravel pack. The application of optically stimulated luminescence (OSL) dating allowed to places a minimum age constraint on the terrace deposit (Section 3.3).

Besides the terrace levels there are also higher and thus probably older planation surfaces up to the volcanic cones of Klöch and Stradnerkogel (Fig. 3.3b). A very prominent denudation plane on top of the Zaraberg (or Zahrerberg) developed. This level corresponds to the last denudation plane prior to the onset of climate deterioration around the Plio-/Pleistocene boundary (Winkler-Hermaden, 1955): the SB/ZB level. The number of the main stream terraces in the region (low terrace gravels, Helfbrunn terrace, Schweinsbachwald and Rosenberg terrace) matches with the four glaciations (Würm, Riss, Mindel and Günz). However, although tempting, it does not mean that they necessarily correlate in time. In contrary, Winkler-Hermaden (1955) argued that the more elevated loam covered terraces are of interglacial origin. Fig. 3.4 indicates various time slices of sediments of different times of deposition. It becomes evident that only the last glacial terrace is almost exclusively constrained along the Mur River and its tributaries from ice-free hinterlands do not contain gravels of the NT. We will address this observation in Section 3.4.2.

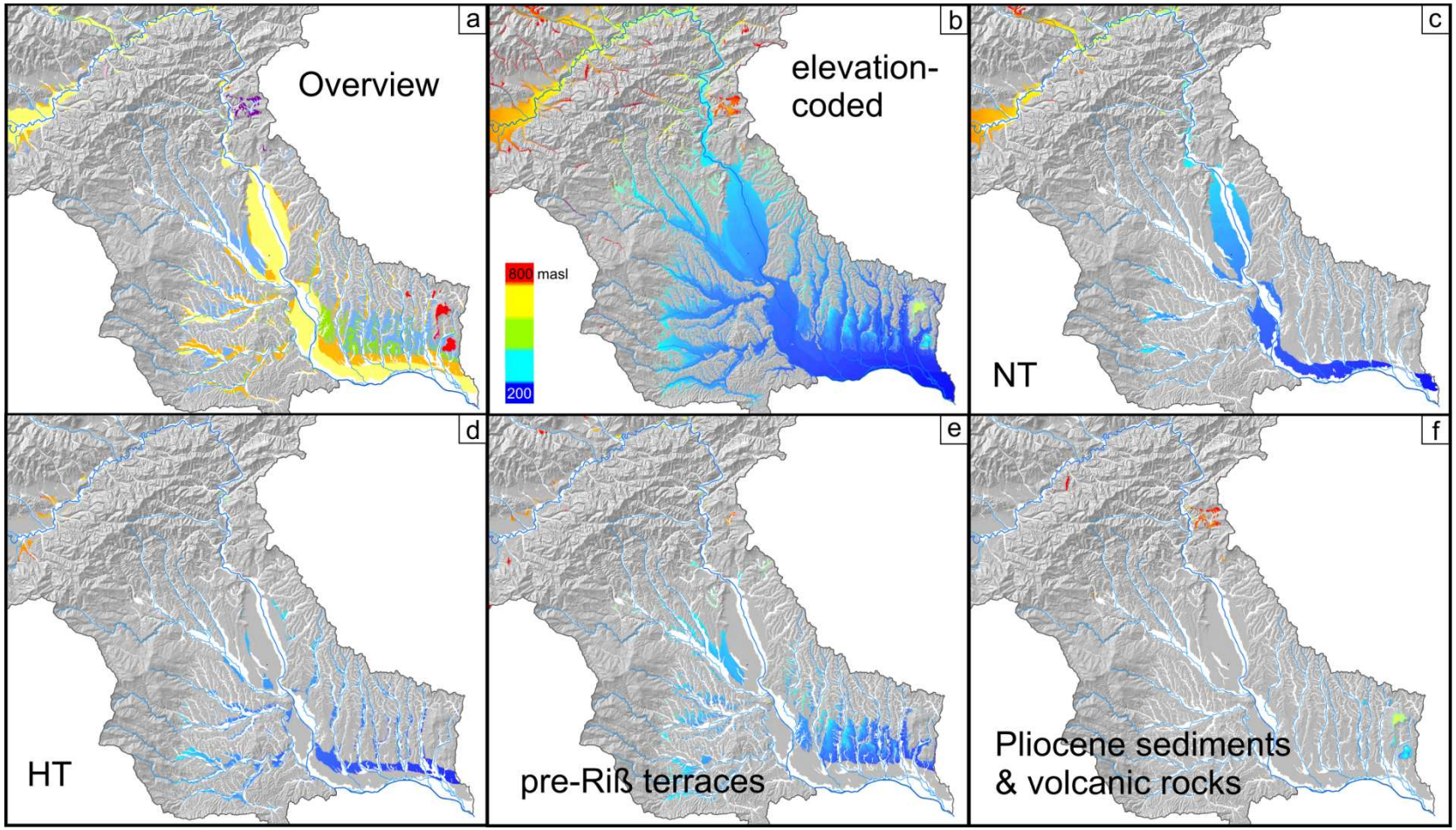

Fig. 3.4. Elevation-correlated sediment distribution of the various time slices from Pliocene to Pleistocene preserved in the Mur catchment. (a) Overview of Pliocene and Pleistocene sediments of the Mur catchment only; labeling according to Fig. 3.1. (b-f) Color-coding according to elevations from 200 m a.s.l. (blue) to above 800 m a.s.l. (red). (b) similar to (a) but color-coded according to elevation. (c) The low terrace gravels (NT) are exclusively found along the Mur River and along tributaries from the glaciated Koralpe summit; (d) the high terrace gravels (HT) are evenly distributed all over the tributaries. (e) The same is true for the higher terrace levels (not further sub-divided). (f) Almost no Pliocene sediments are preserved.

3.4. Absolute age constraints of levels

An essential correlation between surface planation features and cave levels in the Tanneben region was performed by Maurin and Benischke (1992), who realized the potential of the preserved information in the caves versus the more easily eroded surface features. As burial age data were not available at that time, they used the surface forms and their age estimates (based on the work of Winkler-Hermaden, 1955) to get an approximate age of the formation of various cave levels. Here we extend their work further up- and downstream, covering the whole Graz Paleozoic and the Styrian Basin. In our approach, we use the terrestrial cosmogenic nuclide method (TCN; e.g. Granger et al., 1997; Anthony and Granger, 2004), published K/Ar ages of volcanic rocks exposed in the Styrian Basin (Balogh et al., 1994) and new OSL age estimates from fine grained deposits of a stream terrace in the Styrian Basin. Combining these age estimate with speleothem formation happening at the same time (U/Th ages) allows temperature conditions and vegetation cover in the region to be inferred. Combining all this absolute age information, the relative levels along the Mur River are placed into absolute time spans.

3.4.1 Ages of levels in the Highland

Levels in the Highland are best dated through their proxy in the speleogenetic levels. The evolution of the various speleogenetic levels and their age can be constrained by ages of cave deposits (e.g. Stock et al, 2005a). Dissolution caves are younger than the host rock and older than deposited sediments therein if remobilization can be excluded. As the cave deposits provide minimum age constraints for the cave development, they also yield minimum age constraints of parallelized surface forms. Burial ages of allochthonous quartzous cave sediments were found to be best suited to constrain the age of cave passage formation. Table 3.2 is the attempt to extract this information from the data presented in Chapter 1.

The HUB level including the Teichalm planation surface has no corresponding speleogenetic level of known age, so its age remains speculative. Cave level A, and consequently also the TL is at least 4 Ma old, based on burial ages of allochthonous gravels from the Drachenhöhle (DH, Fig. 3.3a). The planation (or dry valley) of Nechnitz is slightly above this elevation, and thus may correlate in age, but has not been dated directly. Level B, analogous to the HL is more than ~3.4 Ma. We suggest to place its formation between 3.4 and 4 Ma; a rather short period of time for its obvious extend in the study area (Untersweg, 1979). Level C and the SB/ZB level have to be placed ~3 Ma. The level D and the associated UTG is constrained by burial ages of ~2.5 Ma and marks the abandoning of cave passages just ~100 m above the current stream. From this time on, speleogenetic levels are more ambiguous. This has been related to episodic aggradation events in the Mur valley (Chapter 1) and suits the fact that the SB/ZB level is recognized as the last pre-glacial denudation plane (e.g. Winkler-Hermaden, 1955).

The actual time constraint of ~2.5 Ma coincides with the onset of the Pleistocene climate deterioration. Level E subsumes various sub-levels which have to be placed within the Pleistocene. A more detailed subdivision is made possible by analyzing the stream terraces further downstream in the Lowland; this will be discussed in the following paragraph. However, burial ages of level E that do not correspond to the actual abandonment of the passage level, indicate an aggradation event ~450 ka most likely related to a damming event in the Mur valley. This concerns samples LG6 and LG8 from two different sub- levels of the Lurgrotte (LG, Figs. 3.3a, 3.7). This rise in sediment load was correlated with MIS 12 and the Mindel glaciations affecting the headwaters of the Mur catchment (Chapter 1). Important for this finding is that, although these samples did not yield information about the time of passage formation, they place lower limits of the passages extent at that period of time. This suggests that at this time, the local base level was already close to the current one. Ongoing re-excavation of gravels from the current river bed demonstrates the current transport limited state of the Mur River. This results in limited bedrock incision since the last glacial maximum in this particular case and also suggests a similar scenario in previous interglacials. This is in accordance with the strong decrease in incision rates in the Pleistocene suggested in Chapter 1.

speleogenetic level	samples	minimum Age (Ma)	comments	elev. above Mur (m)	associated levels
A	DH4	~4	the "1000m" level; Bucheben; Trahütten/Koralpe	500+	TL
B	DH1, DH2	~3.4	Tanneben plateau, Kalkleiten, Stradnerkogel	325-375	HL
C	between LG2 & LG3	~3	last pre-glacial denudation plains	210-250	SB/ZB
D	PWH3, FG1, KG1	~2.5	corresponds to Plio/Pleistocene boundary	~100	UTG
E	between SG3 and today	0-2.5	multiple sublevels, complicated due to aggradations and re-excavations	0-75	MTG - Holocene

Table 3.2. Cave levels and their minimum age constraints based on sediment burial ages from Chapter 1.

3.4.1.1 U/Th ages of speleothems

U/Th age estimates of bottom and top sections of speleothems which are stratigraphically related to some of the allochthonous cave sediments dated by TCN were used as minimum age control for the TCN ages (Chapter 1). These ages (Table 3.3) are an order of magnitude younger than related TCN burial ages, confirming the findings of Stock et al. (2005a) that speleothem ages could considerably underestimate the age of void evolution. However, as their formation is mainly related to appropriate environmental conditions (Spötl and Mangini, 2006; Spötl et al., 2007) and the relation to the individual levels is secondary, we will discuss this data without the reference to the specific levels.

All U/Th ages of speleothems are in the range between 74 ka and 228 ka and were derived from flowstones and calcite false floors. Ages from the Lurgrotte are at the younger end of this spectrum. Sample LG10-FST2 gave the youngest U/Th age of

74.2 ± 0.6 ka and could be correlated to Marine Isotope Stage (MIS) 5a. (Sample names are related to TCN burial age samples and are indicated by the similar sample name, and taken from the top (FST) or the bottom section (FSB) of the flowstone; Table 3.3). Another three of the Lurgrotte samples (LG6-FSB, LG10-FSB and LG10-FST1) yield ages between 90 and 100 ka. Detrital thorium contamination of some of these samples resulted in rather large uncertainties (Table 3.3). Samples LG6-FSB and LG10-FSB are correlated to MIS 5c, LG10-FST2 to MIS 5a. This age range of speleothem formation from the Lurgrotte cave system suggests ice-fee, soil-covered conditions consistent with interstadial conditions of MIS 5a and c. The single age of the Drachenhöhle sample DH4-FST of 228 ± 3 ka correlates to MIS 7 and further documents the match of speleothem formation and interglacial (or interstadial) times. A speleothem from the cave Moosschacht, located in the Tanneben massif close to Ertlhube at level B, indicates discontinuous speleothem growth at a time span of 105 to 80 ka (Spötl et al., 2007), similar to our samples from the Lurgrotte. Interestingly, Spötl and Mangini (2006) reported calcitic flowstone formation in fractures of the Pleistocene Hötting Breccia near Innsbruck at the same periods of time (between 100.5 ± 1.5 and 70.3 ±1.8 ka), thereby demonstrating an ice-free central Inn valley. Although more in detail analysis of speleothem formation in the Central Styrian Karst would be desirable, these initial results are strong evidence for ice-free, soil-covered conditions in the Styrian Block at periods of ~230, ~100 and ~70-80 ka.

Sample	Lab no.	U (ngg^{-1})	$[^{230}Th/^{238}U]$	$[^{234}U/^{238}U]$	$[^{230}Th/^{238}U]$	$[^{230}Th/^{232}Th]$	Age (ka)	$[^{234}U/^{238}U]_i$
LG10-FST2	UMA02798 Jul-2009	51	1.384 (7)	2.632 (5)	0.00296 (3)	3.0	74.2 ± 0.6	3.013 (6)
LG10-FST1	UMA02797 Jul-2009	95	1.328 (8)	1.831 (5)	0.32516 (74)	2.2	92.6 ± 35.6	2.081 (107)
LG10-FSB#	UMA02796 Jul-2009	80	1.285 (7)	1.736 (4)	0.29751 (169)	2.1	99.9 ± 32.2	1.977 (88)
LG6-FSB#	UMA02795 Jul-2009	104	1.081 (5)	1.686 (5)	0.02254 (24)	1.9	99.6 ± 2.1	1.913 (7)
DH4-FST	UMA02794 Jul-2009	127	1.965 (8)	1.980 (4)	0.01681 (21)	2.9	228 ± 2.9	2.871 (14)
DH4-FSB#	UMA02793 Jul-2009	72	1.113 (10)	1.084 (4)	0.22907 (162)	1.4	559 (+inf/-110)	1.427 (+0.53/-inf)

Table 3.3. U-Th age estimates of speleothems from the Lurgrotte (LG) and the Drachenhöhle (DG) caves in the Central Styrian Karst. Samples with a superscript # were previously published see Chapter 1. Sample preparation and measurements done by John Hellstrom, University of Melbourne. Activity ratios were determined with a Nu Plasma MC-ICP-MS following the procedure of Hellstrom (2003). Age is corrected for initial ^{230}Th using Eq. (1) of Hellstrom (2006) and an initial $[^{230}Th/^{232}Th]$ of 1.5 ± 1.5 (uncertainties fully propagated). 95% confidence intervals of the last digits of each value are given in brackets.

3.4.2 Ages of levels in the Lowland

Highest planation levels preserved in the Lowland are on Pliocene to Pleistocene volcanoes and correlate with the HL and the SB/ZB levels. The highest terrace level in the Lowland of Graz (UTG) correlates with the UTG in the Highlands and the dated cave level D (about 2.5 Ma). Thus, all other lower levels in the Lowlands are likely to be younger. In fact, all terrace levels are associated to various glaciation events in the Pleistocene (e.g. Van Husen, 2000). A relatively young phase of volcanic activity in the Styrian Basin is scattered over a time frame of 1.71 ± 0.72 to 3.76 ± 0.41 Ma based on

K/Ar ages of these volcanic rocks (Balogh et al., 1994). This data places maximum age constraints on planation surfaces developing subsequently and gravel accumulations that were deposited on top of these surfaces, the so-called post-basaltic gravels.

In the Mur catchment area, the volcanic cones of Klöch and Stradnerkogel are of particular importance. On both of these, planation surfaces are developed. At about 550 m a.s.l. a striking planation formed on the Stradnerkogel (Fig. 3.3b), the HL is named after this locality. On a lower level of the Stradnerkogel and on the Klöch basaltic rocks, the SB/ZB level can also be distinguished. Balogh et al. (1994) reports a K/Ar-age of the basalt of Klöch to be 2.6 ± 1.2 Ma. This data places a maximum age constraint on the SB/ZB level, and suggests that the formation of this last pre-glacial denudation plane might not be older than 3.76 Ma. From the burial age data of level C which is correlated to the SB/ZB level, we propose an age of at least 3 Ma. These data are in good agreement to each other. A bit more problematic is the K/Ar-age of the Stradnerkogel. A sample was analyzed by Balogh et al. (1994) from the quarry close to the above mentioned striking planation surface on the Stradnerkogel. This sample resulted in the youngest age of all the reported K/Ar-ages (Balogh et al., 1994): 1.71 ± 0.72 Ma. This would imply that the HL is younger than 2.43 Ma which is in contradiction to our data (level B ≥ ~3.4 Ma). This young K/Ar-age does not only disagree with the age constraints of level B (HL), but also with level C (SB/ZB) and to some degree even with level D (UTG). This raises some reasonable doubt about the single K/Ar-age or would suggest a vertical displacement of the Stradnerkogel region of some 100-200 m after the formation of the plain, which is not supported by any field evidence.

All levels below the UTG are not very well constrained in time by absolute age dating. Only the very lowest level (NT) is known to be of Würmian age (Van Husen, 1997). Interestingly, sediments related to the last glaciations (NT) are exclusively deposited in the Styrian Basin along the Mur River and absent in tributary where headwaters originate from ever ice-free regions (Fig. 3.4c, e.g. the ones in the Grabenland). This observation does not apply for higher and thus older terraces (Fig. 3.4d, e). The distinction from the NT is made by the fact that the terraces found at higher elevations all show extensive loamy cover sequences (besides terraces near Frohnleiten at elevated position, likely related to Riss glaciations). The older “floor relics” show, according to Winkler-Hermaden (1955), a succession of gravels - gravel/sand - sand - sandy loam - loam. The terraces with a loamy upper section spread far into the plains downstream of Radkersburg, in contrary to the glacial terraces which taper off closer to the orogen margin. This difference in characteristics resulted in the idea that the more elevated terraces might be of interglacial or interstadial origin, not related to a glacial maximum (Winkler-Hermaden, 1955). However, e.g. Fink (1961) favored a glacial origin.

3.4.2.1 An absolute age constraint for the high terrace gravels

To contribute to the clarification of the absolute age, we report here of the first successful dating of the type locality of the Helfbrunn terrace, which belongs to the HT. The sample location is an abandoned loam pit near Gosdorf (Fig. 3.3b). The HT rises about 10 m above the last glacial gravel spreads (NT, Fig. 3.2i, j) of the Late Würmian glaciation. Because of the higher position, the terrace is believed to be of Riss-Würm interglacial (Winkler-Hermaden, 1955) or possibly Riss glacial origin (Fink, 1961). The terrace sequence can be divided into a loamy upper section and a gravel base. It is conspicuous that individual pebbles of the basal gravels are of a rather decomposed state (heavily weathered) compared to the intact gravels of the NT gravels. This was used to justify an older age of this terrace compared to the lower terrace (Winkler-Hermaden, 1955; Fink, 1961). Based on drillings done in the year 2008, it could be proven that the gravel thickness is not more than about 6-7 m (below about 5-8 m of loam), as Tertiary sediments are encountered thereafter (Fig. 3.5). This is an important confirmation that the Helfbrunn terrace is indeed an individual terrace that was deposited on its independent base level prior to further river incision and deposition of the next lower terrace, the NT. The top section of the terrace consists of up to 8 m thick loams which are interpreted in various ways and termed alluvial clay, dust loam or loess (Suette, 1986). Winkler-Hermaden (1955) suggested them to be mostly warm-temperate alluvial clays; whereas Fink (1961) was of the opinion that at the transition from gravels to loam, fluvial origin is likely but in the higher sections eolian processes were responsible for their formation. Fabiani and Eisenhut (1971) mentioned that pedologically these are cold temperate dust loams. The important point is that the shift from gravels to loams is without doubt of fluvial origin. This is manifested by an intercalation of gravels and loams. Winkler-Hermaden (1955) reported that gravels are found in the lower sections of the loam and vice versa, demonstrating a continuous sedimentation process. This fact was the motivation for dating the top loam section via OSL (Bøtter-Jensen et al., 2003) to obtain a time constraint for this terrace, however the actual absolute age of the base remains speculative. Four samples along a profile of the former loam pit were taken avoiding any contact with sunlight (Fig. 3.5). Sample HBT was taken at the top of the terrace sequence and HBM in the middle of the loam section. HBB came from the bottom of the loam sequence along this profile and sample HBS from a sandy layer (or lens) right below HBB and at the transition to the gravels.

The OSL ages of the two successfully dated samples HBT and HBS are 68.7 ± 4.0 and 80.5 ± 3.7 ka, respectively. Detailed results are presented in Table 3.4 and information about sample preparation and measurement procedure are found in Appendix A. These absolute age estimates place the deposit in the Early Würm and not in the Riss-Würm interglacial or Riss glacial as previously assumed (Winkler-Hermaden, 1955; Fink, 1961). Although the sample HBB had to be rejected due to its grain sizes below 4 µm, its position just above the HBS sample, a more sandy layer or lens at the transition to

the gravel base, it supports the idea that at least the transition of gravels and loams is of fluvial origin and this sample might represent a late stage of an alluvial sedimentation cycle. A continuous sedimentation process of the whole terrace sequence also suggests that the basal gravels belong to the Early Würm. They might indicate outwash from ice advances correlated with MIS 5b or 5d and therefore allows speculation about the existence of this Early Würm stadials which are not yet reported from the Eastern Alps (Ivy-Ochs et al., 2008). The two samples span the whole dust-loam sequence and yield an average rate of deposition of about 0.5 mm/a. This dating attempt can be seen as the first successful study that allows the terrace formation to be constrained by an absolute age estimate.

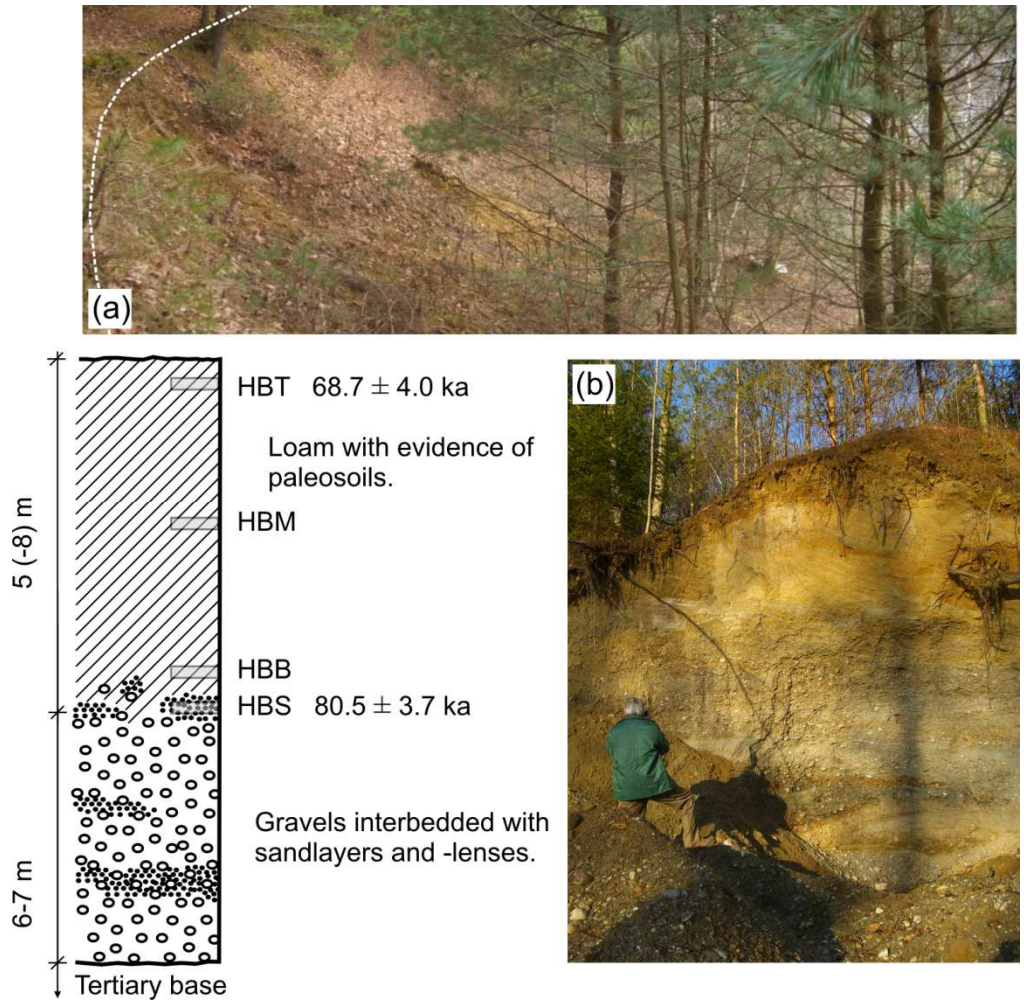

Fig. 3.5. The Helfbrunn terrace sampling location in a former loam pit, the type locality. A schematic profile (modified after Suette, 1986) indicating sampling points and the OSL age of the two dated samples HBT and HBS. HBM and HBB could not be dated, see Appendix. (a) View from the rim of the former loam pit (dashed white line) down the sampled profile. The base is about where the gravels are encountered. (b) An outcrop near the sampled profile, where gravels are exposed. Person for scale.

Sample name	Grain size (µm)	Water content (%)	Potassium (%)	Uranium (ppm)	Thorium (ppm)	Cosmic dose-rate (Gy/ka)	Total environmental dose-rate (Gy/ka)	n	Burial dose (D_b) (Gy)	OSL age (ka)
HBT	4-11	22.7 ± 5	1.68 ± 0.08	4.10 ± 0.21	13.10 ± 0.66	0.18 ± 0.02	3.53 ± 0.13	24	242.3 ± 10.9	68.7 ± 4.0
HBS	4-11	22.7 ± 5	1.78 ± 0.09	4.10 ± 0.21	12.60 ± 0.63	0.09 ± 0.01	3.48 ± 0.13	24	280.1 ± 6.9	80.5 ± 3.7

Table 3.4. Luminescence ages of the Helfbrunn samples. Luminescence analysis was undertaken using the single-aliquot regenerative-dose (SAR) protocol with a preheat of 260°C for 10 s, and a cutheat of 160°C for 0 s. Aliquots consisted of 1 mg of the 4-11 µm quartz fractions. 24 D_e values were derived for each sample, and the final burial dose for the sample was calculated using the central age model. The table includes details of dosimetry calculations showing grain size used in OSL analysis; average field water content of samples measured in the laboratory; potassium, uranium and thorium concentrations; the cosmic dose-rate; and the total effective dose-rate from the environment to quartz grains 4-11 µm in diameter taking into account the alpha efficiency factor; the number of aliquots measured (n); the burial dose; and the calculated age estimate. Sample HBM had to be discarded as scatter in the De values were inexplicable.

3.5 Absolute age correlations between Highland and Lowland

Various terraces and planation relics can be traced continuously from the Lowland into the Highland of Graz (Winkler-Hermaden, 1955). There is no sign of significant misalignment even at the (Alpine) orogen - (Pannonian) basin transition zone north of Graz (Fig. 3.6). A slight increase in the gradients of the individual levels along the Mur River from younger to older (higher up) levels is observed (Fig. 3.6 inset). This indicates the influence of an uplifting realm (e.g. Häuselmann et al., 2007a). However the signal is insignificant to account for high rates of uplift. Large vertical offsets between the Highland and the Lowland are negligible in the time frame covered by these geomorphic markers. This allows the use of relative chronology and relates higher levels to be of generally older age (e.g. Winkler-Hermaden, 1955, 1957). Furthermore, it allows to apply available absolute age data of individual sites for the whole level further up- or downstream along the Mur River course. Fig. 3.7 is the attempt to assemble all these observations and the current knowledge into a single schematic cross section.

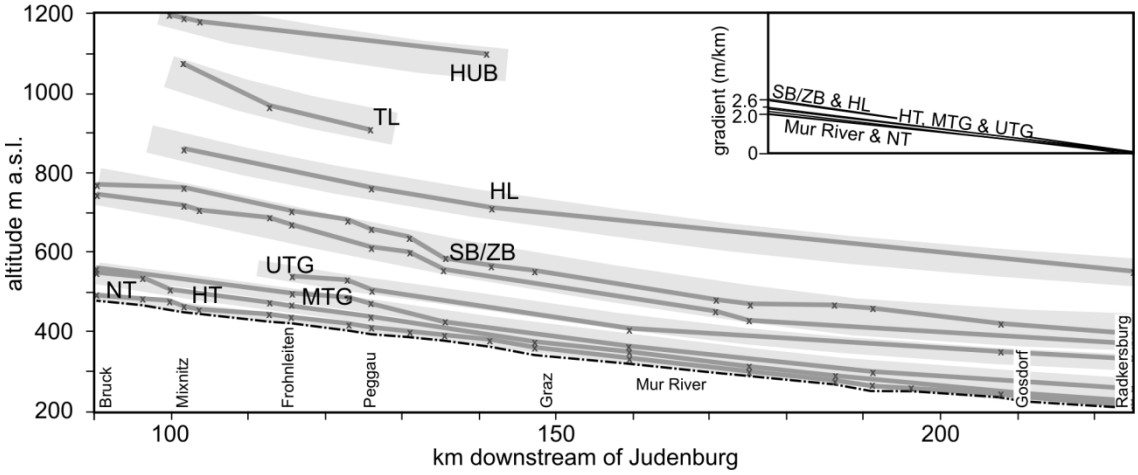

Fig. 3.6. Longitudinal channel profile of the Mur River and reconstruction of the longitudinal sections of the terrace and level spreads along the Mur River between Bruck and Radkersburg. The profile is measured downstream starting at Judenburg, where the LGM terminal moraines are found. Minor deviations from general trends are likely related to various degrees of denudation and not the result of vertical displacements. The inset shows the various gradients indicating increasing gradients with increasing age and/or elevation from ~2 m/km of the current Mur River and the NT to ~2.6 m/km of the SB/ZB and the HL.

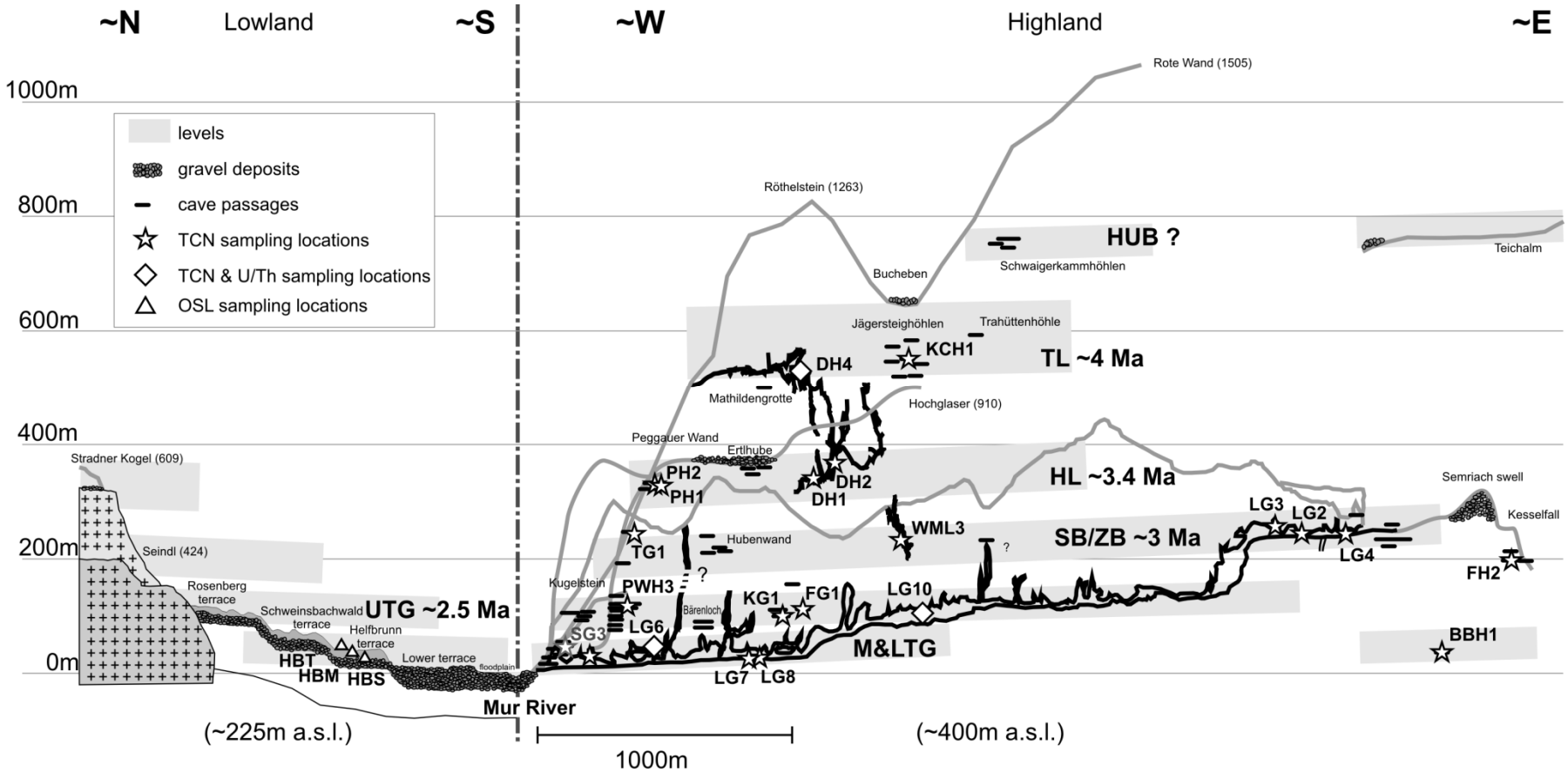

Fig. 3.8. Summary of relief evolution of the Styrian Block deduced from Neogene sediments, their age constraints and planation surfaces preserved in the landscape. Explanation of relief evolution from (a) to (m) see Section 6.

The minimum age constraint of cave level A suggests the TL to be older than about 4 Ma. This is not in contrast to a formation in Latest Pannonian (Winkler-Hermaden, 1955). The HL is suggested to be not younger than about 3.4 Ma; thus the relatively young K/Ar age of the Stradnerkogel basalt is questioned. The SB/ZB level is based on the age constraint of level C at least around 3 Ma, which is in agreement with K/Ar ages limiting it to be not older than ~3.8 Ma. It is supposed to be the last pre-glacial denudation plane. The UTG is suggested to be the first terrace related to climate deterioration at the beginning of the Pleistocene. The associated cave level D of about 2.5 Ma fits to this understanding as it places this level at the Plio-/Pleistocene boundary. This and the lower terraces are influenced by the episodic aggradation and re-excavation of sediment loads, of which some are preserved as stream terraces and shaped the characteristic landscape along the Mur River in the Styrian Basin. These terraces are more developed and / or better preserved in the Styrian Basin than in the Mur valley, especially where it is rather narrow (e.g. north of Peggau). The Schweinsbachwald terrace belongs to the MTG and is placed classically in the Mindel glaciations (~450 ka, MIS 12). This age range is supported by the aggradation event observed in the Lurgrotte dated by the samples LG6 and LG8, although no direct correlation of this event with a terrace in the valley is possible. Winkler-Hermaden (1955) suggested a Great Interglacial origin of this terrace level, based on the up to 17 m thick loams found along the Kaiserwald terrace (e.g. Flügel, 1960) at the southwestern edge of the Graz Basin (equivalent to the Schweinsbachwald terrace). His conclusions were based on the fact that the loams are carbonate free, seen as indication for a warmer climate were decarbonatisation occurred. Terraces that are attributed to the Riss glacial and are loam-free gravel accumulations (high terrace gravels) are rare in the study area. Around the town of Frohnleiten (Fig. 3.3a), gravels situated above the NT are related to the Riss. Some remnants were also documented by Winkler-Hermaden (1955) in the Graz Basin, e.g. in a loam pit of St. Peter which is not accessible anymore. However, in the predominant cases the terraces above the NT are gravels covered by thick loams. The lowest of the loam covered terraces is the Helfbrunn terrace. The above reported OSL age constraints of this terrace suggest an Early Würm origin. This actually makes it somewhat younger than previously assumed and contradicts its glacial development.

The age of deposition of the Helfbrunn terrace coincides with the time of speleothem formation in the Tanneben massif (Section 4.1.1). This indicates that the loamy upper section of the Helfbrunn terrace cannot be a glacial deposit and instead actually supports the idea of Winkler-Hermaden (1955) that this deposit is of an interglacial (or interstadial) origin. However, the formation conditions of the gravel base of this terrace are more speculative as no absolute age of this section is available. A continuous sedimentation process of gravel base and loam top suggests the gravels were deposited right before deposition of the loam base (≥80 ka). If the concept of glacial origin of these gravels from the headwaters of the Mur River catchment is favoured (because of their decomposed state), a possible correlation to ice advance during MIS 5d is

tempting. Major glaciations during MIS 5d and 4 are known from the Swiss Alps (e.g. Preusser et al., 2003), but the evidence in the Eastern Alps is still missing and/or was obliterated during subsequent more extensive Late Würm (MIS 2) advances. At the moment, we can only speculate that these gravels could be the result of Early Würm glaciations. Although tentative, it would explain the diverse interpretation of the Helfbrunn terrace as being either of glacial or interglacial origin (e.g. Suette, 1986). An alternative scenario is to interpret this terrace as a fining upward fluvial deposit with alluvial clay and the occasional soil developed on top.

To conclude, even though OSL dating was performed directly on a stream terrace, the supplementary use of U/Th ages from caves nearby allowed the evidence for temperate conditions during formation of the Helfbrunn terrace to be strengthened. It is suggested that the terrace should be placed in the Early Würm, instead of its previously assumed Riss glacial or Riss-Würm interglacial age and the gravel cover should not simply be termed a loess deposit.

3.6 The bigger picture: relief evolution of the Styrian Block

The elevation, age of the various levels discussed above and their correlation between Highland and Lowland, allow to propose a relief evolution of the Styrian Block. The individual stages of relief development are described in the following: The onset of lateral extrusion east of the Tauern Window in the Ottnangian (~18 Ma) is related to the formation of conjugate strike-slip fault zones: the Mur-Mürz and the Lavanttal fault zones. Intramontane pull-apart basins were filled and the onset of sedimentation in the Styrian Basin also occurred at this time (e.g. Ebner and Sachsenhofer, 1995). Lateral extrusion is mechanically only feasible if collision is aided by slab pull from the Carpathian subduction zone and the existence of conjugate strike-slip faults in the Eastern Alps (Selverstone, 2005; Robl et al., 2008c). Thus, not necessarily much relief and topography development prior to this time is documented (Fig. 3.8 stage (a)).

Shallow marine sediments deposited in the Styrian Basin are related to marine ingressions in Badenian times (Fig. 3.8 stage (b); ~16-13 Ma). This allows to place the elevation of the basin just below sea level. The Noric depression (a term used to summarize all basins along the Mur-Mürz fault system) does not indicate a marine setting, but the evolution of the Fohnsdorf-Seckau Basin (east of Judenburg, Fig. 3.1a) with a brackish influx in relation to the Lavanttal Basin known for Lower Badenian marine sediments suggests only moderate altitudes at these times (Strauss et al., 2001). In Sarmatian and Early Pannonian times (Fig. 3.8 stage (c); ~12 Ma), increasingly brackish conditions are established within the Styrian Basin, related to the constriction of the Lake Pannon (Sacchi and Horvath, 2002; Harzhauser et al., 2004). However, there is still evidence of marine conditions in the Sarmatian related to sea level rises

(Rollsdorf and Gleisdorf Formations; Piller and Harzhauser, 2005). This is evidence for the region to be still lowland. In the intramontane basins sediments of this time are not preserved anymore (Ebner and Sachsenhofer, 1995).

In Pannonian times (Fig. 3.8 stage (d); ~9 Ma) the Styrian Block, especially the Styrian Basin is affected by fluviatile-limnic to terrestrial deposition (e.g. Gross et al., 2007). Quartzous pebbles are peculiar. Their origin (source) is questionable, although the crystalline frame of the Highland and Lowland of Graz is a likely source region (Skala, 1967; Maurin and Benischke, 1992). Again, no such sediments are preserved in the intramontane basins along the Mur-Mürz Fault. Interestingly, the Augenstein sedimentation preserved on top of the Dachstein paleosurfaces and further deposited in the Molasse basin of the Northern Foreland (Frisch et al., 2001) is related to a north-directed transport. Although this sedimentation is as old as 30 Ma and stopped at the onset of lateral extrusion, it still poses the question where these quartz rich pebbles really come from. Ebner and Sachsenhofer (1995) suggested uplift based on subsidence analysis of the Styrian Basin and in Chapter 1 we extended this to the Highland of Graz. Chapter 2 provides reasonable constraint that the Styrian Basin and its surrounding basement behave as a coherent block, the Styrian Block. It can therefore be assumed that during the Latest Pannonian (~5-6 Ma) the region was uplifting. Genser et al. (2007) observed the onset of uplift of the Austrian Molasse at about the same time.

Up to this point sediments are deposited on top of each other in simple stratigraphic order. However, preserved sediments of Ottnangian to Sarmatian/Pannonian times are currently found at varying elevations (Fig. 3.8 stage (e)). Karpatian/Badenian sediments of the Passail Basin are found at ~650 m a.s.l. (Ebner and Gräf, 1982) and Sarmatian sediments found in the Gratkorn Basin (~20 km SW) at currently ~425 m a.s.l. (Gross et al., 2007). This suggests fragmentation of the whole region after deposition although the actual timing of fragmentation is poorly constrained (e.g. Winkler-Hermaden, 1955). In Middle to Late Miocene times a final rather strong subsidence is followed by beginning uplift in the Lowland (Ebner and Sachsenhofer, 1995) and the likely onset of uplift in the Highland (Chapter 1). If the deposition of Pannonian gravels from north happened prior to or after the fragmentation of the whole region is unclear. Ebner and Sachsenhofer (1995) reported fault-controlled subsidence during late Sarmatian times, which might have already caused the fragmentation prior to uplift. This is hard to differentiate because of the only partial preservation of Sarmatian and especially Pannonian sediments. This fact is expressed in Fig. 3.8 by combining stages (d) and (e).

The phase of fragmentation seems to have ceased, giving way to a more continuously uplifting realm as denudation planes started to evolve (Fig. 3.8 stage (f) to (m)). Important here is that denudation planes, planation surfaces and preserved gravel accumulations as well as stream terraces found in the High- as well as in the Lowland are of decreasing elevation with decreasing age, which clearly indicates denudation and

incision related to an uplifting Styrian Block. The actual formation of the today's Mur River course has likely been initiated by the uplift of the region. Headward migration and final stream piracy of the Mur-Mürz catchment has to be placed in the Latest Miocene (Dunkl et al., 2005; Chapter 1).

The HUB level (Fig. 3.8 stage (g)) is only locally conserved in the Highland and absent in the Lowland. However, it is apparent in the Hochlantsch region (Teichalm, Fig. 3.3a) and shows clear signs of karstification (e.g. Schwaigerkammhöhlen, Fig. 3.7), making this the highest level considered to be of significance. The TL (Fig. 3.8 stage (h)) is already preserved to a better extent, although no occurrences in the Styrian Basin are known. Nevertheless, this level is at least 4 Ma old as could be deduced from cave sediments preserved at this level (Chapter 1). The HL (Fig. 3.8 stage (i)) dated to be around 3.4 to 4 Ma and found today at about 325 to 450 m above the Mur River, is the first pronounced denudation plane clearly preserved in the whole region including the Lowland. A continuous level with a slightly increased gradient compared to the current Mur River gradient is observed. This might be the simple result of ongoing uplift in the region. The widespread extent of this level including the Highland and the Lowland of the Styrian Block provides an important constraint on the coherent behavior of the Styrian Block at subsequent times. The double plain system of the SB/ZB level (Fig. 3.8 stage (j)) is suggested to be the last denudation plane prior to the onset of climate deterioration (Winkler-Hermaden, 1955) and could be constrained to be around 3 Ma old. The levels extent is similar to that of the HL, due to its preservation on the young volcanic rocks in the Styrian Basin.

The upper terrace group (UTG) marks a shift in the landscape evolution as uplift and incision rates appear to slow (Fig. 3.8 stage (k)). Based on sediment burial ages of this level, it can be placed right at the Plio-/Pleistocene boundary (~2.5 Ma). The onset of climate deterioration is suggested to be responsible for the strong increase in sediment discharge rates (e.g. Champagnac et al., 2009) reported by Kuhlemann et al. (2001, 2002). However, as shown in Chapter 1, we only observed a decrease of incision rates of the Mur River due to ample sediment supply from the headwaters of the Mur River catchment without a clear sign of its relation to glaciations. The amount of sediments that have to be re-excavated or eroded from the intramontane basins and the Styrian Basin are likely to be considerable, if the former sediment cover of a few hundred meters reconstructed by Sachsenhofer et al. (1997) are taken into account. The MTG (Fig. 3.8 stage (l)) is not well constrained in time by our data, but has to be placed somewhere between ~2.5 Ma (UTG, level D) and ~0.1 Ma (LTG), a rather long time range. However, the MTG as well as the UTG are not single terraces but a potpourri of various terraces hard to be distinguished from each other, suggesting various stages (and times) of deposition. The LTG (Fig. 3.8 stage (m)) is further sub-divided into the NT (low terrace gravels) and HT (high terrace gravels). The NT is related to MIS 2 and the

Late Würm glaciations, respectively. The HT has to be placed, according to our OSL ages of the Helfbrunn terrace, into the Early Würm related to MIS 5 (a-d?).

In general, in the Pliocene and especially Pleistocene (Fig. 3.8, stages (g)-(m)), considerable erosion and re-excavation of Miocene sediments from intramontane basins, the Styrian Basin and the surrounding basement is suggested based on observed sedimentation hiatuses (Piller et al., 2004) and the preservation of planation surfaces of this time. The last about 2.5 Ma (stages (k)-(m)) indicate increasingly erosive times. This is on the one hand supported by the observed decrease in incision rates of the Mur River at this time attributed to increased sediment load from the headwaters of the Mur River (Chapter 1). On the other hand, if erosion would have happened earlier, tributaries in the non-glaciated parts of the Mur River catchment should have reached equilibrium in the meantime. According to Robl et al. (2008a), this is not the case. Moreover, sediment budget data of the Eastern Alps (e.g. Kuhlemann, 2007) shows the same trend. All this evidence suggests that erosion and re-excavation is still adjusting to ongoing tectonic uplift of the whole region and geomorphic steady state is not yet reached (Appendix A).

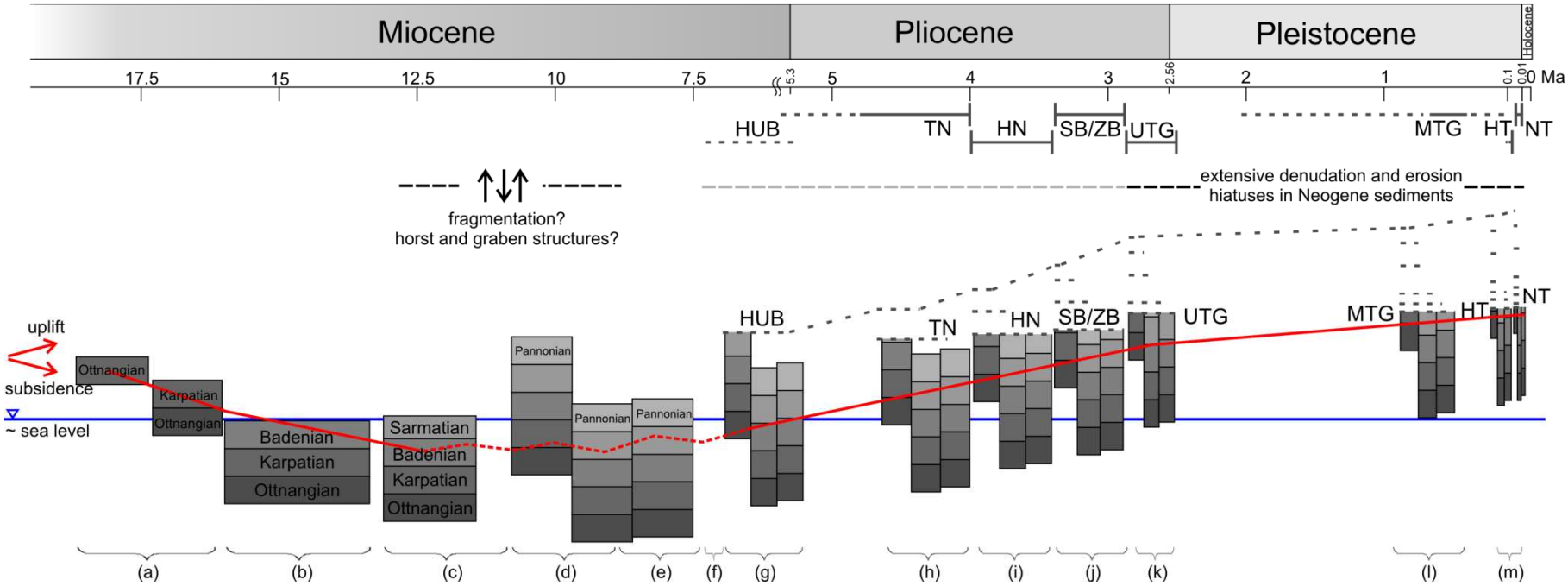

Fig. 3.7. Schematic projected profile of the Highland and Lowland of Graz. Elevations above the Mur River, modified and adapted from Chapter 1. The OSL sample locations are indicated by white triangles and dated TCN cave sediments by white stars. Sample locations where TCN and U/Th ages were measured are represented by white squares. Sample SG3, which is the only sample from the western river side has been shifted to the other river side for the sake of completeness.

3.7 The behavior of the Styrian Block - tectonic and climatic imprint

At the orogen margin of the Eastern Alps, degradational and aggradational settings are closely spaced and are known to have changed in time (e.g. Augenstein sedimentation: Frisch et al., 2001; post-Middle Miocene maximum sediment extent: Dunkl and Frisch, 2002). It is evident that within the last million years climatic changes happened (global Cenozoic cooling trend), but it is even more evident that plate convergence (tectonic processes) have led to the formation of the European Alps and that these processes have not stopped so far (e.g. Appendix A). The current cease in convergence in the Western Alps due to the present position of the Euler pole might be a transitory setting. However, convergence is evident in the eastern parts of the Alps. The Adriatic plate is still pushing northward accompanied by counterclockwise rotation. It is also confirmed that the subduction roll back in the Carpathians ceased and that the Pannonian Basin is inverting since ~5 Ma (Ruszkiczay-Rüdiger, 2007). Moreover, the possible influence of the Pannonian fragment that was proposed by Brückl et al. (2010) is worth mentioning. Underthrusting of this fragment by the European and the Adriatic plate might have caused a spatially broad uplift of the region (Chapter 2).

Pleistocene isostatic rebound in the foreland basins is well described in the Northern Alpine Foreland Basin (Genser et al., 2007). The Po basin shows similar features where the youngest marine sediments are presently above sea level if corrections for the loading of the overlying sediments are made (Scardia et al., 2006). The Styrian Basin provides similar clues: marine sediments (~12 Ma old) are well above sea level (>300 m a.s.l.) and subsidence analysis indicates uplift around 5-6 Ma (Ebner and Sachsenhofer, 1995). A slight tilting of the Neogene basin fill within the Styrian Basin away from the orogen (here towards SE; Winkler-Hermaden, 1957) is similar to observations made in the foreland basin of France (Champagnac et al., 2007). However isostatic rebound is not thought to be the primary mechanism here. The actual inversion of the Pannonian Basin is repeatedly used to account for stress changes in the region (e.g. Ebner and Sachsenhofer, 1995). However, ongoing lateral extrusion (based on GPS data by Bus et al., 2009) and no signs of fault reactivation or reverse faults (Chapter 2) suggests that uplift has to be explained by deep-seated mantle processes.

The period of time investigated by our data (last about 4-5 Ma) seems to be characterized by episodic, but spatially broad processes of uplift. Sediments were transported from the headwaters of the Mur River into the basin (and beyond). This is indicated by missing sedimentary sequences within the Noric depression and parts of the Styrian Basin. This necessitates substantial erosion later in time, however not necessarily a direct influence of climate changes: Mean erosion rates (modern area-weighted mean denudation rates) of 0.125 mm/y for the Eastern Alps in the Holocene from a compilation of Hinderer (2001) is of similar dimension as the ~0.1 mm/y incision rates inferred over the last ~4 Ma in Chapter 1. Palynological records do not

show strong evidence for abrupt climatic changes that correlates with the sediment-yield data ~5.5 Ma ago (Willet, 2010 and references therein). Northern Hemisphere glaciations set in ~2.5 Ma ago (Raymo, 1994), although major glacial erosion in the Alps is reported to have started ~1.8 Ma later (Muttoni et al., 2003; Häuselmann et al., 2007b).

A change in the whole erosional setting of our study area around 2.5 Ma becomes apparent by the change of predominantly preserved denudation plains prior to ~2.5 Ma to primarily stream terraces afterwards and a mean decrease in bedrock incision rates. This has already been attributed to an abundance of sediment transported from the headwaters through the Mur valley (Chapter 1). Furthermore, the OSL ages and morphological observations suggest that not necessarily the four terrace levels prominent in the Styrian Basin need to correlate to the four glacial maxima of Günz, Mindel, Riss and Würm. Direct evidence of Pleistocene glaciations is currently only proven for the last glacial (Würm) terrace (Van Husen, 1997 and references therein). The OSL age of the Helfbrunn terrace (80.5 ± 3.7 to 68.7 ± 4 ka) and contemporaneous speleothem deposition in nearby caves indicates ice-free, soil-covered conditions. No direct indication for glacial origin could be related to the gravel base of the Helfbrunn terrace. Possible outwash material from glaciations in the headwaters of the Mur catchment is a potential source, but not necessarily its final deposition has happened during glacial times. As such the correlation of this terrace (and possible older ones as well) to glaciations in the Alpine region is questioned hereby. Sediments might be the simple product of erosion adjusting to ongoing uplift of the realm and remains as an alternative explanation. The hiatuses of sediments from the intramontane basins and the Styrian Basin are indications for re-excavation of these sediments, possibly related to the decrease in incision rates observed in the Mur valley (Chapter 1).

All the aforementioned evidences for the apparent ongoing uplift pose the question what actually causes this uplift. In Chapter 2, we correlate this to the Pannonian fragment that is underthrust by the European and the Adriatic plates (Brückl et al., 2010). Delamination and/or convective removal of overthickened lithosphere are other possible explanations (Houseman and England, 1981; Genser et al., 2007). An alternative to these ideas is the approach of Appendix A, supposing that the whole topography of the Alps developed just around 5-6 Ma on top of a former relatively low mountain range. As the uplift signal is spatially broad, it becomes likely that some sort of deep-seated change in the geodynamic setting might have occurred at this time. The significance of Adria push (Bada et al., 2007) from the south as a key mechanism for the ongoing uplift is emphasized here. A single uplift pulse around 5-6 Ma is unlikely, because this would have resulted in a decay of topography in the meantime and a cease in the sediment load would have to be observed. Quite the contrary is the case in the Eastern Alps, where an increase around the Plio-/Pleistocene boundary is observed (Kuhlemann et al., 2001). As was already emphasized in Chapter 1, a detailed trend of the uplift signal of the last

4-5 Ma is hard to deduce, as stream piracy events and changing sediment loads are superimposed.

3.8 Conclusions

We constrain the vertical motions of a tectonically important region at the eastern end of the Alps: the Styrian Block, for the last 4-5 my. The area is located outside the region covered by ice during glaciation periods and includes parts of the Alpine basement east of the Lavanttal Fault and south of the Mur-Mürz Fault and parts of the westernmost Pannonian Basin, the Styrian Basin.

Cosmogenic nuclide burial ages of cave sediments show that a cave level ~500-600 m above the current base level formed about 4 my ago. This cave level is correlated with planation surfaces of the so-called Trahütten level (TL), which is preserved in the Highland of Graz. The prominent Hochstraden level (HL, ~325-450 m above base level) could be constrained to have formed between 3.4 and 4 Ma by the same method. The level is pronounced in both, the Styrian Basin and the Highland of Graz. Importantly, it is preserved along different lithologies and across prominent previously active faults. The so-called Stadelberg/Zahrerberg level (SB/ZB, ~180-300 m above base level) could be confirmed to be the last pre-glacial denudation plain with an age of ~3 Ma. In the Styrian Basin, the Upper Terrace Group (UTG) marks the onset of repeated aggradation in the Pleistocene by preserved stream terraces. The corresponding cave level indicates a time of formation around 2.5 Ma. The Middle Terrace Group (MTG) remains loosely constrained. The Lower Terrace Group (LTG) is divided into high terrace gravels (HT) and low terrace gravels (NT). The later has been shown to be of Late Würmian origin. The upper part of the HT in the Styrian Basin, the so-called Helfbrunn terrace could be constrained by luminescence dating to be only about 80-70 ka old. Speleothem formation in various levels of caves in the Highland of Graz show a similar timing based on U/Th ages. This contemporaneous deposition confirms a warm period during formation correlated to the MIS 5a and thus the Helfbrunn terrace not necessarily correlates with glacial advances in the Alpine region.

Incision rates of the Mur River show a decrease around the Plio-/Pleistocene boundary, suggested to be the consequence of increased sediment load from the hinterland. Observed hiatuses in the sediment record of the Noric depression and the Styrian Basin in connection with observed geomorphic disequilibrium of the region imply erosion adjusting to ongoing tectonic activity over Pliocene times. As such, a possible alternative explanation to the commonly blamed response to climate change for repeated aggradation in the Pleistocene is simple erosion, redistribution and re-excavation of Neogene sediments during this period of time up to the present as a consequence of uplift.

Correlation of various planation surfaces, cave levels and stream terraces indicate that the Styrian Block coherently uplifted some 600 m over the last 4-5 my. Our interpretation implies that the observed fragmentation of the block must have occurred prior to this time in the Miocene, thus allowing the preservation of these planar geomorphic markers at distinctive levels.

Acknowledgements Luminescence dating was carried out using the facilities at the University of Innsbruck, Austria. Sincere thanks to Ch. Spötl for hospitality. We greatly acknowledge J. Hellstrom for performing the U/Th dating. M. Gross is thanked for discussing paleontologic aspects of the Miocene evolution. S. Niederl is thanked for permission to collect samples in the former loam pit of Helfbrunn. This research was funded by the "Kooperationsprojekt Erdwissenschaften NAWI Graz (§ 141)" and the ESF project I-152.

3.9 Appendix - OSL sample preparation and measurement procedure

The OSL dating method combines a laboratory-derived estimation of radiation dose that sediment grains have received during the most recent period of burial with the local environmental dose-rate. In fact, although different from the TCN burial age method, the actual result is of similar scope. By measuring the OSL signal from the natural dose (i.e. that received during burial) and OSL signals from a series of laboratory irradiations of known dose (used to calibrate the OSL signal from the natural dose), the amount of radiation that grains have received during burial can be determined, this is termed the equivalent dose (D_e). The radiation flux at a sampling location is termed the environmental dose-rate which has been estimated by laboratory measurements. Calculation of dose rates were done using conversion factors of Adamiec and Aitken (1998), the use of ADELE software (Kulig, 2005) and an alpha effectiveness value for quartz of 0.03 ± 0.01 (Mauz et al., 2006). The actual age of a sample (i.e. the time of burial since last exposure to sunlight) is simply the burial dose (in Gy) divided by the environmental dose-rate (in Gy/ka).

The sample HBB turned out to be of very fine clay-sized particles not suitable for separation of a 4-11 µm fraction and thus had to be discarded. The three samples HBT, HBM and HBS were processed in the OSL laboratory at the University of Innsbruck under dim red-light conditions. Sub-samples were removed for analysis of the radionuclide content (performed commercially by ICP-MS at "Activation Laboratories Ltd.") and water content measurements (an average value of the samples was used in environmental dose-rate calculations). The remaining sample material was pretreated with 10% v.v. dilution of hydrochloric acid followed by 20 volumes hydrogen peroxide to remove carbonates and organic matter prior to dry sieving following standard techniques described in Wintle (1997). The 4-11 µm fraction was further treated with

32% hexaflourosilicic acid (1:40 solid:liquid ratio) for 7 days. Aliquots contained 1 mg of material that was pipetted onto aluminium discs of 9.7 mm diameter by settling through acetone.

Single aliquot OSL measurements were carried out using an automated Risø TL/OSL reader with optical stimulation from blue light emitting diodes (LEDs) with peak emission at 470 nm and IR diodes emitting at 830 Δ10 nm. The OSL signal was measured with an EMI 9635Q photomultiplier tube through 7.5 mm thickness of Hoya U340 filter. Beta irradiation was performed using a calibrated 40 mCi $^{90}Sr/^{90}Y$ source.

Luminescence analysis was undertaken using the single-aliquot regenerative-dose (SAR) (Murray and Roberts, 1998; Murray and Wintle, 2000) protocol with a preheat of 260°C for 10 s, and a cutheat of 160°C for 0 s. 24 D_e values were derived for HBS and HBT. The final burial dose for the samples was calculated from the dataset of D_e values using the Central Age Model (Galbraith et al., 1999). HBM had to be discarded due to inexplicable scatter in the D_e values; from a luminescence point of view the data had to be discarded as no methodical explanation was able to resolve this.

CHAPTER 4

OVERALL CONCLUSIONS

This Chapter gives a brief overall conclusion of this thesis. As each of the previous chapters and appendix A have their individual conclusions, I will give here an overall picture.

The topographic evolution of the Styrian Block has been constrained in some detail in post-Miocene to present time. Geochronological methods were applied to date the time of deposition of cave sediments, fault fillings, terrace sediments and speleothems. Geomorphological observations are combined with these absolute age constraints.

The Styrian Block is especially suited for a geomorphological study, as it remained ice-free over the Pleistocene, allowing to exclude glacial carving as a landforming process. The landscape along the River Mur is the main focus of this study. Numerous distinctive levels, characterized by planation surfaces, stream terraces and cave levels are preserved. A correlation of individual levels observed in the Styrian Basin and the Highland of Graz is feasible.

This Styrian Block is delineated by the Mur-Mürz Fault System in the north, the Pöls-Lavanttal Fault System in the west and the Periadriatic Fault System in the south. The block includes both the eastern most part of the Alps and the westernmost part of the Pannonian Basin. Based on structural and geomorphologic evidence, the Styrian Basin and its surrounding basement have been identified to behave as a kinematically coherent block over Pliocene and Pleistocene times. Currently, the block is seismically inactive. The general stress field is W-E extensional within this block as no reverse faults could be encountered in the region. This is supported by the first absolute age constraints of fault activity by the TCN burial age method. A fault filling gave a burial age of 1.56 ± 1.11 Ma. This age constraint places fault activity in post Miocene time. Hereby, basin inversion as a mechanism for explaining the observed uplift in the Styrian Basin is questioned.

The first successful burial age dating of cave sediments using the cosmogenic isotope pair ^{26}Al and ^{10}Be has been made in the Eastern Alps. It is shown that karstification in the Central Styrian Karst, which belongs to the Paleozoic of Graz, commenced about 5

Ma ago. The burial ages of the cave sediments place minimum age constraints on cave formation and maximum age constraints on rates of river incision. The river Mur incised some 500 m in the last ~4 my resulting in a mean incision rate of about ~125 m/my. A very complex incision history is apparent. A more detailed analysis allows to observe higher rates before ~2.5 Ma and a decrease in river incision rates beginning at ~2.5 Ma. The higher rates of ~250 m/my observed between ~4 and ~2.5 Ma are possibly influenced by a stream capture event where a headward migrating paleo-Mur River increased its drainage area by catching the Mur-Mürz area that previously drained elsewhere. The actual timing of this stream piracy event, although not constrained in detail, is placed in the Late Miocene. The decrease in incision to rates of ~40 m/my for the last ~2.5 Ma is related to an increase in sediment load transported in the river bed derived from upstream sections of the Mur River. This led to a transport-limited state of the river and in the mean, to a decrease in bedrock incision. Pre-burial erosion rates derived from the cave sediments are about constant over the whole time period, suggesting that incision is not triggered primarily by climatic changes.

An absolute age of a terrace level in the Styrian Basin could be constrained by optically stimulated luminescence dating. These results place the Helfbrunn terrace into the Early Würm. This time constraint in combination with speleothem formation in nearby caves based on U/Th age estimates allow to deduce temperate warm climate conditions at the time of deposition of the Helfbrunn terrace. Thus, the terrace not necessarily correlates with glacial advances in the Alpine region. Redistribution of Neogene sediments is proposed as an alternative source of the terrace deposits.

All these absolute time controls allow to place age estimates for individual levels. The information of all these geomorphic markers is further used to deduce the relief evolution of the Styrian Block in more detail over the last ~5 Ma. In addition, this is linked to the existing knowledge of relief evolution since the onset of Neogene sedimentation in the Styrian Block ~18 Ma ago. In particular, the Trahütten level preserved at ~500-600 m above the current base level has formed about 4 Ma ago. Currently at about 325-450 m above the base level, the prominent Hochstraden level is constrained to have formed between 3.4 Ma and 4 Ma. The Stadelberg/Zahrerberg level preserved at ~180-300 m above base level is confirmed to be ~3 Ma old. The Upper Terrace Group formed ~2.5 Ma ago and marks the onset of repeated aggradation in the region. The Middle Terrace Group remains poorly constrained. The high terrace gravels as part of the Lower Terrace Group are shown to be of Early Würmian origin. The low terrace gravels deposited in Late Würmian times.

All these levels developing over the last ~4 Ma are the manifestation of the coherent Styrian Block experiencing periodic uplift of some 600 m over the last 4-5 Ma, starting at low elevations, thereby rejuvenating the landscape. In addition, these preserved levels

imply that the observed fragmentation of the block must have occurred prior to this time in the Miocene.

Observed hiatuses in the sediment record of the Noric depression and the Styrian Basin in connection with observed geomorphic disequilibrium of the region, imply erosion adjusting to ongoing uplift. The decrease in incision rates of the Mur River over the last ~2.5 Ma and the interpreted cause of increased sediment load in the river bed is related to this: Redistribution and re-excavation of Neogene sediments during this period of time up to the present might be the simple consequence of uplift of the Styrian Block.

Analyzing the topography of the whole Alps in combination with a simple model of uplift and erosion allows to estimate the state of geomorphic disequilibrium of the Alpine topography. There is strong evidence that the Alps are still in their infancy and only ~40% of the time towards geomorphic equilibrium has passed. Using available sediment budget data in comparison to the results of the simple model allow to conclude that a substantial part of the formation of the present topography began only 5-6 million years ago. It is suggested that Miocene topography might have been much lower and/or more dissected than the present topography. Importantly, no clear difference between the topographic evolution of the Eastern and the Western Alps is observed. The impact of glaciations seems to be of minor importance and further supports the findings for the Styrian Block listed above.

The cause of the uplift has to remain unanswered. However, basin inversion as observed in the Pannonian Basin system further east, is implausible. Thinning of the mantle part of the lithosphere is an alternative. The Pannonian fragment observed only recently by geophysical experiments might play an important role in explaining the uplift. European and Adriatic plate underthrusting this Pannonian fragment are likely to influence the vertical motion of the Styrian Block. Adria push persists as a major driver for the complex vertical motions of the Alpine – Pannonian region. A multiplate interference system highlights the complex interplay of plate motion and its consequences to topography and landforming processes.

APPENDICES

APPENDIX A

AGE AND PREMATURITY OF THE ALPS DERIVED FROM TOPOGRAPHY

Abstract The European Alps are one of the best studied mountain ranges on Earth, but yet the age of their topography is almost unknown. Even their relative stage of evolution is unclear: Are the Alps still growing, in a steady state or already decaying, and is there a significant difference between Western and Eastern Alps? Using a new geomorphic parameter we analyze the topography of the Alps and provide one of the first quantitative constraints demonstrating that the range is still in its infancy: In contrast to several other mountain ranges, the Alps have still more than half of their evolution to a geomorphic steady state to go. Combining our results with sediment budget data from the surrounding basins we infer that the formation of the present topography began only 5-6 million years ago. Our results question the apparent consensus that the topographic evolution is distributed over much of the Miocene and might give new impulses to the reconstruction of paleoclimate in Central Europe.

Keywords: *Alps; topography; erosion; slope; denudation*

Hergarten, S., et al., Age and Prematurity of the Alps Derived from Topography, Earth Planet. Sci. Lett. 297, 453-460, doi:10.1016/j.epsl.2010.06.048

A.1 Introduction

Geologically, the European Alps are among the best studied mountain ranges on Earth. Curiously, one of the least understood aspects of the range is the very age of its topography. While the structural frame of the present topography evolved in early to middle Miocene (Frisch et al., 1998), even the huge amount of available data seems not to be sufficient for deciphering the history of the Alpine topography. Even their stage of maturity seems to be unclear: Are the Alps still growing, in a steady state or already decaying?

Low-temperature geochronological data – both from detrital record (Dunkl and Frisch, 2002) and from crystalline basement (Vernon et al., 2006, 2008; Luth and Willingshofer, 2008) – constitute a large part of the available data. From these data, mean exhumation rates can be derived, documenting considerable erosion during the Miocene. Sediment budgets from the sedimentary basins around the Alps (Kuhlemann et al., 2001) point towards the same direction, but beyond this, they indicate a sudden rise of sediment supply some five million years ago which has not been explained yet. Even more important, the relationship of exhumation to topography development is in general questionable (Stüwe and Barr, 1998). Topographic change reflects the difference between rock uplift and denudation, and both can hardly be measured on the same time scale.

Erosion history carries some more puzzles such as the Augenstein surfaces on the karst plateaus of the Eastern Alps (Frisch et al., 2001). These and other paleosurfaces from the Eocene indicate very low erosion rates locally (Hejl, 1997).

Drainage patterns also play an important part in the evolution of mountain belts (e.g, Schlunegger and Hinderer, 2001; Robl et al., 2008a,b). However, although they often reveal information on relative base level lowering, they seem not to be suitable for deriving the history of topography.

Several studies based on fossil records provide direct evidence for a high and locally steep relief in and even before the Miocene (e.g., Kocsis et al., 2007). However, we should keep in mind that these results are always local and limited to a few points on the time axis, so that they may only put some constraints on the history of topography. Furthermore, these data are associated with a considerable uncertainty on a quantitative level as demonstrated by Hay et al. (2002).

In sum, the age of formation of the Alpine mountain range remains poorly understood. Even for the present day regime there is only a sketchy understanding about the current uplift and erosion rates: Geodetic measurements of uplift rates were published for the Central Alps (Kahle, 1997) and for the Eastern Alps (Ruess and Höggerl, 2002), and

some measurements of Holocene erosion rates exist (von Blanckenburg et al., 2007; Wittmann et al., 2007; Norton et al., 2010b), but the present day relationship of uplift and erosion or their drivers remains speculative. For the Western Central Alps a pattern arises that suggests that much of the present day uplift is due to isostatic rebound and that the tectonically driven uplift has terminated (Barletta et al., 2006; Champagnac et al., 2007). This is supported by first data that appear to indicate that there is a direct correlation of erosion rate with elevation and with uplift rate (Wittmann et al., 2007; Champagnac et al., 2009). However such information is still in its infancy and usually confined to small areas studied in much detail.

A.2 The Peculiar Topography of the Alps

River profiles become steeper with increasing elevation and slopes show the same tendency in the mean. The straightforward explanation of this phenomenon hinges on the concept of geomorphic equilibrium: Under temporally constant conditions, the land surface evolves towards a steady state where erosion balances rock uplift. As fluvial erosion increases with both slope and catchment size, the smaller catchment sizes found at high elevations must be compensated by steeper slopes in case of spatially uniform rock uplift (Whipple and Tucker, 1999; Wobus et al., 2006). So an increase of slopes with elevation should be expected. If the influence of the catchment size can be eliminated, slopes reveal information on recent erosion rates and, in case of equilibrium, on uplift rates.

This idea is not limited to the case of homogeneous uplift. In mountain belts, rock uplift is in fact often inhomogeneously distributed and tends to increase from the margins toward the crest. Thus, high elevations are often a result of high rock uplift rates and therefore erosion rates should increase with elevation too. For the Alps, this is directly confirmed by measurements of recent uplift rates (e.g., Kahle, 1997) and estimates of erosion rates from cosmogenic nuclei (e.g., Wittmann et al., 2007). Therefore, both decreasing catchment sizes and heterogeneous uplift should lead to a rather strong increase of slopes with elevation. As stated above, deriving erosion rates from slopes requires the elimination of the effect of different catchment sizes. In the so called stream power approach (Whipple and Tucker, 1999; Wobus et al., 2006), this is done by assuming a power-law dependence of the erosion rate on the catchment size. However, as there is still uncertainty about the exponent, we try another approach that avoids the comparison of catchments of different sizes: We compare slopes at different elevations over the entire mountain range, but use only slopes of points in the digital elevation model (DEM) that have approximately the same catchment size. In the following, $\overline{S}_A$ denotes the average slope of all surface points with catchment size close to A. As long as the considered area contains a sufficient amount of points with catchment size A, $\overline{S}_A$ provides a reasonable proxy for the recent erosion rate. In the following we apply this

idea to the topography of the Alps using the freely available SRTM3 DEM. Regions without runoff were filled in order to get consistent catchment sizes, but all points where the elevation had to be increased were excluded from the analysis since filling affects the slopes. For our purpose we define the study area as the connected region of the Alps above 600 m elevation as shown in Fig. A.1.

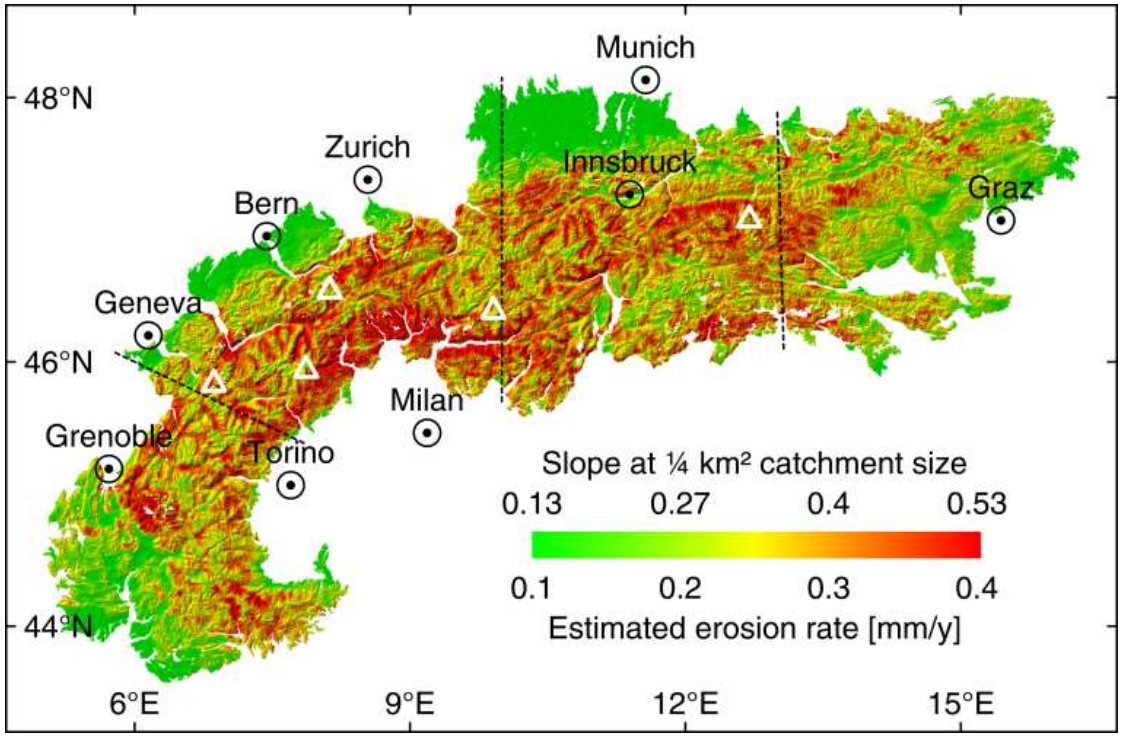

Fig. A.1. Map of mean slope at ¼ km^2 catchment size of the Alps. The conversion of slopes to erosion rates is based on the sediment budget and is discussed later in the paper. White triangles represent the highest peaks of major massifs: Mont Blanc, Monte Rosa, Finsteraarhorn, Piz Bernina, and Groβglockner (from west to east). The separation by the dashed lines is related to Fig. A.5.

Fig. A.2 displays the obtained relationship between $\overline{S}_A$ and elevation for various catchment sizes. The data were averaged with a moving window of 100 m size in elevation, while catchment sizes were subdivided into logarithmic classes. For all considered catchment sizes in the range shown, we find the expected strong increase of $\overline{S}_A$ with elevation only up to about 1500-2000 m. Excitingly, $\overline{S}_A$ decreases again above this elevation for all considered catchment sizes except for the smallest class.

Qualitatively, this finding is not new. Kühni and Pfiffner (2001) found that the increase of mean slope with elevation ceases at about 1600 m in the Swiss Alps. However, they averaged slope values over various catchment sizes and thus found no decrease with elevation. Fitzsimons and Veit (2001) speak of “relatively flat surfaces at higher elevations, especially in the alpine altitudinal belt”. The occurrence of this effect in the average over the entire orogen shows that it is not limited to a few locations.

In the following, we use $\overline{S}_A$ at a catchment size A = 1/4 km^2, which belongs to the uppermost headwater regions and seems to be rather small compared to most studies on fluvial erosion (Wobus et al., 2006, and references therein). More precisely, we analyze all sites with A between 1/16 km^2 and 1 km^2. As an example, Fig. A.3 illustrates the location of these sites in the upper Rhone Valley. Our choice is a tradeoff between the amount of available data and being sure that fluvial processes dominate erosion. If A is too low, hill slope processes will dominate, so that the more or less continuous erosion may turn into threshold behavior. The uppermost curve in Fig. A.2 illustrates this phenomenon as it seems to be limited by a mean slope value of about 0.55. In this case, the slope is no longer a proxy for the erosion rate. On the other hand, the number of available sites rapidly decreases with catchment size, so that the two lower curves show a strong variation at large elevations. Although their shape is essentially similar to the higher curves, the noise at high elevations make these large catchment sizes inappropriate for estimating erosion rates. According to these arguments, the similar shapes of the three solid curves in Fig. A.2 suggest that the range from A = 1/16 km^2 to 1 km^2 is suitable for our analysis. This range covers almost one sixth of the total area of the Alps, while all larger channels contribute less than 4%. The nearly parallel course of the three solid curves suggests a logarithmic dependence of the erosion rate on catchment size, in contrast to a power law mostly assumed for larger catchment sizes. This rather weak dependence is included in the analysis, so that slopes can easily be recalibrated to A = 1/4 km^2, although the data within the considered interval could be taken without recalibration as well.

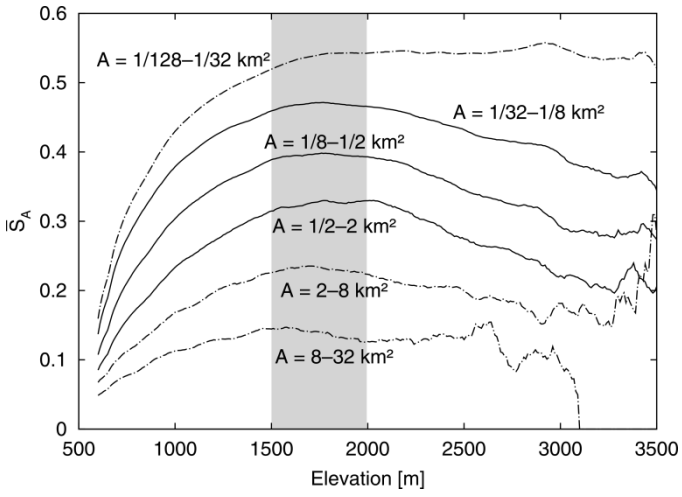

Fig. A.2. Plot of $\overline{S}_A$-elevation relationships for various catchment sizes in the Alps. The gray field marks the range of elevation with the largest $\overline{S}_A$ values.

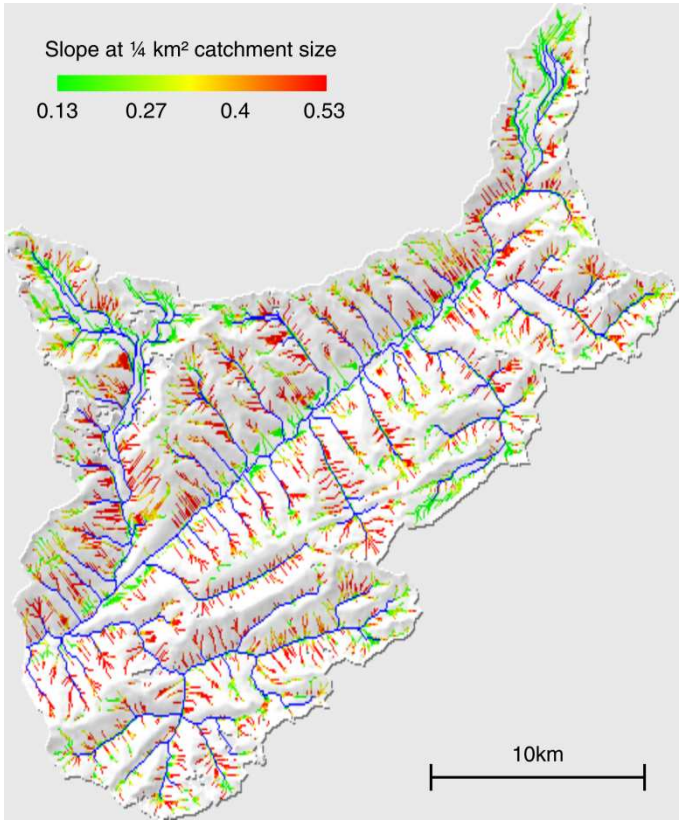

Fig. A.3. Sites with catchment sizes from A = 1/16 km^2 to 1 km^2 (colored according to their slope, rescaled to A = 1/4 km^2 as discussed later in the text) and channels with A >1 km^2 (blue) in the upper Rhone Valley.

The smoothed spatial distribution of $\overline{S}_A$ at A = 1/4 km^2 determines the surface color in Fig. A.1. The decrease in $\overline{S}_A$ at high elevations is immediately visible in the map, too: The highest values occur not in the vicinity of the main crest, but rather north and south of it, and the regions around the highest mountains are characterized by moderate slopes. The corresponding $\overline{S}_A$-elevation curve is shown in Fig. A.4. For comparison, the same analysis was performed for the Rocky Mountains, the Andes, the Atlas Mountains, Taiwan and the South Island of New Zealand. For all orogens, the entire range from the highest peak down to a given elevation was taken, except for the Rocky Mountains, where only the central part from 30° and 50° northern latitude without the Cascades was considered in order not to mix up too many different components. Beside the European Alps, only the Alps of New Zealand show the startling systematic decrease of $\overline{S}_A$ above a certain elevation identifying the Alps as a mountain range with very peculiar topographic characteristics. The $\overline{S}_A$-elevation curves of the Andes and Taiwan show some decrease or at least stagnation of $\overline{S}_A$ at high elevations, too, although not as clear as in the Alps. This will be discussed later.

Comparing the Alps with the Atlas Mountains and the Rocky Mountains in the upper part of Fig. A.4 reveals another apparently striking difference: While the $\overline{S}_A$-elevation of

the Alps is strongly concave even in its increasing part, that of the two other orogens is nearly linear or even slightly convex. However, this finding may not be as important as the decrease at high elevations since it may be a result of the overall shape of the orogen. While the Alps look like a more or less uniform, narrow mountain range, the Atlas Mountains and the Rocky Mountains are easily divisible into several distinct parts. In order to illustrate the effect, we have included an analysis of the entire European topography without Scandinavia (for simplicity, it is in fact the western part of Eurasia to 25° eastern longitude) in Fig. A.4. Obviously, the superposition of several smaller orogens destroys the sharp increase of $\overline{S}_A$ at small elevations and results in a more or less straight curve. The decrease of $\overline{S}_A$ at high elevation of course persists since this elevation range is governed by the Alps.

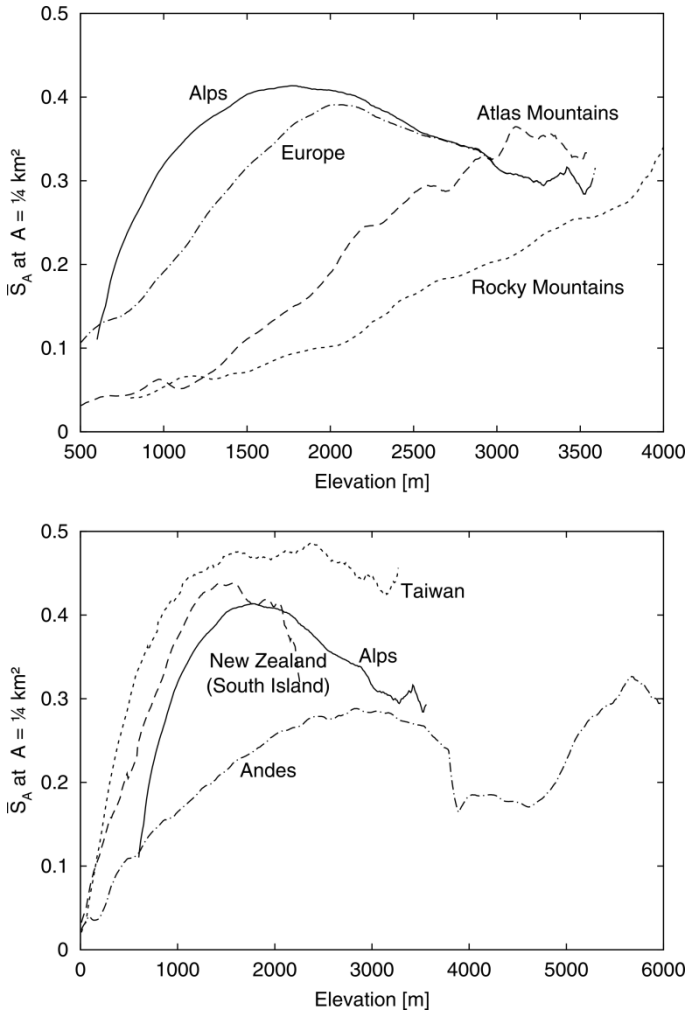

Fig. A.4. The $\overline{S}_A$-elevation relationships of six mountain ranges.

In return, the Alps are not as homogeneous as their DEM suggests. So may the decrease of $\overline{S}_A$ be the result of a superposition of different regions which are not clearly distinguished in the DEM? In order to clarify this, we split up the Alps into the four

regions separated by the dashed lines in Fig. A.1. The parts are numbered I (south-west), II, III (the two central parts) and IV (east). Their $\overline{S}_A$-elevation relations shows a small, but rather unsystematic variation. The decrease of $\overline{S}_A$ is clearly visible in all parts except part IV where elevations in the interesting range become sparse although our method makes almost one sixth of all surface data usable. So the phenomenon originates from the entire Alps and is not the result of a superposition.

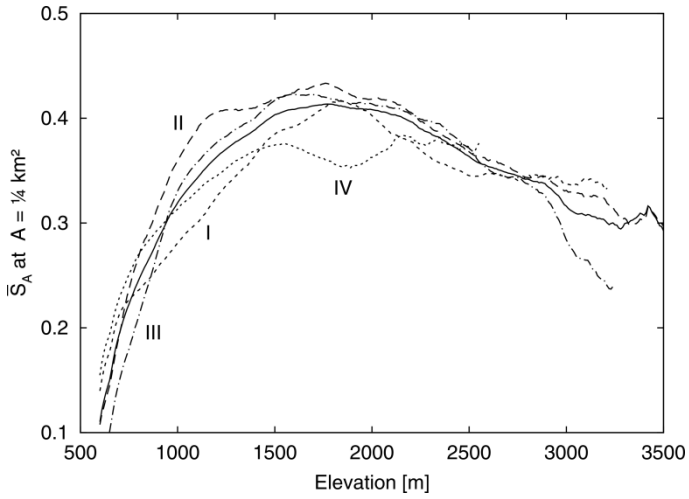

Fig. A.5. The $\overline{S}_A$-elevation relationships of the Alps splitted into four parts.

There are three possible interpretations of the decrease in $\overline{S}_A$ at high elevations in the entire Alps:

1. A systematic lithological, biological or climatological variation making rocks at high surface elevations more erodible, so that equilibrium is maintained by high erosion rates acting on less steep slopes.

2. A lack of uplift at high elevations, so that equilibrium can be maintained by low erosion rates.

3. Geomorphic disequilibrium where erosion has not yet balanced rock uplift at high elevations.

A systematic increase of erodibility with elevation due to rock lithology can be excluded because the highest parts of the Alps are generally characterized by high grade metamorphic rocks. The same applies to biological effects as soil-mantled slopes tend to be less steep than bedrock slopes (Montgomery, 2001) and climatic effects such as permafrost and orographic precipitation. So all these effects should rather support the increase of slopes with elevation than cause a systematic decrease. Furthermore, these effects should be visible in almost all mountain belts.

The second explanation – a lack of uplift at high elevations – was found for the Tibetan Plateau (Molnar and Lyon-Caen, 1989) and the Altiplano (Dalmayrac and Molnar, 1981). The sudden decrease of $\overline{S}_A$above about 3500 m in the $\overline{S}_A$-elevation curve of the Andes (Fig. A.4) in fact originates from the region around the Altiplano. However, for the Alps this idea is not consistent with measurements of recent uplift rates (Kahle, 1997; Ruess and Höggerl, 2002) as there is no systematic decrease of uplift rates at high elevations.

Since both concepts based on equilibrium fail to explain our observations, only the idea that regions above 1500-2000 m are not yet in geomorphic equilibrium remains: Erosion rates are smaller than rock uplift, so that these regions still experience a net increase in elevation (i.e. surface uplift). Further support for this idea might arise from a new study on cosmogenic nuclide-derived erosion rates (Norton et al., 2010b): While erosion apparently keeps track with rock uplift at moderate uplift rates up to about 1 mm/y, significantly lower denudation rates were found at some locations of high uplift.

But what is the signal causing the yet unfinished response of topography? It may originate from tectonics, but glaciation is a candidate, too. Even combinations seem to be possible since a part of the present uplift may be the isostatic response to deglaciation (Barletta et al., 2006; Champagnac et al., 2007). Glaciation itself obviously affects the topography, wide U-shaped valleys instead of rather narrow, V-shaped valleys are the most striking feature. However, U-shaped valleys are found at various elevations, and it may even depend on the total width of the valley whether the Ushape leads to an increase or a decrease in $\overline{S}_A$. Therefore, even some predominance of U-valleys at high elevation seems not to be able to explain the rather sharp transition from a strong increase of $\overline{S}_A$ to a decrease. Of course there may be an overall effect of glaciation. The Alps may have been much higher before glaciation and may have been torn down strongly during the glacial periods. However, this would imply that overall glacial erosion rates are significantly higher than fluvial erosion rates, while recent studies (Koppes and Montgomery, 2009) did not encounter a systematic difference between both.

However, response to deglaciation might have an effect on the analysis. As recognized by Norton et al. (2010a) in the upper Rhone Valley, the transition from glacial erosion to fluvial erosion may result in very high slopes locally, and these extremes might cause a bias in our analysis. Fig. A.6 shows the cumulative distribution of slopes at three elevation slices. While the distributions are similar in total, the highest elevations are characterized by a weaker tail at very high slopes. Thus, very steep slopes occur less frequently at high elevations where the erosional response to deglaciation should in fact be weaker than at lower elevations. However, the effect of the very steep slopes on our

analysis is negligible because all slopes S_A>1 contribute less than 0.01 to the mean value $\overline{S}_A$ at all elevations. Thus, the erosional response to deglaciation can be detected by our method, but its effect causes no bias in our analysis. Moreover, the Rocky Mountains were partly glaciated, too, but exhibit a completely different $\overline{S}_A$-elevation than the Alps, while the Atlas Mountains were not glaciated and seem to be topographically similar to the Rocky Mountains. And finally, an analysis of a small, non-glaciated region at the edge of the Alps east of the Last Glacial Maximum (results not shown here) resulted in a similar $\overline{S}_A$-elevation relationship as for the entire Alps.

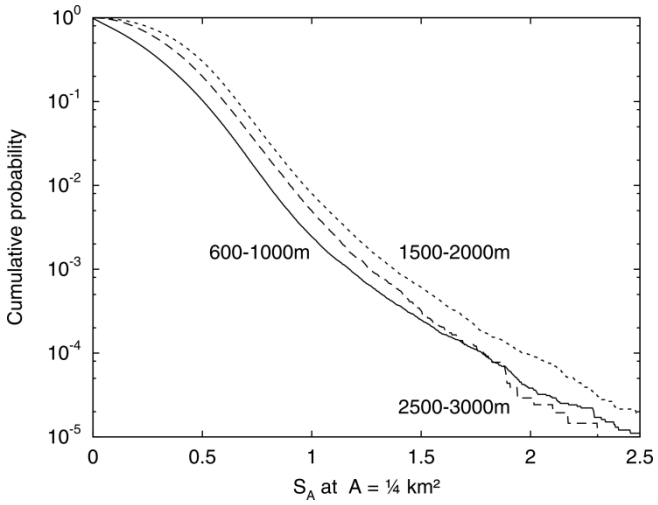

Fig. A.6. Cumulative distribution of the slopes S_A at A = 1/4 km^2 within three elevation slices.

In sum, effects of glaciation on our analysis seem to be insignificant, so that an unfinished response to a tectonic signal remains as the most promising idea.

A.3 A Simple Model

The results of the previous section suggest that the highest regions of the Alps are not in geomorphic equilibrium and thus still grow. In order to test this hypothesis and to quantify their degree of maturity, we derive a simple, one-dimensional model for the evolution of a mountain belt. Compared to more elaborate models involving many parameters, the approach may even be oversimplified, and it seems to be impossible to justify the assumptions with regard to the Alps in detail. Justification will arise from its ability to reproduce and explain the observations.

In contrast to our analysis of the Alpine topography, an erosion model requires an explicit relationship between erosion rate, slope and catchment size. We thus come back to the stream power approach (e.g., Whipple and Tucker, 1999; Wobus et al., 2006). We assume that the erosion rate is proportional to the slope and increases with the distance

from the main drainage divide raised to some power α. The power law exponent α summarizes the increase of erosion rate with the catchment size and the increase of catchment size with the distance from the drainage divide. We furthermore assume a "tentshaped" uplift function corresponding to simple folding of a thin sheet according to compression, i.e., that the uplift rate linearly decreases from the main drainage divide to the margins of the mountain belt. Under these assumptions, uplift and erosion are described by a linear first-order differential equation of the hyperbolic type:

$$\frac{\partial}{\partial t}H(x,t) = \underbrace{U\left(1-\frac{x}{l}\right)}_{\text{uplift rate}} - \underbrace{\left(-Ex^{\alpha}\frac{\partial}{\partial x}H(x,t)\right)}_{\text{erosion rate } R(x,t)} \tag{A1}$$

for $0 \leq x \leq l$ where x is the coordinate perpendicular to the crest (the main drainage divide) and l is the distance from the crest to the margins. For symmetry reasons, we only consider one half of the mountain belt. The negative sign within the erosion rate $R(x,t)$ originates from the fact that $\frac{\partial}{\partial x}H(x,t)$ will become negative for our coordinate choice. Furthermore, U denotes the uplift rate at the crest, and E is a parameter that quantifies erodibility, precipitation, etc.

As shown in the Appendix A, Eq. (A1) can be solved analytically starting from a flat surface $H(x,0) = 0$. It is found that the surface reaches a steady state after the time $T = \frac{l^{1-\alpha}}{(1-\alpha)E}$, and that the maximum elevation (at the crest) finally becomes $H_{max} = \frac{l^{1-\alpha}U}{E(1-\alpha)(2-\alpha)}$. This result suggests nondimensional variables, i.e., to measure x in terms of l, t in terms of T, $H(x,t)$ in terms of H_{max}, and $R(x,t)$ in terms of U. With these nondimensional variables it is found that the region with $x \geq (1-t)^{\frac{1}{1-\alpha}}$ is in equilibrium at the time t, and

$$H(x,t) = (2-\alpha)(1-x^{1-\alpha}) - (1-\alpha)(1-x^{2-\alpha}) \tag{A2}$$

$$R(x,t) = 1 - x \tag{A3}$$

In the region with $x < (1-t)^{\frac{1}{1-\alpha}}$, erosion does not keep track with uplift, resulting in an increase of elevation. We obtain:

$$H(x,t) = (2-\alpha)t - (1-\alpha)\left((x^{1-\alpha}+t)^{\frac{2-\alpha}{1-\alpha}} - x^{2-\alpha}\right) \tag{A4}$$

$$R(x,t) = (x^{1-\alpha}+t)^{\frac{1}{1-\alpha}} - x \tag{A5}$$

Apart from the scaling parameters in the nondimensional variables, the power law exponent α is the only nontrivial model parameter.

Fig. A.7 illustrates the behavior of the solution given by Eqs. (A2) - (A5). On the way to geomorphic equilibrium reached at $t = 1$, the erosion rate has a maximum somewhere between the central divide and the margins. As uplift continues and the range equilibrates, the maximum moves towards the watershed and thus towards higher elevations. In the surface topography itself the transition point is reflected by a discontinuity in curvature which separates a quite linear part (in the upper reaches) from a more concave part (in the lower reaches). This change in curvature is not a "knickpoint" in the well-known sense, but still defines an important departure from an exponential equilibrium profile of a graded river bed. As this characteristic point of the stream morphology is barely noticeable in plots of longitudinal river profiles, its substantial implications for the erosion rate remained unnoticed before.

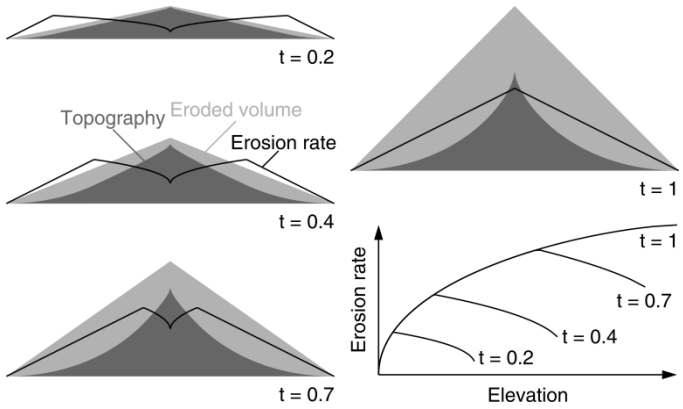

Fig. A.7. Concept of the one-dimensional uplift/erosion model. The cartoons illustrate a mountain belt at four time steps approaching geomorphic equilibrium ($t = 1$).

Excitingly, plotting erosion rates versus elevation for this simple model (Fig. A.7) reproduces our findings from Fig. A.4: A convex increase up to a certain elevation, and a slow decrease at higher elevations. The model reproduces the $\overline{S_A}$-elevation curves of the European Alps and the Alps of New Zealand at least qualitatively and indicates that both are far off from geomorphic equilibrium. Taiwan appears to be in or very close to equilibrium. Interpreting the curve of the Andes remains difficult, but the recovery of the slopes at high elevations points towards geomorphic equilibrium.

A.4 The State of Maturity of the Alps

The dashed line in Fig. A.8 shows a visual fit of our model to the $\overline{S_A}$ elevation curve of the Alps. We found that the curvature in the left hand part, the position of the turnover

at maximum $\overline{S_A}$, and the decrease to the right constrain the model parameters well. In contrast, the sharp bend at the point of maximum erosion rate is an artefact of the one-dimensional approximation because each elevation is assigned to only one location and thus to only one uplift rate here. In contrast, the same elevation occurs at many locations and thus at various uplift rates in reality. Thus, focus was laid on fitting the rest of the curve.

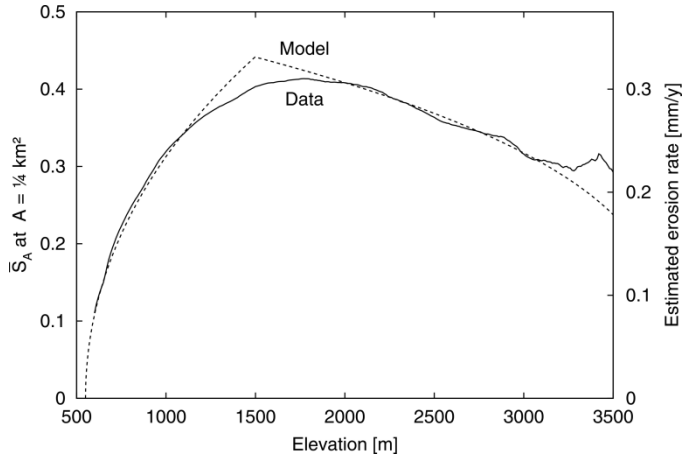

Fig. A.8. Visual fit of the model result to the $\overline{S_A}$-elevation curve of the Alps. The scale of erosion rate is explained in Section A.5.

The visual fit results in a power law exponent $\alpha = 1/3$ and a nondimensional time $t = 0.4$, which means that only 40% of the time towards geomorphic equilibrium has passed. Testing the fit with other parameters we found that the uncertainty of this value is lower than 0.1.

The combination of the excellent match between data and model for the Alps with the well constrained parameters allows a series of far reaching interpretations: The Alps are not even half way from a rather low (in the simple model completely flat) topography to their state of geomorphic equilibrium. While regions lower than 1500 m have already reached their final height, higher regions will still rise if the convergence between Adriatic plate and European plate continues. From the model results we can further derive that the net rise of the highest regions may amount to 2000 m. However, this number should be treated with caution as it hinges on the assumption that Pliocene and Quaternary rock uplift persists in the future. Furthermore, the gain in elevation may be limited by effects of slope instability above a critical slope. The $\overline{S_A}$-elevation curve floors at an elevation of 550 m: This suggests that the Alpine range is built on a base level of this elevation which is indeed close to the elevation of the Molasse basins.

The model also allows an estimate of the cumulative erosion during a hypothetic evolution of the topography from a nearly flat surface towards the present state. Maximum erosion amounts to about 900 m thickness and occurs at a present elevation

of 1300 m. This value decreases to 600 m at 3000 m elevation, which means that these regions should have experienced about five times more uplift than erosion so far. Such predictions are consistent with the observations that Miocene surfaces are largely preserved in several places (Hejl, 1997; Frisch et al., 2001; Dunkl and Frisch, 2002; Kuhlemann, 2007), but are inconsistent with mean erosion rates since the Miocene. We will take up this discussion after constraining the absolute time scale in the next section.

A.5 The Absolute Age of the Alpine Topography

As the time axis of our model can be arbitrarily rescaled, it does not allow any direct estimates of the absolute age of the topography. Combining the cumulative erosion with the hypsographic curve of the Alps leads to a total eroded volume of about 120,000 km^3, but this can in principle be distributed over an arbitrary time interval. However, recent uplift rates in the order of 1 mm/y found in high regions (Kahle, 1997) give a first hint: If these rates are representative during the formation of topography and only a few hundred meters were lost by erosion, the whole process cannot have taken more than a few million years.

Quantitative data on the sediment budget of the Alps (Kuhlemann et al., 2002; Kuhlemann, 2007) allow a more precise estimate. The observed sediment data (crosses in Fig. A.9) show only one strong, continuous increase through time, beginning 5-6 my ago. Although climatic effects have been suggested as a cause for this (Cederbom et al., 2004; Willett et al., 2006), no consistent explanation has been found for this increase so far. Indeed, it has been argued (Molnar, 2004) that, even if the global sudden increase of erosion in the late Cenozoic is related to climatic effects it remains questionable how it did so. Our model predicts a nearly linear increase of sediment yield per time from beginning of topography build up to the present state. Therefore, we argue here that – for the European Alps – these 5-6 my relate to the onset of considerable topography build up and corresponds to the 40% of time towards morphological equilibrium. Then another 8-9 my are required for the Alps to reach a geomorphic steady state, and the increase in sediment yield shall strongly decelerate in future, as is shown in the trend of the modeled curve in Fig. A.9.

In order to test this hypothesis we have calculated the sediment volumes predicted by our model, and plotted them as the solid line in Fig. A.9. The modeled curve is shifted to a base level of 25,000 km^3/my (dashed line), assuming a more or less constant background sedimentation rate throughout the Miocene. It may be seen that the sediment yield predicted by the model (grey area corresponding to 120,000 km^3, representing the nondimensional time $t = 0.4$) is even slightly lower than the amount of sediment found in nature. In other words, the sediment found in nature is enough to capture the volume lost by erosion during topography build up. This result clearly

supports our hypothesis that the formation of the present Alpine topography (at least of major parts) started only 5-6 my ago. This correlates well to the onset of uplift in the Molasse basins (Genser et al., 2007), so that the formation of the Alpine topography and the uplift of the Molasse basins may be more related to each other than previously assumed.

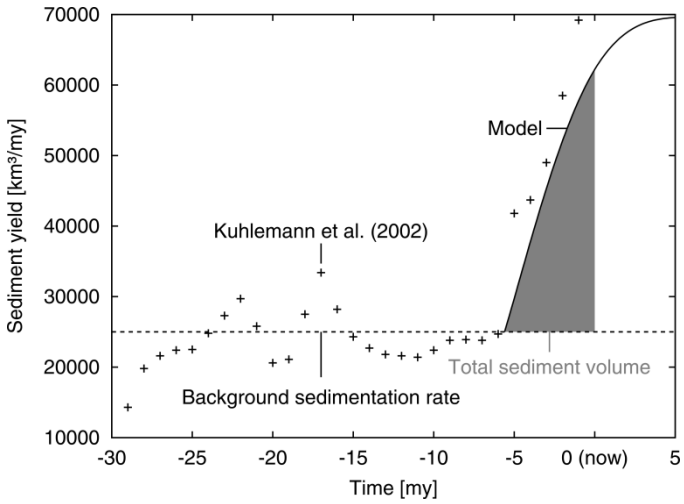

Fig. A.9. Predicted sediment yield of the model (continuous line) in comparison with the sediment yield data for the Alps (crosses) (Kuhlemann et al., 2002). The dashed line represents the background sedimentation rate throughout the Miocene; the gray area represents the nondimensional time $t = 0.4$ up to present.

Finally, constraining the time scale through the sediment budget allows the translation of $\overline{S}_A$ to erosion rates as anticipated in Figs. A.1 and A.8: Under the lithologic and climatic conditions of the Alps, erosion rate in millimeters per year is roughly three quarters of the slope at a catchment size of 1/4 km^2.

A.6 Limitations of the Model

We now come back to the circumstance that we used a perhaps oversimplified model. The one-dimensional approach itself is a very crude approximation, and the time-independent, tent-shaped uplift function may be qualitatively reasonable, but the real uplift pattern of the Alps is much more complex. Furthermore, effects of isostasy, perhaps in combination with lithospheric flexure, are disregarded. However, the main result concerning the equilibrium topography is an increase of erosion rate with elevation, and this hinges on an increase of uplift rate with elevation, but not on mapping this increase on a spatial pattern in detail. Both the curvature of the rising branch in Fig. A.8 and the shape of the curve around the maximum may of course depend in detail on the spatial pattern, but the general result on disequilibrium does not.

Isostatic adjustment as the result of deglaciation or redistribution of sediment may in reality result in a time-dependent uplift rate. However, the main effect would be a non-linear timescale, which means that the transfer from the non-dimensional model time to the real time scale is not constant through time. This obviously affects the shape of the increase in sediment yield starting at 5-6 my b.p., which is indeed not reproduced perfectly. However, the point of onset itself should not be affected.

Therefore, the limitations of the perhaps oversimplified realization of our model approach should neither affect our results on the state of maturity nor on the absolute age of topography.

A.7 Earlier Topography

In Section A.5 we found that building up the Alps from a base of 550 m elevation during the last 5-6 my reproduces the present topographic characteristics and the observed increase in sediment yield very well. However, we shall not conclude that the Alps were just a hilly flat throughout the Miocene. This would obviously contradict to measured exhumation rates as well as to the mean Miocene sediment delivery of about 25,000 km^3/my (dashed line in Fig. A.9). Although opening and filling of basins lead to huge redistribution of sediment, this seems to be impossible without any topography.

Our analysis does not enable us to reconstruct the Miocene topography. But if we assume that it was close to geomorphic equilibrium and from its overall structure similar to the present topography, we can make a rough and, of course, speculative estimate. From the simple model we first estimate the increase of elevations towards geomorphic equilibrium and compute the corresponding hypsographic curve. As Fig. A.10 illustrates, regions above 2000 m elevation will significantly rise if uplift persists. Since sediment yield is about 70,000 km^3/my in equilibrium (asymptotic behavior in Fig. A.9), we then rescale the equilibrium state (relative to a base of 550 m) by a factor 25,000/70,000 to obtain an estimate of the Miocene hypsographic curve. The result shown in Fig. A.10 suggests that only 4% of the area might have been above 1500 m in Miocene, compared to more than 40% today.

As a consequence of geomorphic equilibrium, the estimated hypsographic curve of the Miocene is relatively steeper in the upper part compared to the present. Although this is only a guess, it fits well to the idea that Miocene topography was more dissected than the present (e.g. Fitzsimons and Veit, 2001).

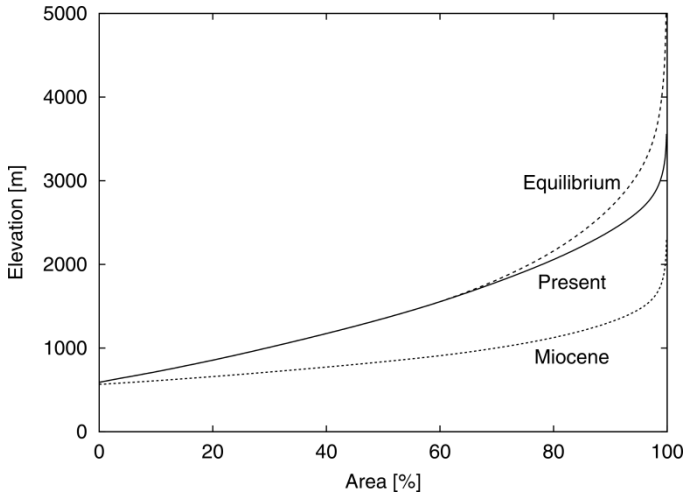

Fig. A.10. Hypsographic curves of the Alps: Present, estimated for geomorophic equilibrium, and downscaled according to the Miocene sediment yield.

A.8. Conclusions

Our analysis of the Alpine topography in combination with a simple model of uplift and erosion gives strong evidence that the Alpine topography is still in its infancy and far off from geomorphic equilibrium. Comparing our results with sediment budget data leads to the conclusion that the formation of the present topography began only 5-6 million years ago at the end of the Messinian. Miocene topography should have been much lower and/or more dissected than the present topography. A clear difference between the topographic evolution of the Western and Eastern Alps was not found.

These findings question the apparent consensus that the topographic evolution was distributed over much of the Miocene. A thorough discussion of these results in relation to existing knowledge on paleo-elevations will have to follow.

In return, “rewriting” the topographic history of the Alps might give new impulses to the reconstruction of paleoclimate in Central Europe.

Admittedly, this large-scale analysis does neither put any serious constraints on the shape of the Miocene topography nor explain why topography was formed or reshaped at the end of the Messinian. Ceasing of lateral extrusion may be a candidate for an explanation. More detailed studies of the present topography will show whether the slight and so far not very systematic differences found between western and eastern parts help us to understand these phenomena.

Acknowledgements The authors thank the TOPO-ALPS group for discussions and the ESF project TOPO-ALPS for funding.

A.9 Appendix - Mathematical Background

Our model of uplift and erosion is described by Eq. (A1) for $0 \leq x \leq l$with the initial condition $H(x,0) = 0$. This linear hyperbolic differential equation can be solved analytically using the method of characteristic curves.

In a first step, we rescale x to a nondimensional coordinate $\hat{x} = \frac{x}{l}$, which transforms Eq. (A1) to

$$\frac{\partial}{\partial t}H(\hat{x},t) = U[1-\hat{x}]_+ + \hat{E}\hat{x}^{\alpha}\frac{\partial}{\partial \hat{x}}H(\hat{x},t) \tag{A6}$$

where $\hat{E} = \frac{E}{l^{1-\alpha}}$, and $[...]_+$ denotes the positive part of its argument, so that $[1-\hat{x}]_+ = 1-\hat{x}$ if $\hat{x} \leq 1$ and 0 else. This is introduced to allow values $\hat{x} > 1$. In the following, we omit the hats for convenience.

The characteristic curves of Eq. (A6) are given by the equation

$$\frac{d}{dt}x(t) = -Ex(t)^{\alpha}. \tag{A7}$$

Its solution is

$$x(t) = (\,x(0)^{1-\alpha} - (1-\alpha)Et)^{\frac{1}{1-\alpha}} \tag{A8}$$

so that

$$\frac{d}{dt}H(x(t),t) = \frac{\partial}{\partial x}H(x(t),t)\frac{d}{dt}x(t) + \frac{\partial}{\partial t}H(x,t) \tag{A9}$$

$$= U[1-x(t)]_+ \tag{A10}$$

$$= \left[\,1-(x(0)^{1-\alpha} - (1-\alpha)Et)^{\frac{1}{1-\alpha}}\right]_+ \tag{A11}$$

Starting from a flat surface at $t = 0$, $H(x,0) = 0$, integrating this result leads to

$$H(x(t),t) = U\int_0^t \left[\,1-(x(0)^{1-\alpha} - (1-\alpha)E\tau)^{\frac{1}{1-\alpha}}\right]_+ d\tau \tag{A12}$$

$$= U \int_0^t \left[1 - (x(t)^{1-\alpha} + (1-\alpha)Et - (1-\alpha)E\tau^{\frac{1}{1-\alpha}} \right]_+ d\tau \tag{A13}$$

and thus

$$H(x,t) = U \int_0^t \left[1 - (x^{1-\alpha} + (1-\alpha)E(t-\tau))^{\frac{1}{1-\alpha}} \right]_+ d\tau \tag{A14}$$

$$= \frac{U}{E(1-\alpha)} \int_{x^{1-\alpha}}^{min\{1, x^{1-\alpha}+(1-\alpha)Et\}} (1 - \xi^{\frac{1}{1-\alpha}}) d\xi \tag{A15}$$

$$= \frac{U}{E} \text{ x } \begin{cases} Et - \frac{(x^{1-\alpha}+(1-\alpha)Et)^{\frac{2-\alpha}{1-\alpha}} - x^{2-\alpha}}{2-\alpha} & \text{for } x < (1-(1-\alpha)Et)^{\frac{1}{1-\alpha}} \\ \frac{1-x^{1-\alpha}}{1-\alpha} - \frac{1-x^{2-\alpha}}{2-\alpha} & x \geq (1-(1-\alpha)Et)^{\frac{1}{1-\alpha}} \end{cases} \tag{A16}$$

The lower expression is time-independent, which means that erosion balances uplift for $x \geq (1-(1-\alpha)Et)^{\frac{1}{1-\alpha}}$. The entire mountain belt has reached its steady state at the time $T = \frac{1}{(1-\alpha)E}$, and the elevation at the main drainage divide becomes

$$H_{max} = H(0,T) = \frac{U}{E(1-\alpha)(2-\alpha)}. \tag{A17}$$

Transforming Eq. (A.17) to the nondimensional variables $\frac{H}{H_{max}}$ and $\frac{t}{T}$ immediately leads to Eqs. (A2) and (A4). The rate of erosion (Eqs. A3 and A5) finally emerges from inserting this result into Eq. (A1).

APPENDIX B

TREATMENT OF SAMPLES FOR AL AND BE EXTRACTION - A "COOKING RECIPE"

This appendix is a short description of the sample preparation and treatment for cosmogenic burial age dating we adopted and applied for our samples. Most of the work was done in Vienna at the Center of Earth Sciences in the frame of the Earth Science Cooperation between the University of Vienna and the University of Natural Resources and Applied Life Sciences, Vienna under supervision of Dr. Philipp Häuselmann. The final step was done at the SUERC AMS Laboratory by Dr. Derek Fabel prior to the actual AMS measurements there (Scottish Universities Environmental Research Centre, Scottish Enterprise Technology Park, East Kilbride, UK).

The actual procedure is based on a compilation by Ph. Häuselmann, Darryl Granger, Amy Wolkowinsky, Mike Bourgeois, and Tom Clifton and adapted by Diana Sahy and Thomas Wagner for the processing done in the cosmo lab in Vienna, Austria.

Summary of the procedure: The goal of sample preparation is to extract the nuclides of interest from the raw sample material, which involves a variety of physical and chemical pretreatments and isotopic extractions. The exact procedure depends on what form your sample starts out as, what is in it, and what you want to get out. EVERY SAMPLE IS UNIQUE. However, usually, the procedure will involve the following steps:

- Brushing/cleaning the pebbles to get rid of dust and loam; crushing and sieving to get your sample into the right grain size.
- Then dissolve $CaCO_3$ and organic material in aqua regia.
- Next, do the magnetic separation, which will remove magnetite, other magnetic minerals, and some of the micas.
- The next step is to dissolve everything except for quartz and a few of the most stubborn other minerals such as zircon. This is done in a weak HF/HNO_3 solution over a period of several days up to two weeks. The purity of this is tested visually and eventually by doing an aluminum assay by ICP-MS. If there is feldspar, the aluminum content will be high and you will know you need to leach it some more. In between the leaches you will do a heavy liquid separation and a H_2O_2 treatment to get rid of heavy minerals (and feldspars) and muscovite, respectively.
- Next, the quartz is dissolved in a nasty cocktail of hot HF and nitric acid. A split is removed for the final aluminum (FinAl) analysis.
- Then the sample is fumed in sulfuric acid to remove fluorides. Ti, Fe, Al and Be hydroxides are formed, concentrated by centrifuging, and everything else poured off.
- Then the sample is run through an anion column to remove iron.
- Afterwards, Ti is removed by selective precipitation.
- A cation column is used to separate Be and Al.
- During hydroxide precipitation of Be, an aliquot is measured to assure that there is no Al in the Be and the separation worked alright.
- The resulting pure Be and Al hydroxides are oxidized in a furnace, then packed into sample holders.
- In the end, they got measured for $^{26}Al/^{27}Be$ and $^{10}Be/^{9}Be$ ratios on an accelerator mass spectrometer (AMS).
- Finally, the number crunching will lead to burial ages and pre-burial erosion rates (based on the assumptions taken, especially on the model used to explain the exposure history prior to burial and after blank corrections).

Note: for up-to-date information on cosmogenic isotopes and sample preparation, check the homepage of the CRONUS-Earth project: http://hess.ess.washington.edu/. Useful procedures and remarks and an online calculator are accessible.

Always THINK before ACTING! Each machine/equipment/bottle/etc is cleaned thoroughly after (and/or before) its use to avoid sample contamination.

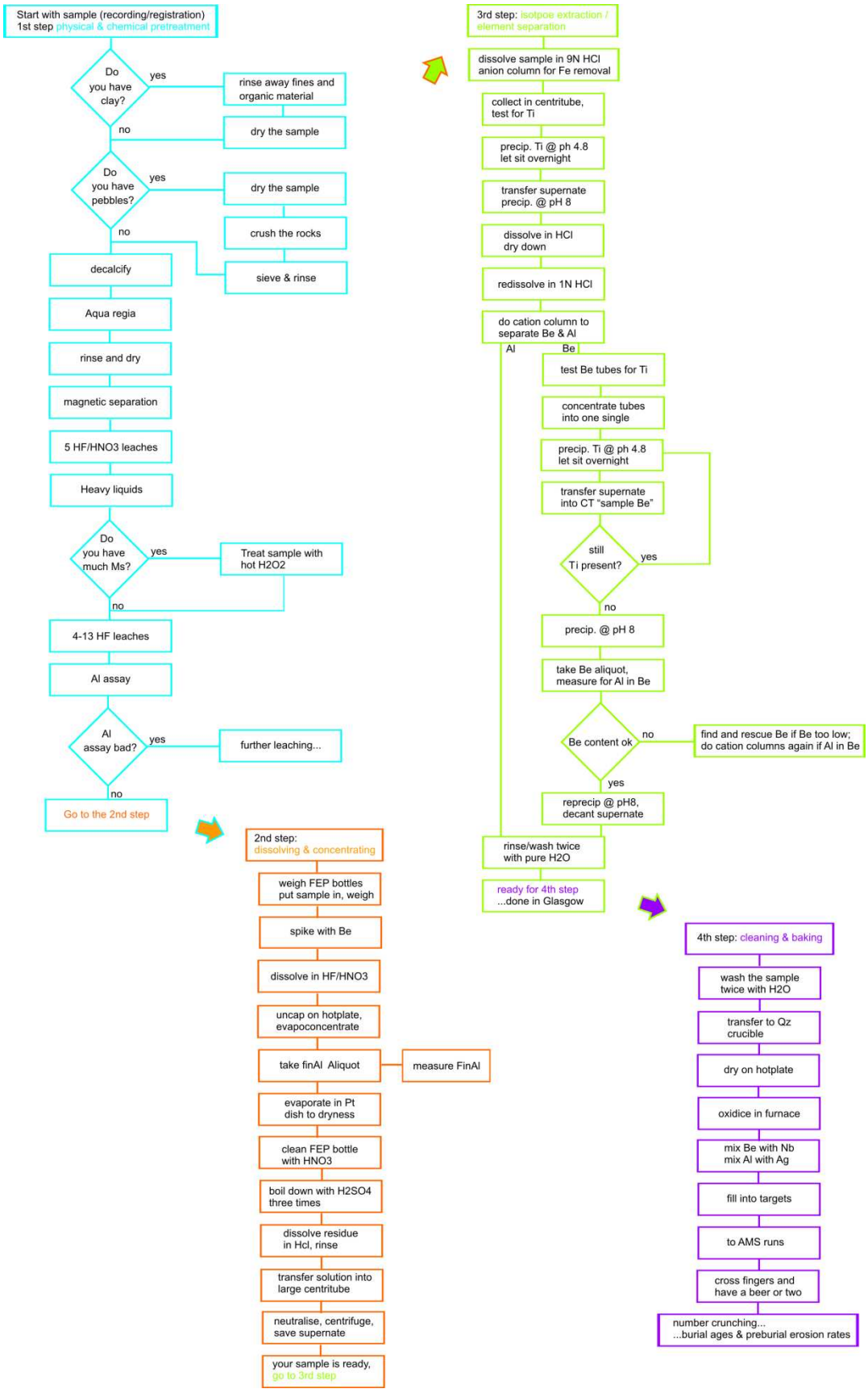

Fig. B1. Sample preparation flow chart

B.1 1st step: physical and chemical pretreatment

Sample ID:		
Date:		
Sample Description & Comments:		

If the sample is silty and/or has much organics, rinse it before all. This eliminates complications from organics as well as fines that could clog up further steps. Dry the sample. If there are pebbles or clasts, **crush and grind** the sample to a grain size where Quartz is separated from other minerals (depending also on the type of machine). Take care to clean the crusher accordingly before and afterwards with pressurized air and a wire brush. Now wet sieve the fines; build a tower of various sieves, use >2 mm, 2-1 mm, 1-0.5 mm, 0.5-0.25 mm sieve fractions and smaller ones (at least one e.g. 0.25-0.63 mm). Rinse the sample fractions with water several times to get rid of clay and silt; this is basically done when you proceed from the coarsest fraction down to the finest fraction, always rinse until only clean water is coming out.

Generally, the **fraction between 0.5 and 1 mm** proved good, however, you may want to include also the finer (0.25-0.5 mm) or even the finest sand fraction – it depends on your sample (size & amount), especially if there is only little of it. For pure quartz pebbles, the 1-2 mm fraction is in most cases to favor. No generalization possible (as holds true for all the procedure!). Dry in the oven. Temperature does not matter here as it might for noble gas work.

Decalcify the sample in a glass beaker using either 37% HCl, or 25% HNO_3 which was previously used to clean lab instruments (but under no circumstance in a bowl made out of aluminium because this is the stuff you want to measure). The reaction might be strong and loads of foam might be developed, keep a water bottle aside to dampen the reaction if necessary. Beware of calcium saturation: If the samples stopped fuzzing and the solution is still acidic (test via pH paper), it might be that the solution simply is oversaturated with Ca – discard the acid (into the appropriate waste acid carboy) and start over to be sure. The purpose of this step is to dissolve any carbonate. If no visible reaction occurs when fresh acid is added to the sample, prepare aqua regia by adding an equal amount of the other acid (HCl if HNO_3 was used for decalcifying, and HNO_3 if HCl was used initially).

Aqua regia is a powerful acid that oxidizes the remaining organics and dissolves all metal (e.g. from grinding) present in the sample.

Let it soak for a couple of hours (at least 3), then pour off the acid into the waste canister (if you directly neutralize the aqua regia with NH_3, you will need a whole lot of

it!); rinse with pure H_2O (or distilled water, which works fine at this stage, provided that it is available. We use pure water because it is the only kind of water we have in the lab besides tab water) and discard again into the waste canister; neutralize the remaining acid with NH_3 (after a pH of ~7 is reached, the rather yellowish to brownish solution turns into more or less clear one with red precipitate!), rinse out several times (~10 times) with distilled water until the solution is completely clear. Dry the sample and weigh to get a first estimate of how much of sample material you have of the 1-0.5 mm fraction.

Magnetic separation: The purpose of this step is to remove ferromagnetic and diamagnetic minerals. It is possible that it removes some quartz with a high density due to rutile inclusions, however, this may be a good thing. And usually there is still plenty of sample left to work with despite minor quartz loss.

You may first remove magnetite (and other ferromagnetic minerals) with a strong magnet by attaching a magnet to a funnel and pouring sediment through the funnel. Periodically dump magnetic sediment to keep funnel from clogging.

(If there is no magnetite,) Let the sample pass through the magnetic separator. Get instructed on the individual machine, each “behaves” differently! First, clean magnetic separator carefully with vacuum and compressed air. Take care not to plug any parts of the separator to avoid any sample loss.

Combine everything into a bag or other container and label as the “sample” magnetic split. Label the non-magnetic split as well and proceed with the sample preparation.

Clean the machine carefully afterwards.

Quartz purification:

Crush pebbles		
Sieve & rinse fines		
Decalcify		
Aqua regia soak (3hrs - overnight):		
Neutralize (NH_3), rinse & dry:		
Magnetic separation:		

From now on, **USE ONLY PURE WATER**.

Leach in 1 liter 1% HF and 1% HNO_3 on a shaking table at ~125 rpm

The purpose of this step is to dissolve pretty much everything. Quartz (and a few other minerals such as zircon and graphite) is exceptionally resistant to dissolution, and therefore this treatment will attack and dissolve everything else in the sample, but only minimally dissolve the quartz (this is actually important to dissolve the outer portion of the quartz and along any fractures, as this will remove atmospheric/meteoric Be). Untreated samples can take up to 18 leaches to become pure quartz. 40 g original material will be reduced somewhat (down to a maximum of 30 g if the sample contained a reasonable amount of Quartz) after 5 leaches, and bottles can then be combined to make room on the shaking table and to reduce the amount of chemicals needed. The shaking table in use will only take 16 bottles.

Load ~40 g of sample into weighted (to know later on how much sample material was "lost") 1 l-PP-bottles (the "normal" Nalgene bottles). Note: according to Kohl and Nishiizumi (1992): 7.5 g sample / L leachant is best; higher volumes decrease the natural Al reduction, but the 40 g worked appropriately. Fill them with pure water (to max about 1 inch below upper curve). Add 10 ml of concentrated HF (48%). **Be careful!** Dry area and gloves first to make spilled drops easier to spot.) Using the same graduated cylinder (this will wash out the HF), add 10 ml of concentrated HNO_3 (65%). Alternatively, **better and safer**: have a canister with a pump where you can pre-mix a solution of: 1 l pure H_2O, 10 ml HF and 10 ml HNO_3.

Put the bottles on the shaking table (125 rpm), let them rotate for a day; samples should leach for 24 hrs.

Changing the acids: Decant the acid (and not the sample!). Rinse well three times with pure water; dump each rinse into HF waste canister. Finally refill the Nalgene bottles.

Repeat the whole leaching procedure five times; than heavy liquid separation will follow. If leaching is complete or if you want to combine the contents of bottles, rinse once more and transfer to oven to dry. This takes about a half day.

Neutralize the HF storage canister with NaOH when it is about 2/3 full (do not allow to get it filled up too much or you will get in trouble neutralizing it). Mix the solution from NaOH flakes. Fill a plastic beaker (or a nalgene) to ~700 ml with tab water (no need of pure water!). Add about 20 spoons (plastic ones) of NaOH flakes. Stir a bit until all flakes are dissolved. Be careful, this is very exotermic and can get hot to handle. Add about one and a quarter of the beaker / bottle to the HF canister. Shake canister to mix (close it beforehand). Test pH of canister by dropping in a small piece of pH paper. If

acid is neutralized, pH paper will essentially stay the same color. If you have added too much base, add a little acid, best done by adding some of the bottles from the shaking table (which means that it is best to neutralize the waste canisters in the morning before changing the acids on the shaking table!). If it is still too acidic, add some more NaOH. Be careful and add small amounts, it is easy to overrun the neutral point.

Finally, pour the neutralized acid down the sink. Run water before and after. Be careful not to get this on your skin, it still has a calcium affinity and can hurt you.

Heavy liquids: The purpose of this step is to separate heavy minerals (such as zircon, rutile, epidote and tourmaline) from the quartz; then diluting the heavy liquid further until the quartz finally sinks and light minerals (such as feldspar) floats and can be separated as well.

Check density of LST Fastfloat (solution of sodium hetropolytungstates in water). Do this by pouring into a graduated cylinder and reading density gauge (or tare on a balance). This heavy liquid is non-toxic and non-carcinogenic, so no need for extreme caution; you can do the whole procedure out of the fume hood somewhere in the lab, but it is expensive, so avoid spillage in any case. Density should be higher than quartz, so between 2.7 and 2.8. If it is too dense, add water a few drops at a time, if too light, then put on a hot plate with a magnetic stirrer until it reaches the appropriate density.

Fill 2 bottles of dried and weighted sample material (~60-80 g) into a 250 ml separator funnel, add about twice as much liquid (~100-150 ml LST of density 2.7), close and shake vigorously (but take care not to get the sand and liquid up to the plug). Put on a stand, wait to separate. Pour the heavies (and as little as possible of the liquid) out, through a filter paper (commercial coffee filters) into a flask (from which all the used LST can be recycled). Close the funnel, add a drop of pure water to lower density and repeat. Repeat this as many times as necessary (i.e. if almost no grains fall out any more). Now you got rid of the heavy minerals. To get rid of the light stuff (especially feldspars), pour some more water droplets in the funnel, shake and observe the Quartz - when it sinks to the ground (and the feldspars remain on top), stop watering (tricky thing; but better to remove a bit of the Quartz together with the feldspars to have a clean Quartz remaining). Now use a new filter paper (and flask) and pour out the Quartz (beware: non-linear pouring! Be prepared to close rapidly!). Rinse both filters carefully to wash all the LST out of the sand and the filter paper to minimize LST loss. Dry the Quartz and the “waste” (heavies and lights) in the oven; collect the “waste” for further analysis if needed, or simply discard. This whole process may take some time (hours - days). Measure the weight of the remaining sample and note in the table to compute sample loss at each stage.

Recycle LST: the used LST from the flask is filled into a labeled Nalgene bottle for storage ("LST to recycle"). Whenever time and space is available, filter the LST through a filter paper into the small plastic beaker attached to the vacuum pump. Put the LST in a heat resistant beaker and onto a heat plate with a magnetic stirrer. Let the water evaporate until the desired density of 2.7 is reached; regularly check the density with a graduated cylinder on a balance. If the density is ok, let it cool and filter it once more. Now transfer the recycled LST back into the appropriate bottle, ready to be reused.

H_2O_2 treatment: If very much (1/3) Muscovite is present, treat the sample with hot H_2O_2 (if you are not really sure, do it anyway, cause it does not take too much time and does no harm to your sample).

Put your sample in a beaker; add some pure H_2O just to cover the sample to have some sort of buffer before you add the acid, but especially to decrease the chance of evaporating the whole water and leaving pure oxygen, which is explosive! Pour in H_2O_2 in excess (~300-400 ml). Bring to the boil on the hotplate (stir occasionally with a glass rod). The mica will pop up and float at the surface. Note that you will not get rid of all the micas! Skim them off. When there are no more micas appearing, switch the heat back, let it cool, pour of the liquid (just in the sink, this is ok), rinse it several times with pure H_2O until it is clear and no more mica is appearing (maybe there will be mica still appearing, or even most of it will be at this stage).

Now dry it again and measure how much material has been lost during LST and hot H_2O_2 treatment.

Fill again sample material into the 1l-PP-bottles (normally you will be able to decrease the amount of bottles per sample due to the sample loss, again around 40 g per bottle), put back onto shaking table.

The amount of leaches depends on the purity of your Quartz but ranges somewhere between **12 and 18 leaches in total** (check by sight, needs some experience), do the acid change every day.

Finally dry the sample and measure again, how much sample material is left.

Repeated leaching in 1 liter 1% HF / 1% HNO_3:

Bottle ID	bottle tare	mass in [g]	# of leaches	mass out [g]	LST	H_2O_2	mass in [g]	# of leaches	mass out [g]	sample loss

Aluminimum assay: This is used at this step to assess the amount of Aluminium in the sample. Quartz will contain a small background amount of Al, but not more than about 200 ppm. Higher Al content indicates that there are still feldspars in the sample and the sample should be further leached or cleaned.

Measure a small amount of sample into a Teflon beaker. About 0.5 g (as accurate as possible, 5.00-5.01 g, makes the calculations easier!). Do this using the high precision balance in the 4th floor, adding the sample with a small plastic spittle. Take care of "statics".

Add 25 ml HF and 10 ml 1:1 (32.5%) HNO_3 to the beaker. Place on hotplate under heat lamp. Sample should dissolve and dry down completely. If sample is not completely dissolved, repeat (which is the usual case and assures that all the Quartz gets into solution). The drying down process will take several hours. After sample is dissolved and dry, fume with 1:1 HNO_3 to remove fluorides. Do this by adding 10 ml 1:1 HNO_3 and drying; repeat for another time (2 times 10 ml total). Now dissolve in 5 ml 1:1 HNO_3. Because you are using a Teflon beaker, the drying liquid will form a bead, and therefore when it finally dries, the dissolved material will form a residue right where the bead was. So once that bead residue dissolves you will have completely dissolved the sample and there is no need to worry about the residue still adhered to other parts of the beaker. Tare the centrifuge tube (high precision balance). Transfer beaker contents to centrifuge tube with a transfer pipette. Quantitative transfer is the goal. Rinse beaker with 45 ml pure H_2O and transfer to the centrifuge tube. Rinse transfer pipette with this as well. Measure the Al content with the ICP-MS (Inductively Coupled Plasma - Mass Spectrometry); this was done by Wilfried Körner by Thomas Prohaska. In this case dilute the aliquot further, this means take 2 ml (with the 1000 µl fixed volume Eppendorf pipette) out of the CT and transfer it to a new, now tared CT, dilute to a total volume of 20 ml with pure H_2O.

Remember that at this stage we are interested in an approximate value anyway. This means that although everything under 200 ppm is ok, if you get 195 ppm, you might want to consider cleaning the sample a little more.

Cleaning: Clean the Teflon beaker in pure water, take care not to scratch the inside of the beaker. Soak in 25% HNO_3 for 24 hrs, rinse with pure H_2O and dry (Always use gloves when handling Teflon beakers).

quartz aliquot mass (0.5 g nominal): into Teflon beaker			
volume HF (25 ml nominal):			
volume 1:1 HNO_3 (10 ml nominal):			
Dissolve (on hotplate)			
repeat if not dissolved (usual case)			
add 10 ml 1:1 HNO_3 (32.5%) and dry			
add another 10 ml 1:1 HNO_3 and dry			
dissolve in 5 ml 1:1 HNO_3 use edge of hotplate to speed up (do not evap!)			
tare centrifuge tube (high precision)			
transfer to centrifuge tube with pipette labelled “sample AlAssay”			
rinse beaker with 45 ml pure H_2O add to tube via pipette (to rinse as well) note: 50 ml total, full CT			
tare full CT (CT & solution) (high precision):			
For ICP measurements by Th Prohaska ➔ take 2 ml of diluted solution out of the CT in to a new CT (now tared!!!) and dilute further to 20 ml with pure water ➔ ready, wait for ICP results (proceed in the meantime with other stuff)			
solution mass (total mass – CT mass):			
quartz [Al]:			
if not acceptable (>200 ppm), repeat ultrasonic leach			

That is it! You have done the most time-consuming and boring steps. Now, the "real chemistry" begins. Be sure to use pure water only, be sure to use the **right acids**. **Think before acting!** The time you spend thinking is way shorter than the time you need to restart all over because you did a small and important mistake. **If you are not sure, ask!**

Beware of cross-contamination and general contamination: before dealing with the open bottles (evaporation), clean the lab thoroughly, hassle the people until they do not dare enter the lab any more (to prevent materials import), and speed up with the open-lid chemistry! You have time to wait (and to re-clean the lab) when your sample is in the centrifuge tubes. **Label everything!**

B.2 2nd step: dissolving and concentrating

Quartz Digestion: Once you have pure Quartz (meaning your sample passed the AlAssay (<200 ppm)), dissolve it. The HF complexes and volatilizes the silicon as H_2SiF_6 or as SiF_4. The strong oxidizing HNO_3 aids mineral dissolution and prevents the formation of insoluble fluorides. While the silica is volatilized, the Al and Be remain as a residue in the beaker. There is enough Al of a known isotopic ratio in quartz, but there is no ^9Be, so you need to add a Be spike. Then dissolve the spike and quartz in HF / HNO_3, analyze a split for Al and Be on the ICP (use these results in the end to compute the Al and Be concentrations in the total sample solution), and evapoconcentrate the rest. Evapoconcentration can take a few days, especially with high volume samples. Also you need to add an Al spike to the blank.

So, use clean FEP bottles and decide which sample goes in which bottle, label the bottles accordingly (caps as well). The FEP bottles have to be big enough to hold 5 times HF and 1 time HNO_3 than Quartz. Record the weight of each bottle (bottle + cap); high precision balance on the 4th floor. There could be a problem with static electricity so getting several measurements and averaging them seems like a good idea. Tare bottle very carefully on large balance, use an air shield if necessary to get a better read. Fill in approximately 100 g of sample (clean Quartz by now) in each bottle (beware of statics). Cap bottles and weigh them again in order to determine the exact weight of the sample and record this in the sample flowchart (bottle mass as well). You do this usually with 7 samples plus a blank; but due to space constraints we do 3 and a blank and another 4 afterwards.

bottle tare (high precision balance):	
Sample (~100 g) + bottle (high precision balance):	
mass quartz (compute by subtracting first from second):	

Be Spike: Spike bottle with 100 µl (= 736 µg) of Be (carrier solution; make sure that you are using the Be carrier and not the Be standard) via a fixed volume Eppendorf pipette (2% error according to the manufacturer; use the smaller, yellow pipette tips). Be careful to avoid evaporation of spike carrier and spillage!

Note: use the yellow tips that tightly fit onto the pipette and do a "test run" with pure water. There are three points of resistance when pressing the pipette. Press down to the first one, put tip into solution, release to soak up the solution. Now you have exactly 100 µl of solution "in" the pipette. To get it into the FEP bottle press down to the first point of resistance, then further to the second to even get out the last small drop (do this rather at once, so that this drop does not remain in the tip), then remove the pipette and place it over the trash, then press down to the last point of resistance and the tip (the yellow one) should jump off (be cautious that this does not happen before and the tip falls into one of the FEP bottles).

Note exact weight of spike; meaning measure the bottle with the Be carrier prior and after the 100 µl have been taken out.

Remark: 736 µg is rather high of a value, Derek Fabel in Glasgow usually uses 250 µg, but less than 200 is already problematic, because it might be below the detection limit of the AMS. So if some is lost during the preparation / processing (Why? Where?), use higher values. Anyway use the ICP results from the FinAl for the computations for Al and Be concentrations.

Be carrier ID:	
carrier [Be]:	
mass carrier added:	
mass Be spike (µg):	

Chemical blank: Do the same for the blank; additionally add 1 ml (note exact weight) of Al standard. According to Derek F this is enough, but due to (generally) low Al currents on measuring, it is recommended that you add 3 ml of Al into the blank to improve accuracy; check the specific AMS experiences. 3 ml is equal to 3000 µg of Al spike.

3 ml Al standard	
100 µl Be carrier	
500 ml HF / 100 ml HNO_3	

Dissolve the quartz: Now it is time to add the acids: for concentrated HF, you have to add a volume equivalent to 5 times the weight of the sample (so, for 100 g- 500 ml, for 110 g-550 ml), and for concentrated HNO_3, a volume equivalent to the weight of the sample (100 g-100 ml, 110 g-110 ml).

Pour the appropriate amount of acids in, put the lids loosely (so that fumes can escape and pressure will not build up), let dissolve. For the blank, take 500 ml HF and 100 ml HNO_3. Use extreme caution here. Think out the entire pouring process and create enough space before starting. Normally the HF is added first, and the HNO_3 right afterwards, otherwise the sample plus the HF, if left alone for some time (more than 5 minutes!), starts boiling and it can supposedly melt the bottles. Watch the first couple of hours for any sign of boiling of the sample: reaction is exotherm. If it is going too hot, the bottles will melt! If necessary cool them by immersing them in a water bath and change the water as necessary. Watch for expansion of the HF solution, which can overflow your bottle. The next days, you may slightly shake the bottles (Leave the bottles inside the fume hood!).

After two days, close the lids tightly, put them on the shaking table (if this is occupied, use the IR lamps, heat also helps to speed up the whole process of dissolution), let them react. Wait until all Quartz is dissolved (may take 1-2 weeks!).

Transfer to big hot plate, heat it up to max. ~150°C, do not put the bottles too close to the heat lamps (they will melt), uncap the lids, let the HF evaporate down to about 2-3 cm (yes, one inch!) or better said below 400 g total weight, because this is the maximum the high precision balance can handle. Will need 3-4 days, even up to one week.

volume HF/HNO_3 added (5 X quartz mass/1 X quartz mass nominal):	
cap **loosely** and control for the first 2 hours reaction is exotherm	
The next day you may slightly shake the bottles	
After 2 days, lids tightly, put on shaking tables (or IR lamps) Wait until Quartz is dissolved completely (1-2 weeks)	
when dissolved, put on hotplate, uncap, evaporate to 1 inch (below 400 g in total, upper limit of balance)	

Split and transfer: Mix well the solution of dissolved sample material and HF/HNO_3 to assure it is homogenized (dense H_2SiF_6 settles at the floor of the bottle) and your split will be representative. Take an Al aliquot that corresponds to about 200 µg Al (calculate on the basis of your Al assay and the amount of Quartz; note: if the measurements are done by ICP, simply take 2 ml of solution (do not use 1000 µl Eppendorf pipette)). Evaporate it (~150°C) and treat as described. Calculate the Be loss with the amount you take – there should be a minimum of 500 µg Be left in the sample bottle. Weigh everything.

Measure the FinAl assays or have them measured; Al and Be! High precision is needed here.

mass bottle + solution:	
mass solution:	
transfer 200 µg Al to Teflon beaker for FinAl analysis here simply 2 ml via disposable pipette	
mass FinAl aliquot (tare FEP bottle afterwards and compute difference to previous weight)	

FinAl analysis: When sample is getting close to evaporate, after 24-48 hrs, split sample for FinAl analysis. Because of the fact that we use an ICP-MS and the detection limits are very good, simply use 2 ml of solution; transferred via a disposable pipette into a Teflon beaker. Note: using the fixed volume Eppendorf pipette is not recommended, because the inside of it contains glass components and the solution still contains HF; and because it is not really relevant how precisely you measure the 2 ml, you are going to measure the weight of the aliquot anyway.

Pour solution into Teflon beaker, then cap bottle and weigh, substract from original measurement to determine amount of solution in beaker. Do not remove the beaker from the fume hood, it has HF in it! Only weigh the capped Nalgene bottle.

Proceed with FinAl process with split in Teflon beaker. Dry down. This is like the first step of the first AlAssay in which you added HF and HNO_3 and dry down.

- Add 15 ml 1:1 HNO_3 to Teflon beaker, dissolve sample, dry down.
- Add 15 ml 1:1 HNO_3 to Teflon beaker, dissolve sample, dry down.
- Dissolve the "dot" in 5 ml 1:1 HNO_3 (preferably overnight), tare centrifuge tube, pour sample into tube.
- Rinse beaker with about half of 45 ml pure H_2O, transfer to centrifuge tube, repeat with the rest of the 45 ml pure H_2O.
- Cap and weigh centrifuge tube. Now it is ready for FinAl analysis.
- The result of the FinAl should be within 10% of your initial AlAssay. If not!? Out of our own experience some samples had up to 50% of difference between AlAssay and FinAl, which might be explained by sample bias.

dry aliquot	
add 15 ml 1:1 HNO_3 and dry	
add 15 ml 1:1 HNO_3 and dry	
dissolve in 5 ml 1:1 HNO_3	
tare centrifuge tube (label: „sampleName_AlBe")	
transfer to centrifuge tube	
rinse beaker with 45 ml pure H_2O & add to tube	
solution mass:	
atomic absorption [Al]:	
quartz [Al]:	

Fluoride Fuming: This step is to eliminate remaining fluoride. While most of the fluorides are evaporated during the quartz dissolution and fuming, some remain in the residue. This fluoride must be eliminated, since fluorine complexes with Al and will interfere with future analysis and Al separation.

This is accomplished by fuming samples in sulfuric acid. Sulfuric acid boils at a higher temperature than HF, so when fluorides are separated, any F^- will be volatized. Do this in a Pt dish because the temperatures involved will melt Teflon and fluorides will dissolve or bond to glass.

Pour the rest of the sample in a Pt dish and dry it on the hotplate under a heat lamp – make sure that it will not boil (~150°C as usual). Do not fill the Pt dish to the rim; leave about 1/3 of total height. This is necessary because when adding the H_2SO_4 to do the fluoride fuming, the stuff will creep over the rim of the Pt dishes. When the bottles are empty, wash them with HNO_3. Pour only the amount of acid that can be taken up by the Pt dish (usually bottom is not completely covered; ~15 ml). Try not to transfer whatever insoluble residue. It should not matter, but it may react with the sulfuric acid in the next step. Repeat the cleaning another two times.

Cleaning the FEP bottles: although you rinsed the bottles 3-4 times with HNO_3 still they should be cleaned with 25% HNO_3, and the cleaning solution for this should be freshly prepared. First wipe out the inner surface with paper towels and a Teflon tong (not the normal one, you will scratch the surface!). Fill in the freshly prepared cleaning solution. Let it soak for 24 hrs. After the cleaning solution is poured off (and used for further cleaning of other lab instruments), dry the bottles in the oven at max 40°C for 1-2 hours; do not use paper towels inside cleaned FEP bottles. Now they are ready for the next batch of samples.

Pour sulfuric acid into the Pt dish. Fill about to 1/2 mm below the residue. Heat the whole so that it just will not boil under the heat lamps (~450°C). Fume down the acid to dryness. Lots of fumes will be produced. Very important, remove Pt dish from heat immediately upon drying, or insoluble things will form. Color should be toasty, but not black. So, take away when there are no more fumes (use tong; put onto watch glass – do not melt the hood).

Repeat with about 10 ml sulfuric acid.

Repeat with about 5 ml sulfuric acid.

Transfer dry Pt dish to rim of big hotplate. Pour HCl (37%), wait for Sulfates to dissolve completely. You may "stir" by pipetting liquid in and out a transfer pipette (use the same pipette throughout - beware of cross-contamination). When the solution is clear (wait up to 2 h without stirring) transfer it to a 50 ml centrifuge tube with the transfer pipette.

Repeat until all the Sulfates are dissolved; begin to clean the inside walls of the Pt dish by pipetting HCl over it. Be patient! It takes a long time! This means 3-4 more fill-ups to the residue, wait ~1 hr each. Any residue (e.g. black stuff) should remain in the Pt dishes, save this in an extra CT as well; label.

Neutralize solution to pH 8 after each (or every other – depending on volume, simply take care because it is not possible to neutralize the total volumes in one CT, only 50

ml) transfer with NH_4OH (check with sight: hydroxides fall out; with nose: smells mildly but not strongly of ammonia; with 1/10 drop of liquid transferred to a pH paper with the pipette. DO NOT put the paper into the solution). Regularly mix the liquid. Take care that no liquid will reach the lid of the tube: cap does not close tightly. Thus a mixing by hand or by Vortex around 1 is preferred. Centrifuge, precipitate will form a gel in the tip of the CT; save supernate in 250 ml bottle "pre-column supernate".

Now, you have a concentrate of Al, Be and all the other possible elements (without Si). The next step will be to get rid of the different elements without losing any Al or Be.

transfer concentrated solution from FEP to Pt dish & dry	
rinse bottle with 15 ml 1:1 HNO_3(32.5%), transfer to Pt dish, dry	
rinse bottle with 15 ml 1:1 HNO_3, transfer to Pt dish, dry	
rinse bottle with 15 ml 1:1 HNO_3, transfer to Pt dish, dry	
add H_2SO_4 just below marks, dry @ 450°C and remove immediately	
add 10 ml H_2SO_4 & dry @ 450°C	
add 5 ml H_2SO_4 & dry @ 450°C	
dissolve in 37% HCl (so that sample/bottom is covered, wait to dissolve!) to speed it up, use a pipette to "stir"	
transfer to centrifuge tube with pipette, label "sample AFF" note: AFF …after fluoride fuming	
add NH_4OH to pH 8, centrifuge and decant into labeled bottle labeled "sample pre-column supernate"	
rinse Pt dish 3-4 times with HCl and transfer rinsate neutralize each time!	
add NH_4OH to pH 8, centrifuge and decant into labeled bottle labeled "sample pre-column supernate"	

B.3 3rd step: isotope extraction / element separation

Take the CT and redissolve the precipitate in 9N HCl. Very often, the stuff will not dissolve easily. The secret here is: TIME. Begin to dissolve it about 2 days before you plan to go on the columns, regularly observe and care for the solution. If there is some

very fine material left that will not dissolve, it could be TiO_2, which is favorable since we want all the Ti out. Centrifuge and decant, in any rate save the material.

Go and let the material through the anion columns to get rid of the iron as described. Take care that the resin is free of bubbles (bubbles will channel flow through the column and ruin the separation) and no dirt whatsoever is in there, discard and use new one if necessary. If the columned material that you collect in a 50 ml centrifuge tube is still yellow, the acid concentration was too low and you have to repeat it.

Fe removal by anion exchange columns: column volume = 2 (-3) ml

This step removes Fe on an anion exchange column. Fe (and some Ti) is tightly bound by the resin in 9N HCl, but Al, Be, most of the Ti and some other things will pass through.

- Dissolve precipitate in 9N HCl (done in the CT), the less solution you have to run through the column, the faster it will go, so try to minimize HCl added.
- Choose a cleaned and conditioned anion column.
- Condition column for what you are about to put in it: add 1 ml 9N HCl (the resin will shrink as it adjusts to the higher acid strength), allow to drain. Now the 1ml of HCl will have moved about halfway down the column. It will continue to move down and then out the column when the sample is added, condition the column as it goes. Discard the drips from this step.
- Place CT “sample anion” under column.
- Add the sample to the column, gently (try not to disrupt the top surface of the resin).
- Rinse CT with enough 9N HCl and add to columns to make 1 column volume total (note: normally this does not work, because 2-3 ml is already the dissolved sample volume; so simply rinse CT with one column volume of 9N HCl); the solution should be colorless (not yellowish), because the Fe should be bounded to the resin at this stage.
- Add another cv of 9N HCl and drain to get all the Al and Be out.
- Place bottle “sample anion rinse” under column.
- Add 4 column volumes of 0.012N HCl and drain; this should be yellowish, because this weak acid allows the Fe to drain and end up in the anion rinse.
- Recondition the columns.

Note: the resin is NOT toxic, so if the resin is contaminated, one can throw it out like normal waste - simply wash it down the sink. Make sure to replace it with the anion resin – the yellow one – free of bubbles.

Dissolve precipitate in 9N HCl (1 ml nominal; 2 (-3) ml usually):	
condition anion column (if not recently conditioned, especially check for bubbles in the resin; if so, discard or put it back into resin-bottle if not contaminated and fill again the column, no bubbles are allowed!)	
drain resin bed (means let the water get out)	
add 2 column volumes 9N HCl & drain (waste)	
add 4 column volumes 0.012 N HCl & drain (waste)	
add 1 ml of 9N HCl to column & drain (waste)	
place centritube labeled "*sample* anion" under column	
add solution *gently* to column & drain	
add enough 9N HCl to centritube to make 1 column volume total note: normally this does not work, because normally already 2-3 ml is already the dissolved sample volume; so simply rinse CT with one column volume of 9N HCl	
add rinse *gently* to column & drain	
add 1 column volume 9N HCl *gently* to column & drain ***note:*** if this is yellowish, redo columning with fresh prepared 9N HCl, because most likely the acid was not strong enough!	
place bottle labeled "*sample* anion rinse" under column	
add 4 column volume 0.012 N HCl *gently* to column & drain **note:** should be yellowish, because this is where the Fe should end up!	
recondition column, leaving some solution on bed	
hang "conditioned" sign from top of column	

Selective precipitation to remove Ti: Add a drop of H_2O_2 to the solution. If it turns reddish, you have Ti in your sample and therefore have to do the selective precipitation to get rid of it.

Add 3-4 drops of acetic acid (buffer to be able to reach pH value of 4.8; without the acetic acid, you will probably be always below or above 4.8) to your sample and "neutralize" with NH_4OH to pH 4.8. Before reaching this pH, the colour will fade away. The results are best when the pH is approached slowly from below – so take care not to

add too much ammonia. Towards the end, adding it 10-dropwise still results in overshoot it sometimes. Remark: Do not measure the pH on the narrow-range paper within the fume hood - the fumes affect the liquid and will therefore indicate a false pH within tenths of seconds! Usually use the same pipette for every operation from now on – in order not to lose sample. Take great care not to cross contaminate and to keep the pipette tip away from everything but the sample; put into small plastic beakers (100 ml) upside down and label them not to get confused and to prevent cross contamination.

Spin it down, transfer the supernate to another centrifuge tube (the precipitate in this tube should contain the Ti now, relabel!). Add a few drops of NH_4OH to the supernate in the new CT labeled “sample AlBe” (this will bring the pH up to 8 – check by smell and paper). Spin it down and collect the supernate in a bottle labeled “sample Ti selective precipitation”.

Naturally, you most probably will have Ti within transferred to your sample even if you observed the pH closely. Do not worry yet and proceed to the columns.

Dissolve the concentrated Al&Be hydroxides in 2 ml 1:1 (6N) HCl, transfer it to a small Teflon beaker; rinse the CT with another 2 ml of 6N HCl and dry it down on the hotplate.

add 3-4 drop of H_2O_2 to centritube. If red, precipitate Ti:		
	add NH_4OH to centrifuge tubes to pH 4.8 (exact, use acetic acid as a buffer)	
	precipitate Ti overnight	
	centrifuge 10 minutes @ 3000 rpm	
	decant supernate into a centritube labelled "*sample* AlBe" the precipitate obtains the Ti (should…), relabel CT as such!	
	precipitate sample with NH_4OH to pH 8	
	Centrifuge	
	Decant supernate into labeled bottle: “sample Ti selective precipitation”	
dissolve in 2 ml 1:1 HCl, transfer to Teflon beaker, rinse centritube with another 2 ml 1:1 HCl and transfer		
dry down sample on hotplate		

Al / Be separation by cation exchange columns: column volume = 20 ml

Please note that the column, bottle, and centrifuge volumes depend on the Al content of the sample and may vary from sample to sample.

Cation Columns: This step is done to separate Be and Al; Be is going through the cation columns first using 1N HCl (if there is any Ti left, this will show up even earlier), and then comes the Al using a 2.5N HCl.

First, choose the good column size! Generally, the smaller the volume, the quicker and faster the process goes. But if the volume is too small, the separation is bad and needs to be repeated. Rule of fist: for every 1000 µg of Al present in the solution (FinAl assay), take 1 ml of column volume. Round up rather than down. (14 mg to 20 ml). Usually we use 20 ml column volume.
Re-dissolve sample in 1:1 HCl. Most of the time, it will not dissolve very well. Add enough H_2O to make it 1N, (attention: often there is too much Cl-ions in the cake, so that the solution will be more than 1N. Tentatively try to make it 0.3 to 0.6N nominal – try and watch the results after columning!! Generally if you have added 2 ml 6N HCl, you have to add 10 ml of pure H_2O), warm the solution a bit on the hotplate, stir with the pipette; transfer to a 15 ml tube, spin it down - the residue will most probably be TiO_2 (yes you have got rid of a tiny bit more!).

Add the solution to the conditioned column. Rinse the Teflon beaker with 1N HCl, transfer to the tube, vortex, spin down, transfer to the column.

Adjust the bottle and centrifuge tube size to the column volume. If you work with 20 ml columns, you have to split the Be into three tubes and the Al into 2. Take great care not to fill the Al's to more than exactly 40 ml or you will not be able to neutralize it!

dissolve in 1:1 HCl (1 ml nominal) note: not too much, because 3 ml of 6N HCl means already 15 ml of pure H_2O to get a 1N HCl, this is already almost a whole column volume!	
transfer to centrifuge tube note: you can use the previously used ones („sample AlBe“)	
rinse beaker w/enough pure H_2O to make 1N HCl (5 ml nominal)	
transfer rinsate to centrifuge tube	
Centrifuge – residue if present might be TiO_2 –save material	

condition cation column (if not recently conditioned)	
drain resin bed	
add 10 (5 + 5) column volumes 6N HCl & drain	
add 3 column volumes pure H_2O & drain	
add 1 column volume 1N HCl *gently* to column and drain	
place bottle labeled "*sample* cv 1-3 Be" under column	
add solution *gently* to resin bed & drain	
add enough 1N HCl to column to make 3 column volumes total & drain *note: if CT has already a volume of 18 ml, than only 42 ml of 1N HCl is added*	
place centrifuge tube labeled "*sample* cv 4-5 Be" under column	
add 2 column volumes 1N HCl *gently* to column & drain	
place centrifuge tube labeled "*sample* cv 6-7 Be" under column	
add 2 column volumes 1N HCl *gently* to column & drain	
place centrifuge tube labeled "*sample* cv 8-9 Be" under column	
add 2 column volumes 1N HCl *gently* to column & drain	
place bottle labeled "*sample* cv 10-14 Be" under column	
add 5 column volumes 1N HCl *gently* to column & drain	
place centrifuge tube labeled "*sample* cv 15-16 Al" under column	
add 2 column volumes **2.5N** HCl *gently* to column & drain **note: stronger acid now!!!**	
place centrifuge tube labeled "*sample* cv 17-18 Al" under column	
add 2 column volumes **2.5N** HCl *gently* to column & drain	
recondition column [10 cv 6N HCl & 3 cv pure H_2O), leaving some water on bed	
hang "conditioned" sign from top of column	

Hydroxide precipitation: This step is to precipitate some of the things we want and pour off everything else. Be and Al (as well as Fe and Ti) will all form hydroxides with Ammonium Hydroxide (NH_4OH) at pH of 8. The actual separation of Fe and Ti is already done on the anion columns and the selective precipitation, respectively. Be careful with the pH here, if it is too high Al will redissolve. If it is too low, Be will be in solution.

Add four drops of H_2O_2 to the Be separates. If it turns yellow, you still have Ti.

In case you used three tubes, and the first one is less yellow, you may want to analyze its contents for Be: Generally the Ti comes first, and if there is no Be in the tube, you may discard it (of course, into a labeled bottle!).

Precipitate the first of the Be and Al tubes to pH 8 with NH_4OH (smell, paper). Spin down, pour off the supernate, pour the contents of the 2nd tube into the first (to concentrate Be and Al). The same for the 3rd Be tube.

If this was the last Be tube, and if there is Ti present (an almost invisible yellow is still ok, best compare to blank if possible), do the selective precipitation once more as described above. Spin it down and pour the now hopefully- Ti-free supernate into the now spare Be tube.

Dissolve and acidify the Be concentrates (and the Ti fractions, if you measure the Ti fraction for Be, but this is not done in our lab) with 2 ml of 1:1 (6N) HCl, make the volume a total of 50 ml; mix!

For the Be fraction, take a Be aliquot: Take 1 ml into a CT (using the fixed volume 1000 µl Eppendorf pipette; note exact weights), dilute to 25 ml with pure H_2O. Measure the Be fraction for its Al content. Small amounts of Al in the Be (up to 40 µg) are acceptable, otherwise you will have to repeat the columning.

Re-precipitate the Be fraction if everything is in order, centrifuge and decant supernate. Finally rinse / wash the Al & Be sample two times with pure H_2O (it might be that not all dissolves, but be patient and vortex…).

Hydroxide precipitation for Be:

add four drops H_2O_2 to Be CT (optional), if yellow precipitate Ti	
first, concentrate elements into one centrifuge tube by precipitating: - add NH_4OH to pH 8 to the first tube - centrifuge - decant into labeled bottle "sample Be neutralized" - transfer solution of 2nd tube to first tube - add NH_4OH to pH 8 to the first tube -centrifuge - decant into labeled bottle - transfer solution of 3rd tube to first tube - add NH_4OH to pH 8 to the first tube -centrifuge - decant into labeled bottle	
add 2 ml of 6N HCl	
dilute to 25-30 ml with pure H_20	
add 5 drops acidic acid as a buffer to get the right pH of 4.8	
add NH_4OH to centrifuge tube to pH 4.8 (exact)	
precipitate Ti overnight	
centrifuge 10 minutes @ 3000 rpm	
decant supernate into a centritube labeled "*sample* Be"	
relabel the Ti tube as such (you might have to reuse it if some Be ended up in there!)	
add 2 ml 6N HCl; if yellow precipitate Ti again	
precipitate sample with NH_4OH to pH 8	
centrifuge 10 minutes @ 3000 rpm	
decant supernate into labelled bottles note: use previous bottles: "sample Be neutr."	
dissolve Be in 2 ml 6N HCl, dilute to 50 ml with pureWater	

take Be aliquot from sample: take 1 ml with fixed volume Eppendorf pipette (1000 µl); transfer to CT and diluted to 25 ml with pure H_2O label: *"sample Be aliquot"*	
analyze for Al and Be content	
reprecipitate Be (remaining 49 ml) with NH_4OH to pH 8	
centrifuge 10 minutes @ 3000 rpm	
decant supernate into labeled bottles note: use the large ones used previously!	
Rinse 2 times:	
add 5 ml pure H_2O	
vortex & centrifuge 10 minutes @ 3000 rpm	
decant supernate into labeled bottles "sample Be rinse"	
add 5 ml pure H_2O	
vortex & centrifuge 10 minutes @ 3000 rpm	
decant supernate into labeled bottles	

Hydroxide precipitation for Al:

first, concentrate elements into one centrifuge tube by precipitating: - add NH_4OH to pH 8 to the first tube - centrifuge - decant into labeled bottle "sample Al neutralized" - transfer solution of 2nd tube to first tube - add NH_4OH to pH 8 to the first tube -centrifuge - decant into labeled bottle	
Rinse 2 times:	
add 5 ml pure H_2O note: if it does not fully dissolve the first time, it should the second time	
vortex & centrifuge 10 minutes @ 3000 rpm	
decant supernate into labeled bottles "sample Al rinse"	
add 5 ml pure H_2O	
vortex & centrifuge 10 minutes @ 3000 rpm	
decant supernate into labeled bottles	
You are done now; the oxidation is done by Derek in Glasgow, because it would not be possible to "press" the targets here and it is also easier to send the hydroxides instead of the oxides, because they are less toxic! Tell your friends and go have a beer!	

B.4 4th step: cleaning and baking

Since the Be was already precipitated at least twice, this is not necessary any more. For Al, it is not necessary to precipitate once more either. Usually keep the hydroxides in the same tubes – this avoids transfer losses.

Rinse, vortex, and spin the samples twice. The problem here is to get rid of virtually every ammonia and ammonia salt that is interlaced with the hydroxides, without getting these dispersed and disposed. Especially for Be, take great care not to smear the

$Be(OH)_2$ up to the walls of the centrifuge tubes – better vortex slowly and a long time than quick and dirty. Take the black box, put Quartz crucibles in the holes, make a plan where which sample sits. Put some drops of H_2O to the Be sample, make a gel by stirring it up with a pipette (here, the pipette is changed) and transfer it quantitatively (!) to the crucible. It may be needed to wash the tube several times (letting the crucibles dry on the hotplate in the meantime) in order to get all out. For Al, there is usually enough material that one pipetteful is enough. Do not fill it up to the rim, or there is a chance that it will overflow when drying. Dry it on the hotplate a last time at very low temperature, because otherwise it boils and spits and makes a terrible mess. Go to the furnace, and transfer the crucibles in there with the special tweezers. Cap it when you have them in the air. Remember to place them in the correct order! Heat the furnace up and oxidize at 1100°C for one hour. Turn it off and let it cool. Mix the samples accordingly (Al is mixed with a silver binder, while Be is mixed with niobium for the AMS facility in Glasgow; Cu is used as a binder for the AMS facility in Zürich). Take care for BeO which is very toxic and powdery. If you have to fill the targets, do not fill the holes up to the top – leave a diameter's depth empty. You cannot hammer too hard – unless you break the rod, which is very unfortunate to do.
…wait for AMS results…

Oxidation:

take 2 clean* quartz vials	
add ~2 drops pure H_2O to hydroxides	
transfer hydroxides to quartz vials	
dry at low heat (<100°C)	
cap quartz vials	
oxidize in furnace at 1100°C for one hour	
add same volume Ag to Al and crush	
add same volume Nb to Be and crush	
label quartz vials clearly	
cap, cover with parafilm & place in tray	
*to clean quartz vials boil vials and caps in 10% HF / 50% HNO_3 for one hour	

B.5 Some useful side notes

B.5.1 Glossary

HNO_3: Salpetersäure / nitric acid: 65%
HCl: Salzsäure / hydrochloric acid: 37%
HF: Flusssäure / hydrofluoric acid: 47%
NH_3: Ammoniak / ammoniac: 25%
H_2O_2: Wasserstoffperoxid / hydrogen peroxide: 25%
CH_3COOH: Essigsäure / acetic acid
H_2SO_4: Schwefelsäure / sulfuric acid: 95%

Notes: most chemicals have to have the purity grade "per Analyse"; besides NaOH (which is techn.) and the "used" acids for decalcifiying.

FEP bottles: the Nalgenes that are almost transparent and have a smaller opening than the "normal" Nalgenes.
Pt dishes: Platinum "bowls", take care not to dent them, they are really expensive.
Teflon beaker: the small white beakers. Never touch the inside to avoid scratching the surface!
Pipette: use the disposable ones or fixed volume Eppendorf pipette (nevertheless always weigh/tare to be sure!).

B.5.2 First Aid Kit

- Calziumgluconatgel to put onto skin for smaller chemical burns, especially HF.
- Spray "Pulmicort" to inhale after (unintended) HF inhalation.
- Syringe with Calciumgluconat to injected under the skin for larger chemical burns.
- Calcium fizzy tablets.

B.5.3 Cleaning of bottles

The cleaning solution should be 25% HNO_3 (which is prepared using the 65% HNO_3 and diluted accordingly; 1 parts of 65% HNO_3 and 2 parts of pure H_2O). You can reuse this cleaning solution, store it if not in use in the 2.5 L bottles labeled accordingly "25% HNO_3 cleaning solution". Usable for multiple cleanings.

The bottles (normal Nalgene bottles) are cleaned by rinsing them carefully with pure H_2O, then by filling them up to the rim with the 25% HNO_3 cleaning solution, with closed lid, let it soak for 24 hrs. After this period of time fill them in other bottles that have to be cleaned or back into the large storage bottles "25% HNO_3 cleaning solution".

Rinse the cleaned bottles again with pure H_2O and wipe carefully with paper towel. Use a tong to reach the bottom of the bottle.

Empty bottles of chemicals: rinse with tab water, pour into waste canister, rinse some more, discard.

APPENDIX C

CONFERENCE ABSTRACTS RELATED TO THIS THESIS

This appendix is a collection of abstracts, which were presented at various national and international conferences as talks or posters in the time frame of the thesis. Additionally the abstract of a paper initiated by the Styrian Doctoral School of Earth Sciences in 2009 where I could contribute is attached here. The list is in chronological order beginning from the most recent contribution.

C.1
Pliocene to Pleistocene faulting at the transition between Alps and Pannonian Basin: Constraints from dating fault activity by the $^{26}Al/^{10}Be$ burial age method

For the geodynamic interpretation of the Alpine-Carpathian-Pannonian realm, the Pliocene to Pleistocene tectonic evolution at the transition between the Eastern Alps and the Pannonian Basin poses a series of open questions: (1) What is the significance of the fault pattern that evolved during latest orogenic evolution? The general Lower- to Middle Miocene fault pattern accommodated much of the Eastern Alpine eastward extrusion and is fairly well known. However, some of these major faults are found to be still active at kinematics typical for Middle Miocene times (e.g. Bus et al. 2009), although it has been suggested that the stress regime at the orogen-basin transition changed substantially during the Miocene. (2) Why are there apparently no structures related to basin inversion at the Alpine - Pannonian transition as found elsewhere in the central Pannonian Basin? General consensus holds that roll back and retreat of the Carpathian Slab steered extensional tectonics in the Miocene, but ceased around Late Miocene. This resulted in inversion of the Pannonian Basin (Horváth and Cloetingh, 1996). The observed surface uplift at the western termination of the Pannonian Basin, i.e. the Styrian Basin is commonly associated with this process. (3) What is the interpretation of ~10 km vertical steps of the Moho at the transition between Eastern Alps and the Pannonian Basin as revealed by seismic experiments? Brückl et al. (2010) identified a triple junction between European, Adriatic and Pannonian / Tisza plates west of the SE corner of the study area. Hence, the question arises whether the simple picture of Miocene extension by extrusion between Adriatic and European plates and

renewed Pliocene compression induced by cease of the Carpathian slab pull has to be modified.

Lineament analysis and fault plane solution data in the transition between Alpine orogen and Pannonian Basin shows that a kinematically coherent and seismically inactive block can be defined in this region. This block – here called the "Styrian Block" – is delineated by the Mur-Mürz Fault System in the north, the Pöls-Lavanttal Fault System in the west and the Periadriatic Fault System in the south and includes both the eastern most part of the Alps and the westernmost part of the Pannonian Basin. Fault analysis shows that the young stress field within this block appears to be extensional in W-E direction. An 1.56 ± 1.11 Ma age of fault activity is constraint by burial age data of quartz rich sediments entrapped within a fault using the nuclide pair ^{26}Al and ^{10}Be. Here we interpret the post-Miocene fault pattern as result of north-south convergence between European and Adriatic plates and displacement partitioning along margins of coherent crustal fragments. The Styrian Block is part of the Pannonian fragment. Strike-slip displacement resolved along margins of this coherent block, especially along the northern Mur-Mürz Fault System. Here the European plate acts as a rigid backstop along which N-S plate motion trajectories are deflected into eastward flow, thereby releasing strike slip displacement. The Styrian Block is continuously extending since Early to Middle Miocene and it experiences uplift since about the Miocene-Pliocene boundary. We explain this by two interfering processes: (1) The weak Pannonian fragment is underthrusted from north and southwest by European and Adriatic plates and (2) decreasing extension rates towards east. While the eastern Pannonian Basin experiences W-E convergence since the cease of Carpathian subduction, the Styrian Block is still extending eastwards. This scenario reflects a multiplate interference system and highlights the complex interplay of plate motion and its consequences to topography and landforming processes.

C.2
Young uplift in the non-glaciated parts of the Eastern Alps

We report the first incision rates derived from burial ages of cave sediments from the eastern margin of the Eastern Alps. At the transition zone between the Alpine orogen and the Pannonian basin, the Mur river passes through the Paleozoic of Graz – a region of karstifiable rocks called the Central Styrian Karst. This river dissects the study area in a north-south trend and has left behind an abundance of caves which can be grouped into several distinct levels according to their elevations above the present fluvial base level. Age estimates of abandoned cave levels are constrained by dating fluvial sediments washed into caves during the waning stages of speleogenesis with the terrestrial cosmogenic nuclide method. These ages and the elevations of the cave levels relative to the current valley bottom are used to infer a history of 4 million years (my) of

water table position, influenced by the entrenchment and aggradation of the Mur river. We observe rather low rates of bedrock incision over the last 4 Ma (~0.1 mm/y on average) with a decrease in this trend to lower rates around 2.5 Ma. However the pre-burial erosion rate estimates from backward modeling of the data show even lower rates, indicating disequilibrium between the incision in the main river and its tributaries and their hinterland. We relate this to the increase of drainage area of the Mur river due to stream piracy of the paleo-Mur-Mürz in Late Miocene to Pliocene times. The decrease in valley lowering is attributed to the rise of the base level related to aggradation of sediments within the valley. We explain this observation by continuous sediment transport through the valley from the upstream section of the Mur river limiting the erosional potential of the river in a transport limited state. Putting these relative rates into a vertical reference frame allows us to attribute most of the inferred incision to surface uplift of the region in the range of 0.1 mm/y over the last 4 Ma.

C.3
Age and Prematurity of the Alps

Although the Alps are among the best studied mountain ranges on Earth, the age of their topography is almost unknown. Even their relative stage of evolution is unclear: Are the Alps still growing, in a steady state or even decaying? Using the mean slope at given catchment size as a new geomorphic parameter we analyse the topography of the Alps. Our analysis provides one of the first quantitative constraints that shows that the range is still in its infancy: In contrast to several other mountain ranges, the Alps have still more than half of their evolution to a geomorphic steady state to go. Combining our results with sediment data from the surrounding accumulation spaces we infer that the formation of substantial topography began only 5-6 million years ago. Our results challenge a general consensus that the topographic evolution is distributed over much of the Miocene.

C.4
Geology of Styria: An overview

In 2009 the Styrian Doctoral School of Earth Sciences organized a field trip work-shop on the geology of Styria. The field trip was led by PhD students of the three participating universities: KFU Graz, TU Graz, MU Leoben. As an outcome of this field trip, we present here the geology of the entire province in a simplified way, taking into account modern concepts of the tectonic evolution. In a first part, the tectonic units building up Styria are presented; in a second part the geodynamic evolution of these units through time is described. A third part deals with the economic significance of

mineral resources in Styria. The figures of this contribution are available online on the pages of the naturwissenschaftlicher Verein and at http://wegener.uni-graz.at.

C.5
Slope-elevation relation of an orogen, a chance to decipher its stage of evolution?

Slope-elevation distributions for particular drainage areas show the actual stage of development for an active orogen. Analytical solutions of an uplifting orogen and its decay by surface erosion perfectly fit the observed data (extracted from digital elevation models). This consistency suggests young (5 Ma) additional topographic build up of the Alps, thereby provoking general geological believe.

C.6
The significance of cave bears for passage morphology

Cave walls polished by passing cave bears (so called Bärenschliffe) are known from some dozen caves in Europe that were populated by cave bears in the Middle and Upper Pleistocene. Bärenschliffe are rounded and polished parts of cave walls and boulders originating from the passing cave bears, rubbing their fur along the walls. They mainly occur on edges that project into the passages but also on straight walls. Bärenschliffe were first noticed and interpreted as animal traces in 1806 from Drachenhöhle near Mixnitz (Styria, Austria), where they are very pronounced. However for some caves it is doubted that these features are traces of cave bears.

The aim of this presentation is to show that the features are Bärenschliffe by excluding any other geological or anthropogenic process that could have caused these features. Further we want to point out the significance of cave bear presence for the mesomorphology of that caves. We found that in some caves like Drachenhöhle, Arzberghöhle, and Peggauerwandhöhle, many boulders and often whole sections of cave walls (often several square meters) were reshaped due to passing by cave bears. To constrain the age of the Bärenschliffe a stalagmite that has grown on such a polished surface is being dated using the U/Th-disequilibrium method.

C.7
Cave sediments as records of landscape evolution in the Eastern Alps

Landscape evolution in the European Alps has been a major topic of research for Earth scientists during the past several decades. The effects of landscape modeling processes are quantified using estimated sediment budgets, fission track analysis, and the dating of geomorphic markers like fluvial terraces, glacial moraines and erosional surfaces. Caves can provide additional clues for understanding landscape development because the position of phreatic cave passages, which form close to the local water table, is linked to the position of springs and valley bottoms. Lowering of the valley floor by erosion leads to the development of progressively younger phreatic passages at lower elevations. Therefore, valley incision rates can be obtained, provided that the age of a cave is known with reasonable accuracy. The minimum age of a cave can be determined by dating the sediments it contains, which are younger than the cave itself. The available techniques are U-Th dating, paleomagnetic analysis, and burial age dating based on the differential decay of the $^{26}Al/^{10}Be$ isotope pair in quartz.

The Northern Calcareous Alps (NCA) of Austria provide an ideal application for landscape evolution studies based on cave sediments because caves, which developed in thick limestone sequences, show a clear vertical distribution. Attempts have been made to empirically link this distribution pattern to the geomorphic history of the Alps, but numerical ages for the caves have yet to be determined. In the high karst plateaus of the central and eastern NCA (Dachstein, Tennengebirge, Totes Gebirge) speleogenesis probably started in the Miocene. The oldest known caves are currently located at altitudes of more than 1800 m asl. Progressive valley incision led to the development of a second level of caves at altitudes of 1400-1800 m asl. The third and youngest level is situated close to modern valley floors and is still active today. In the largest cave systems of the NCA (Hirlatzhöhle, Schönbergsystem, Dachstein-Mammuthöhle), distinct levels of horizontal passages which developed during times of relative tectonic calm, are connected by series of vertical shafts which formed during times of rapid valley incision, when the development of underground systems was forced to keep up with rapid geomorphic changes at the surface.

A project funded by the Austrian Science Foundation is currently underway, with the goal of investigating cave sediments from the NCA and the Slovenian Alps using the $^{26}Al/^{10}Be$ dating method. The goal of this study is to answer questions regarding the timing of speleogenesis in the NCA and to compare the pace of landscape modeling processes along a N-S transect of the Eastern Alps, as well as other available records from the alpine region.

C.8
Burial Age Dating in caves applied in current Austrian research projects

Burial age dating provides a tool to date Pliocene and Pleistocene sediments. Quartz grains exposed to cosmic radiation at the surface accumulate ^{26}Al and ^{10}Be with a definite ratio of 6.8:1. When the quartz grains are buried, the different half-live of these radioactive nuclides causes the ratio to decrease with time. Caves are buried repositories for Quartz grains in clastic sediments and thus cave sediments can provide minimum ages for the cave genesis. The decrease of the mentioned ratio of the radio nuclides is the key to determine the time since the grain was buried. The current research projects aim to determine valley incision rates in the European Alps during the Neogene and Quaternary. Burial age dating is up to now primarily used for landscape development studies, but applications in other fields of cave science like for example cave paleontology is also possible. The current projects are funded by the Austrian Science Foundation.

C.9
Active tectonics at the Eastern end of the Alps: The Alps are certainly not “dead” at all

In the literature many contributions have recently claimed that: "the Alps are tectonically dead". Much of this work has followed the recognition that the central part of the Alps appears to have changed their tectonic regime since the Miocene and deformation has propagated into the foreland. The inactivity of the Central Alps comes to no surprise, as the geophysical community has long established that the (counter clockwise) rotation pole of the Adriatic plate relative to Europe is due south of the central Alps near Torino implying zero convergence in the Central Alsp to north of it. Conversely, this rotation pole implies north-south extension in the western Alps and north-south convergence east of the rotation pole in the Eastern Alps. In the Eastern Alps, seismology, active tectonics and recent uplift patterns show indeed that this region is currently highly active. In this contribution we defend the tectonic activity in the Eastern Alps against a growing body of opinion that the Alps are tectonically dead. For this we present two aspects: First we summarize our preliminary studies from the past including (i) cosmogenic burial ages suggesting up to 700 m of surface uplift within the last 4 my (ii) U/He age suggesting massive exhumation within the last 10 my (iii) morphometric studies showing substantial uplift of fluvial terraces. Secondly, we present our working groups plan to tackle this subject within the current TOPO-ALPS initiative.

C.10
Incision rates based on burial age dating of cave sediments along the Mur river in Austria and their correlation to the nearby landscape formation

Dating appropriate cave deposits using the radioactive decay of cosmogenic nuclides like ^{26}Al and ^{10}Be allows a lower limit estimate of absolute cave ages and consequently an upper limit of relative incision rate of an adjacent river system. Alternating stages of erosion and stagnation lead to the development of planation surfaces in the landscape and coeval formation of horizontal cave passages. This interplay can be used to date the surface levels by correlating them with the associated cave levels and their associated ages.

This study focuses on the area around Graz along the Mur river in the Central Styrian Karst. There is apparent interest in this area as it is located at the transition zone from the mountainous region, the so-called Highlands of Graz as part of the Eastern Alps to the Styrian Basin, being the western-most part of the Pannonian Basin system.

First results of age dated cave deposits as well as geomorphic features extracted from digital terrain models, show a strong evidence of substantial changes of the recent (Pliocene and younger) drainage system characteristics. In this work results from (i) burial age dating, (ii) historical information and (iii) morphological and structural data are merged to distinguish between the relative roles of tectonic activity and erosion driven incision in this area. This will provide an insight to further constrain the landscape evolution and the complicated uplift history of that marginal area in space and especially in absolute time in relation to the ongoing basin inversion processes.

C.11
Rates of valley incision in the European Alps approached by cosmogenic nuclides

Burial age dating provides a tool to date Pliocene and Pleistocene sediments. Quartz grains exposed to cosmic radiation at the surface accumulate ^{26}Al and ^{10}Be with a definite ratio of 6.8:1. When the quartz grains are buried, the different half-live of these radioactive nuclides causes the ratio to decrease with time. Caves are buried repositories for Quartz grains in clastic sediments and thus cave sediments can provide minimum ages for the cave genesis. The decrease of the mentioned ratio of the radio nuclides is the key to determine the time since the grain was buried. The current research projects aim to determine valley incision rates in the European Alps during the Neogene and Quaternary. Burial age dating is up to now primarily used for landscape development

studies, but applications in other fields of cave science like for example cave paleontology is also possible. The current projects are funded by the Austrian Science Foundation.

C.12
River incision based on cave sediment analysis along the Eastern Alpine orogen – Pannonian Basin System transition zone

Dating cave deposits via the Terrestrial Cosmogenic Nuclide (TCN) method allows a lower limit estimate of absolute cave ages and consequently an upper limit of relative incision rates of an adjacent river system. This study focuses on the area around Graz along the Mur river, which is located at the transition from the mountainous region, the so-called Highlands of Graz as part of the Eastern Alps to the Styrian Basin, being the western-most part of to the Pannonian Basin system. First results of age dated cave deposits as well as geomorphologic manifestations using digital terrain modeling show a strong evidence of much recent (Pliocene and younger) actual drainage system characteristics. In this work various cognitions will be merged to emphasize the role of tectonic activity versus erosion driven incision in this area, particularly focusing on the karstified domains. This will provide an insight to further constrain the landscape evolution and the complicated uplift history respectively of that marginal area in space and absolute time in relation to ongoing basin inversion processes.

C.13
The western margin of the basin: highlights of young morphologies formed by basin inversion

The western margin of the Pannonian Basin includes: (a) the Vienna Basin and (b) the Styrian Basin. The Vienna Basin is dominated by a large transform fault that extends well into the Carpathian arc and that created an enormous pull-apart basin along its northwest margin. This pull apart basin and the Vienna transform fault clearly also dominated the geometry of basin inversion over the last 10 my. In contrast, in the Styrian Basin, no major transform faults have been mapped and the thickness of the sedimentary pile in the basin increases successively and continuously eastward - bar some north-south striking basement swells (Middle Styrian Swell, South Burgenland Swell). As such, the basin extension and its subsequent inversion are likely to have followed a more ‘normal’ pattern and the Styrian Basin and its bounding regions are an ideal area to study basin inversion processes. In this contribution we highlight three eye catching morphological features of the Styrian Basin and its surroundings that apparently relate to the basin inversion.

· ***Caves in the Palaeozoic of Graz***: The river Mur is the major Alpine drainage that crosses the transition zone from the orogen into the basin in a unit called the Palaeozoic of Graz. This unit is made of karstified carbonates hosting hundreds of caves, many of which include long horizontal stretches. These caves obviously formed at (or below) ground water level, but they occur on various elevations from active caves on the present day elevation of the Mur up to 600 m above the current water table. Many of these caves contain crystalline basement pebbles that are likely to have been deposited during their active time. We are currently dating the burial ages of these sediments to infer the incision history of the river Mur and obtain vertical reference levels for the basin inversion. Preliminary ages show a rough age increase with elevation from zero to about 4 my at 600 m above the current river level corresponding to an incision rate of 0.15 mm per year.

· ***Pohorje Dome***: The Pohorje Dome in Slovenia rises some 1.000 vertical metres above the basin amidst the suture zone between Adriatic and European plates. The river Drava crosses the dome through its centre, apparently indicating an antecedent relationship of dome and river. This implies that the dome is likely to be a very young feature, probably younger than most of the offset along the Lavanttal fault which constrains its uplift to the last 5 my. Preliminary cosmogenic exposure ages have not revealed a systematic pattern, but confirm active tectonics in the region.

· ***Terraces in the basin***: In the Styrian Basin itself, the morphology also indicates active tectonics: The hilly landscape of the Styrian wine growing area fluctuates between 200 m and 500 m above sea level on relatively short length scales and shows – in some regions – a very strict parallel organisation of drainages with asymmetric valley profiles. This asymmetry in the morphology is enhanced by various glacial and interglacial terraces that often occur on side of the valley only. Using channel profiles of streams and displaced young marine deposits (e.g. Leitha Kalk) as reference levels we constrain which landforms were formed by basin inversion and which are formed by drainage incision.

C.14
The Evolution of the Styrian Basin in the Neogene – Indications and First Conclusions

We present some observations on the neotectonic evolution of the transition zone between the Alpine orogen and the Pannonian Basin in the region of the Styrian Basin. In particular, we discuss the nature of some peculiar morphological features in this region, such as asymmetric valley profiles or parallel orientation of drainages in discretely defined zones of the basin. These features can be interpreted in terms of the

interplay of erosion and a complicated uplift history during the inversion of the basin margin. Two methods are used to constrain our observations in absolute time: 1. Marker horizons of known age and equivalent deposition environment are correlated across the basin with respect to their elevation. This information is used to infer later tectonic activity. 2. Burial ages of 'Augensteine' in karst caves and in fault gouges are obtained using terrestrial in situ cosmogenic nuclides. Burial ages are used to constrain river incision and age of activity of fault systems. Early results indicate that most of the landscape evolution in the basin-orogen transition zone occurred in the last 6-8 my. Our findings provide a deeper understanding of the relative importance and possible feedback effects of erosion driven incision and tectonic uplift in the shaping of inverted basin margins.

C.15
An Elevation Correlated Map of the Neogene in the Styrian Basin

This contribution is a progress report on a digital map of the Styrian Basin (as part of the Alpine Orogen - Pannonian Basin transition zone), in which we correlate marker horizons across the transition zone in elevation and time. The Styrian Basin was inverted about 7-10 my ago and is currently characterised by a hilly landscape between 200 and 600 m in elevation. In the bounding orogen, mountains rapidly rise to 2200 m asl. A series of conspicuous features in the basin indicate that the region experienced a complicated uplift history during the inversion of the basin margin. These include asymmetric valley profiles, parallel orientation of drainages in discretely defined zones of the basin and others. The aim of the map is to understand the relative importance of erosion driven incision and tectonic uplift in the shaping of the surface morphology in the transition zone. For this we extract the tectonic component by mapping the elevation of marker horizons of constant age and equivalent deposition environment across the basin. As marker horizons we use various Neogene sediments like coeval fluvial terraces and shallow marine deposits in the basin. Currently we use existing maps, and preliminary dating of cosmogenic nuclei from cave deposits as well as unpublished information. Further work will use low temperature geochronology, morphological mapping and numerical landform modelling to constrain the uplift history in space and absolute time.

C.16
Conspicuous features and their indications for the evolution in the Styrian Basin

We present a digital map of the Alpine Orogen - Pannonian Basin transition zone, in the region of the Styrian Basin, in which we correlate marker horizons across the transition zone in elevation and time. The Styrian Basin was inverted about 7 my ago and is currently characterised by a hilly landscape between 200 and 600 m in elevation. In the bounding orogen, mountains rapidly rise to 2200 m asl. A series of conspicuous features in the basin (including asymmetric valley shapes and parallel orientation of drainages in discretely defined zones of the basin) indicate that the region experienced a complicated uplift history during the inversion of the basin margin. The aim of the map is to understand the relative importance of erosion driven incision and tectonic uplift in the shaping of the surface morphology in the transition zone. Documenting the relative length scales of these two processes will ultimately help us to understand the mechanics governing the basin inversion. As marker horizons we use coeval fluvial terraces, top surfaces of shallow marine deposits in the basin and caves. This contribution is very much a progress report of a study in its early stages. Currently we use existing maps, preliminary dating of cosmogenic nuclei from some caves and unpublished information. Further work will use low temperature geochronology, morphological mapping and numerical landform modelling to constrain the uplift history in space and absolute time.

REFERENCES

Adamiec, G., Aitken, M.J., 1998. Dose-rate conversion factors: update. Ancient TL 16, 37-49.

Anthony, D.M., Granger, D.E., 2004. A Late Tertiary origin for multilevel caves along the western escarpment of the Cumberland Plateau, Tennessee and Kentucky, established by cosmogenic ^{26}Al and ^{10}Be. Journal of Cave and Karst Studies 66, 46-55.

Audra, Ph., Bini, A., Gabrovsek, F., Häuselmann, Ph., Hobléa, F., Jeannin, P.-Y., Kunaver, J., Monbaron, M., Sustersic, F., Tognini, P., Trimmel, H., Wildberger, A., 2006. Cave genesis in the Alps between the Miocene and today: a review. Z. Geomorph. N.F. 50 (2), 153-176.

Bada, G., Horváth, F., Dövényi, P., Szafián, P., Windhoffer, G., Cloething, S., 2007. Present-day stress field and tectonic inversion in the Pannonian basin. Global Planet. Change 58, 165-180.

Balogh, K., Ebner, F., Ravasz, C., 1994. K/Ar-Alter tertiärer Vulkanite der südöstlichen Steiermark und des südlichen Burgenlandes. – in: Lobitzer, H., Csaszar, G., Dauer, A. (eds.): Jubiläumsschrift 20 Jahre Geologische Zusammenarbeit Österreich-Ungarn. 2. – 55-72, Geologische Bundesanstalt, Wien.

Barletta, V.R., Ferrari, C., Diolaiuti, G., Carnielli, T., Sabadini, R., Smiraglia, C., 2006. Glacier shrinkage and modeled uplift of the Alps. Geophys. Res. Lett. 33, L14307.

Behm, M., Brückl, E., Chwatal, W., Thybo, H., 2007. Application of stacking and inversion techniques to three-dimensional wide-angle reflection and refraction seismic data of the Eastern Alps. Geophys. J. Int. 170, 275-298.

Bøtter-Jensen, L., McKeever, S.W.S., Wintle, A.G., 2003. Optically Stimulated Luminescence Dosimetry. Amsterdam, Elsevier Science B.V.

Brückl, E., Bleibinhaus, F., Gosar. A,, Grad, M., Guterch, A., Hrubcová, P., Keller, G.R., Majdanski, M., Sumanovac, F., Tiira, T., Yliniemi, J., Hegedüs, E., Thybo, H., 2007. Crustal structure due to collisional and escape tectonics in the Eastern Alps region based on profiles Alp01 and Alp02 from the ALP 2002 seismic experiment. J. Geophys. Res. 112, B06308. doi:10.1029/2006JB004687.

Brückl, E., Behm, M., Decker, K., Grad, M., Guterch, A., Keller, G.R., Thybo, H., 2010. Crustal structure and active tectonics in the Eastern Alps. Tectonics 29, TC2011. doi:10.1029/2009TC002491.

Bus, Z., Grenerczy, Gy., Tóth, L., Mónus, P., 2009. Active crustal deformation in two seismogenic zones of the Pannonian region – GPS versus seismological observations. Tectonophys 474, 343-352.

Cederbom, C.E., Sinclair, H.D., Schlunegger, F., Rahn, M.K., 2004. Climate-induced rebound and exhumation of the European Alps model. Geology 32, 709-712.

Champagnac, J.D., Molnar, P., Anderson, R.S., Sue, C., Delacou, B.F., 2007. Quaternary erosion induced isostatic rebound in the Western Alps. Geology 35, 195-198.

Champagnac, J.D., Schlunegger, F., Norton, K., von Blanckenburg, F., Abbühl, L.M., Schwab, M., 2009. Erosion-driven uplift of the modern Central Alps. Tectonophysics 474, 236-249.

Cloetingh, S., Lankreijer, A., 2001. Lithospheric memory and stress field controls on Polyphase deformation of the Pannonian basin – Carpathian sytem. Mar. Pet. Geol. 18, 3-11.

Dalmayrac, B., Molnar, P., 1981. Parallel thrust and normal faulting in Peru and constraints on the state of stress. Earth Planet. Sci. Lett. 55, 473-481.

Decker, K., Peresson, H., 1996. Tertiary kinematics in the Alpine-Carpathian-Pannonian system: links between thrusting, transform faulting and crustal extension. In: Wessely, G., Liebl, W. (eds), Oil and Gas in Alpidic Thrustbelts and Basins of Central and Eastern Europe, EAGE Special Publication 5, 69-77.

Dunkl, I., Frisch, W., 2002. Thermochronological constraints on the Late Cenozoic exhumation along the Alpine and West Carpathian margins of the Pannonian basin. EGU Stephan Mueller Special Publication Series 3, 135-147.

Dunkl, I., Kuhlemann, J., Reinecker, J., Frisch W., 2005. Cenozoic relief evolution of the Eastern Alps – constraints from apatite fission track age-provenance of neogene intramontane sediments. Aust. J. of Earth Sci. 98, 92-105.

Ebner, F., Gräf, W., 1982. Bentonite und Glastuffe der Steiermark. Arch. F. Lagerst.forsch. Geol. B.-A. 2, 31-45.

Ebner, F., Sachsenhofer, R.F., 1995. Paleogeography, subsidence and thermal history of the Neogene Styrian Basin (Pannonian basin system, Austria). Tectonophysics 242, 133-150.

Eide, E.A., Trosvik, T.H., Andersen, T.B., 1997. Absolute dating of brittle fault movements: Late Permian and late Jurassic extensional fault breccias in western Norway. Terra Nova 9, 135-139.

Fabiani, E., Eisenhut, M., 1971. Bodenbedeckung und Terrassen des Murtales zwischen Wildon und der Staatsgrenze. Ber. Wasserwirtsch. Raumplanung 20, 1-121.

Fink, J., 1961. Die Südostabdachung der Alpen. Mitt. Österr. Bodenkundl. Ges. 6, 123-183.

Fitzsimons, S.J., Veit, H., 2001. Geology and geomorphology of the European Alps and the Southern Alps of New Zealand: A comparison. Mt. Res. Dev. 21, 340-349.

Flügel, H.W., 1960. Die jungquartäre Entwicklung des Grazer Feldes (Steiermark). Mitt. Österr. Geogr. Ges. 102, 52-64, Wien.

Fodor, L., Bada, G., Csillag, G., Horváth, E., Ruszkiczay-Rüdiger, Zs., Palotás, K., Síkhegyi, F., Timár, G., Cloetingh, S., Horváth, F., 2005. An outline of neotectonic structures and morphotectonics of the western and central Pannonian Basin. Tectonophysics 410, 15-41.

Fodor, L., Gerdes, A., Dunkl, I., Koroknai, B., Pécskay, Z., Trajanova, M., Horváth, P., Vrabec, M., Jelen, B., Balogh, K., Frisch, W., 2008. Miocene emplacement and rapid cooling of the Pohorje pluton at the Alpine-Pannonian-Dinaric junction, Slovenia. Swiss J. Geosci. 101, Supplement 1, 255-271.

Frisch, W., Kuhlemann, J., Dunkl, I., Brügel, A., 1998. Palinspastic reconstruction and topographic evolution of the Eastern Alps during late Tertiary tectonic extrusion. Tectonophysics 297, 1-15.

Frisch, W., Kuhlemann, J., Dunkl, I., Szekely, B., 2001. The Dachstein paleosurface and the Augenstein Formation in the Northern Calcareous Alps; a mosaic stone in the geomorphological evolution of the Eastern Alps. Int. J. Earth Sci. 90, 500-518.

Fritz, H., 1991. Stratigraphie, Fazies und Tektonik im nordwestlichen Grazer Paläozoikum (Ostalpen). Jahrb. Geol. Bundesanst. 134, 227-255.

Galbraith, R.F., Roberts, R.G., Laslett, G.M., Yoshida, H., Olley, J.M., 1999. Optical dating of single and multiple grains of quartz from Jinmium rock shelter, northern Australia: Part I, Experimental design and statistical models. Archaeometry 41, 339-364.

Gasser, D., Stüwe. K., Fritz, H., 2009. Internal structural geometry of the Paleozoic of Graz. Int. J. Earth Sci. DOI 10.1007/s00531-009-0446-0.

Genser, J., Cloetingh, S., Neubauer, F., 2007. Late orogenic rebound and oblique Alpine convergence: New constraints from subsidence analysis of the Austrian Molasse basin. Global Planet. Change 58, 214-223.

Gollner, J., Zier, C., 1985. Zur Geologie des Hochlantsch (Grazer Paläozoikum, Steiermark). Jb. Geol. B.-A. 128, 43-73.

Gosse, J.C., Phillips, F.M., 2001. Terrestrial in situ cosmogenic nuclides: theory and application. Quat. Sci. Rev. 20, 1475-1560.

Granger, D. E., Kirchner, J.W., Finkel, R.C., 1997. Quaternary downcutting rate of the New River, Virginia, measured from differential decay of cosmogenic ^{26}Al and ^{10}Be in cave-deposited alluvium. Geology 25, 107-110.

Granger, D.E., Fabel, D., Palmer, A.N., 2001. Pliocene-Pleistocene incision of the Green River, Kentucky, determined from radioactive decay of cosmogenic ^{26}Al and ^{10}Be in Mammoth Cave sediments. Geol. Soc. Am. Bull. 113, 825-836.

Granger, D.E., Muzikar, P.F., 2001. Dating sediment burial with in situ-produced cosmogenic nuclides: theory, techniques, and limitations. Earth Planet. Sci. Lett. 188, 269-281.

Grenerczy, G., Kenyeres, A., Fejes, I., 2000. Present crustal movement and strain distribution in Central Europe inferred from GPS measurements. J. Geophys. Res. 105, 21835-21846.

Grenerczy, G., Sella, G., Stein, S., Kenyeres, A., 2005. Tectonic implications of the GPS velocity field in the northern Adriatic region. Geophys. Res. Lett. 32, L16311, doi: 10.1029/2005GL022947.

Grenerczy, G., Kenyeres, A., 2006. GPS velocity field from Adria to the European Platform. In: Pinter, N., Grenerczy, G., Medak, D., Stein, S., Weber, J.C. (eds). The Adria Microplate: GPS Geodesy, Tectonics, and Hazards, Springer, Dordrecht, pp 321-334.

Gross, M., Fritz, I., Piller, W.E., Soliman, A., Harzhauser, M., Hubmann, B., Moser, B., Scholger, R., Suttner, T.J., Bojar, H.P., 2007. The Neogene of the Styrian Basin: Guide to Excursion. Joannea – Geologie und Paläontologie 9, 117-193.

Harzhauser, M., Daxner-Höck, G., Piller. W.E., 2004. An integrated stratigraphy of the Pannonain (late Miocene) in the Vienna Basin. Austrian Journal of Earth Sciences 95/96, 6-19.

Häuselmann, Ph., Granger, D.E., 2005. Dating of caves by cosmogenic nuclides: method, possibilities, and the Siebenhengste example (Switzerland). Acta Carsologica 34 (1), 43-50.

Häuselmann, Ph., 2007. How to date nothing with cosmogenic nuclides. Proceedings Time in Karst, Acta Carsologica 36 (1), 93-100.

Häuselmann, Ph., Fiebig, M., Kubik, P.W., Adrian, H., 2007a. A first attempt to date the original „Deckenschotter“ of Penck and Brückner with cosmogenic nuclides. Quaternary International 164-165, 33-42.

Häuselmann, Ph., Granger, D.E., Jeannin, P-Y., Lauritzen, S-E., 2007b. Abrupt glacial valley incision at 0.8 Ma dated from cave deposits in Switzerland. Geology 35, 143-146.

Hay, W.W., Soeding, E., DeConto, R.M., Wold, C., 2002. The Late Cenozoic uplift – climate change paradox. Int. J. Earth Sci. 91, 746–774.

Hejl, E., 1997. 'Cold spots' during the Cenozoic evolution of the Eastern Alps: thermochronological interpretation of apatite fission-track data. Tectonophysics 272, 159-173.

Hellstrom, J., 2003. Rapid and accurate U/Th dating using parallel ion-counting multi-collector ICP-MS. Journal of Analytical Atomic Spectrometry 18, 1346-1351.

Hellstrom, J., 2006. U-Th dating of speleothems with high initial ^{230}Th using stratigraphical constraint. Quaternary Geochronology 1, 289-295.

Hilber, V., 1912. Die Taltreppe, eine geologisch-geographische Darstellung.- 50 p., Graz.

Hinderer, M., 2001. Late Quaternary denudation of the Alps, valley and lake fillings and modern river loads. Geodinamica Acta 14, 231-263.

Horváth, F., Cloething, S., 1996. Stress-induced late-stage subsidence anomalies in the Pannonian basin. Tectonophysics 266, 287-300.

Houseman, G.A., McKenzie, D.P., Molnar, P., 1981. Convective instability of a thickened boundary layer and its relevance for the thermal evolution of continental convergent belts. J. Geophys. Res. 86, 6115-6132.

Ivy-Ochs, S., Kerschner, H., Reuther, A., Preusser, F., Heine, K., Maisch, M., Kubik, P.W., Schlüchter, Ch., 2008. Chronology of the last glacial cycle in the European Alps. Journal of Quaternary Science 23 (6-7), 559-573.

Kahle, H.G. et al., 1997. Recent crustal movements, geoid and density distribution: contribution from integrated satellite and terrestrial measurements. In: Pfiffner, O.A., Lehner, P., Heitzmann, P., Müller, St. and Steck, A. (Eds.): Results of the National Research Program 20 (NRP 20). Birkhäuser, Basel, pp. 251-259.

Kocsis, L., Vennemann, T.W., Fontignie, D., 2007. Migration of sharks into freshwater systems during the miocene and implications for alpine paleoelevation. Geology 35, 451-454.

Koppes, M.N., Montgomery, D.R., 2009. The relative efficacy of fluvial and glacial erosion over modern to orogenic timescales. Nat. Geosci. 2, 644-647.

Kralik, M., Klima, K., Riedmüller, G., 1987. Dating fault gouges. Nature 327, 315-317.

Kröll, A., Flügel, H.W., Seiberl, W., Weber, F., Walach, G., 1988. Steirisches Becken – Südburgenländische Schwelle. Geologische Themenkarten und Erläuterungen, Geol B.-A., Wien, 49p.

Kuhlemann, J., 2007. Paleogeographic and paleotopographic evolution of the Swiss and Eastern Alps since the Oligocene. Global Planet. Change 58, 224-236.

Kuhlemann, J., Frisch, W., Dunkl, I., Szekely, B., 2001. Quantifying tectonic versus erosive denudation by the sediment budget; the Miocene core complexes of the Alps. Tectonophysics 330, 1-23.

Kuhlemann, J., Frisch, W., Szekely, B., Dunkl, I., Kazmer, M., 2002. Postcollisional sediment budget history of the Alps: Tectonic versus climatic control. Int. J. Earth Sci. 91, 818-837.

Kühni, A., Pfiffner, O.A., 2001. The relief of the Swiss Alps and adjacent areas and its relation to lithology and structure: topographic analysis from a 250-m DEM. Geomorphology 41, 285-307.

Kulig, G., 2005. Erstellung einer Auswertesoftware zur Altersbestimmung mittels Lumineszenzverfahren unter spezieller Berücksichtigung des Einflusses radioaktiver Ungleichgewichte in der ^{238}U-Zerfallsreihe, Unpublished BSc thesis, Technical University Bergakademie Freiberg.

Luth, S.W., Willingshofer E., 2008. Mapping of the post-collisional cooling history of the Eastern Alps. Swiss J. Geosci. 101, Supplement 1, 207-223.

Marton, E., Fodor, L., Jelen, B., Marton, P., Rifelj, H., Kevric, R., 2002. Miocene to Quaternary deformation in NE Slovenia: complex paleomagnetic and structural study. J. Geodyn. 34, 627-651.

Mason, P.R.D., Seghedi, I., Szákacs, A., Downes, H., 1998. Magmatic constraints on the geoidynamic models of subduction in the East Carpathians, Romania. Tectonophysics 297, 157-176.

Maurin, V., 1953. Über jüngste Bewegungen im Grazer Paläozoikum. Verh. Geol. B.-A. 1953 (1-4), 216-220, Wien.

Maurin, V., Benischke, R., 1992. Morphogeny, Paleohydrography and Karst Development, in: H. Behrens et al., Investigations with Natural and Artificial Tracers in the Karst Aquifer of the Lurbach System (Peggau-Tanneben-Semriach, Austria). Steir.Beitr. z. Hydrogeologie 43, 22-33.

Mauz, B., Packman, S., Lang, A., 2006. The alpha effectiveness in silt-sized quartz: New data obtained by single and multiple aliquot protocols. Ancient TL 24, 47-52.

Molnar, P., Lyon-Caen, H.D., 1989. Fault plane solutions of earthquakes and active tectonics of the Tibetan plateau and its margins. Geophys. J. R. Astron. Soc. 99, 123-135.

Molnar, P., 2004. Late Cenozoic increase in accumulation rates of terrestrial sediment: How might climate change have affected erosion rates? Annu. Rev. Earth Planet. Sci. 32, 76-89.

Montgomery, D.R., 2001. Slope distributions, hillslope thresholds and steady-state topography. Am. J. Sci. 301, 432-454.

Mottl, M., 1949. Die Kugelsteinhöhlen bei Peggau und ihre diluvialstratigraphische Bedeutung. Verh. Geol.B.-A. 1949, 61-69, Wien.

Murray, A.S., Roberts, R.G., 1998. Measurement of the equivalent dose in quartz using a regenerative-dose single –aliquot protocol. Radiation Measurements 29, 503-515.

Murray, A.S., Wintle, A.G., 2000. Luminescence dating of quartz using an improved regenerative-dose single-aliquot protocol. Radiation Measurements 32, 57-73.

Muttoni, G., Carcano, C., Garzanti, E., Ghielmi, M., Piccin, A., Pini, R., Rogledi, S., Sciunnach, D., 2003. Onset of major Pleistocene glaciations in the Alps. Geology 31, 989-992.

Neubauer, F., Dallmeyer, R.D., Dunkl, I., Schirnik, D., 1995. Late Cretaceous exhumation of the metamorphic Gleinalm dome, Eastern Alps: kinematics, cooling history and sedimentary response in a sinistral wrench corridor. Tectonophysics 242, 79-98.

Nishiizumi, K., Winterer, E.L., Kohl, C.P., Klein, J., Middleton, R., Lal, D., Arnold, J.R., 1989. Cosmic ray production rates of ^{10}Be and ^{26}Al in quartz from glacially polished rocks: J. Geophys. Res. 94, 17907-17915.

Kohl, C.P., Nishiizumi, K., 1992. Chemical isolation of quartz for measurement of in-situ-produced cosmogenic nuclides. Geochemica et Cosmochimica Acta 56, 3583-3587.

Norton, K.P., Abbühl, L.M., Schlunegger, F., 2010a. Glacial conditioning as an erosional driving force in the Central Alps. Geology 38, 655-658.

Norton, K.P., v. Blanckenburg, F., Kubik, P.W., 2010b. Cosmogenic nuclide-derived rates of diffusive and episodic erosion in the glacially sculpted upper Rhone Valley, Swiss Alps. Earth Surf. Process. Land. 35, 651-662.

Palmer, A.N., 1987. Cave levels and their interpretation. NSS Bulletin 49, 50-66.

Peresson, H., Decker, K., 1997. Far-field effects of Late Miocene subduction in the Eastern Carpathians: E-W compression and inversion of structures in the Alpine-Carpathian-Pannonian region. Tectonics 16(1), 38-56.

Piller, W.E., Egger, H., Erhart, C.W., Gross, M., Harzhauser, M., Hubmann, B., Vav Husen, D., Krenmayr, H.-G., Krystyn, L., Lein, R., Lukeneder, A., Mandl, G.W., Rögl, F., Roetzel, R., Rupp, C., Schnabel, W., Schönlaub, H.P., Summesberger, H., Wagreich, M and

Wesseley, G., 2004. Die stratigraphische Tabelle von Östereich 2004 (sedimentäre Folgen). Komm. paläont. stratigr. Erforsch Österr., Österr. Akad. Wiss. und Österr. Stratigr. Komm., Wien.

Piller, W.E., Harzhauser, M., 2005. The myth of the brackish Sarmatian Sea. Terra Nova, 17, 450-455.

Pischinger, G., Kurz, W., Übleis, M., Egger, M., Fritz, H., Brosch, F.J., Stingl, K., 2008. Fault slip analysis in the Koralm Massif (Eastern Alps) and consequences for the final uplift of "cold spots" in Miocene times. Swiss J Geosci 101, Supplement 1, 235-254.

Plan, L., Grasemann, B., Spötl, Ch., Decker, K., Boch, R., Kramers, J., 2010. Neotectonic extrusion of the Eastern Alps: Constraints from U/Th dating of tectonically damaged speleothems. Geology 38, 483-486.

Preusser, F., Geyh, M.A., Schlüchter, Ch., 2003. Timing of Late Pleistocene climate change in lowland Switzerland. Quaternary Science Reviews 22, 1435-1445.

Ratschbacher, L., Frisch, W., Neubauer, F., Schmid, S.M., Neugebauer, J., 1989. Extension in compressional orogenic belts: The eastern Alps. Geology 17, 404-407.

Ratschbacher, L., Frisch, W., Linzer, H.-G., Merle, O., 1991. Lateral extrusion in the Eastern Alps 2. Structural analysis. Tectonics 10, 257-271.

Raymo, M.E., 1994. The initiation of northern hemisphere glaciations. Annu.Rev. Earth Planet. Sci. 22, 353-383.

Reinecker, J., Lenhardt, W.A., 1999. Present-day stress field and deformation in eastern Austria. Int. J. Earth Sci. 88, 532-550.

Robl, J., Hergarten, S., Stüwe, K., 2008a. Morphological analysis of the drainage system in the Eastern Alps. Tectonophysics 460, 263-277.

Robl, J., Stüwe, K., Hergarten, S., 2008b. Channel profiles around Himalayan river anticlines: Constraints on their formation from digital elevation model analysis. Tectonics 27, TC3010.

Robl, J., Stüwe, K., Hergarten, S., Evans, L., 2008c. Extension during continental convergence in the Eastern Alps: The influence of orogen-scale strike-slip faults. Geology 36, 963-966.

Royden, L., Horváth, F., Nagymarosy, A., Stegena, L., 1983. Evolution of the Pannonian Basin system 2. Subsidence and thermal history. Tectonics 2(1), 91-137.

Ruess, D., Höggerl, N., 2002. Bestimmung rezenter Höhen- und Schwereänderungen in Österreich, in: Friedl, G., Genser, J., Handler, R., Neubauer, F., Steyrer, H.-P. (Eds.),

Pangeo Austria. Institut für Geologie und Paläontologie. Universität Salzburg, Salzburg, p. 151.

Ruszkiczay-Rüdiger, Zs., 2007. Tectonic and climatic forcing in Quaternary landscape evolution in the Central Pannonian Basin: A quantitative geomorphological, geochronological and structural analysis. PhD Thesis, Vrije Universiteit, Amsterdam, Netherlands.

Sacchi, M., Horváth, F., 2002. Towards a new time scale for the Upper Miocene continental series of the Pannonian basin (Central Paratethys). European Geosciences Union, Stephan Mueller Special Publication Series 3, 79-94.

Sachsenhofer, R.F., 1989. Das Inkohlungsbild im Jungtertiär der Norischen Senke (Östliche Zentralalpen, Österrreich) und seine paläogeothermische Deutung. Jb. Geol. B.-A. 132 (2), 489-505.

Sachsenhofer, R.F., Lankreijer, A., Cloetingh, S., Ebner, F., 1997. Subsidence analysis and quantitative basin modelling in the Styrian Basin (Pannonian Basin System, Austria), in: Neubauer, F., Cloetingh, S., Dinu, C. and Mocanu, V. (Eds.), Tectonics of the Alpine-Carpathian-Pannonian Region, II Tectonophysics 272, 175-196.

Sachsenhofer, R.F., Jelen, B., Hasenhüttl, C., Dunkl, I., Rainer, T., 2001. Thermal history of Tertiary basins in Slovenia (Alpine-Dinaride-Pannonian junction). Tectonophysics 334, 77-99.

Scardia, G., Muttoni, G., Sciunnach, D., 2006. Subsurface magnetostratigraphy of Pleistocene sediments from the Po Plain (Italy): Constraints on rates of sedimentation and rock uplift. Geological Society of America Bulletin 118, 1299-1312.

Schadler, J., 1931. Die Ablagerungen, in: Abel, O. and Kyrle, G. (Eds.), Die Drachenhöhle bei Mixnitz. Speleologische Monographien 7-8, pp. 169-224.

Schlunegger, F., Hinderer, M., 2001. Crustal uplift in the Alps – why the drainage pattern matters. Terra Nova 13, 425-432.

Schlunegger, F., Hinderer, M., 2003. Pleistocene/Holocene climate change, re-establishment of fluvial drainage network and increase in relief in the Swiss Alps. Terra Nova 15, 88-95.

Selverstone, J., 2005. Are the Alps collapsing? Annu. Rev. Earth Planet. Sci. 33, 113-132.

Skala, W., 1967. Kurzbericht über die Untersuchung von Fließrichtungen in den Basisschottern des Obersarmats im Steirischen Becken. Mitteilungen des Naturwissenschaftlichen Vereins für Steiermark, 97, 28-31.

Sölva, H., Stüwe, K., Strauss, P. 2005: The Drava River and the Pohorje Mountain Range (Slovenia): geomorphological interactions. Mitt. d. Naturwissenschaftlichen V. für Stmk. 134, 45-55.

Spötl, Ch., Mangini, A., 2006. U/Th age constraints on the absence of ice in the central Inn Valley (eastern Alps, Austria) during Marine Isotope Stages 5c and 5a. Quaternary Research 66, 167-175.

Spötl, Ch., Offenbecher, K.-H., Boch, R., Meyer, M., Mangini, A., Kramers, J., Pavuza, R., 2007. Tropfstein-Forschung in österreichischen Höhlen – ein Überblick. Jb. Geol. B.-A. 147, 117-167.

Stock, G.M., Anderson, R.S., Finkel, R.C., 2004. Pace of landscape evolution in the Sierra Nevada, California, revealed by cosmogenic dating of cave sediments. Geology 32, 193-196.

Stock, G.M., Granger D.E., Sasowsky, I.D., Anderson, R.S., Finkel R.C., 2005a. Comparison of U-Th, paleomagnetism, and cosmogenic burial methods for dating caves: Implications for landscape evolution studies. Earth Planet. Sci. Lett. 236, 388-403.

Stock, G.M., Anderson, R.S., Finkel, R.C., 2005b. Rates of erosion and topographic evolution of the Sierra Nevada, California, inferred from cosmogenic ^{26}Al and ^{10}Be concentrations. Earth Surf. Process. Landforms 30, 985-1006.

Strauss, P., Wagreich, M., Decker, K., Sachsenhofer, R.F., 2001. Tectonics and sedimentation in the Fohnsdorf-Seckau Basin (Miocene, Austria): from pull-apart basin to a half-graben. Int. J. Earth Sci. 90, 549-559.

Stüwe, Barr, T.D., 1998. On uplift and exhumation during convergence. Tectonics 17, 80-88.

Suette, G., 1986. Geologische Karte der Republik Österreich 1:50.000, Erläuterungen zu Blatt 208 Mureck. Geol.B.-A., Wien.

Székely, B., Reinecker, J., Dunkl, I., Frisch, W., Kuhlemann, J., 2002. Neotectonic movements and their geomorphic response as reflected in surface parameters and stress patterns in the Eastern Alps. EGU Stephan Mueller Special Publication Series 3, 149-166.

Thöni, M., 2006. Dating eclogite-facies metamorphism in the Eastern Alps – approaches, results, interpretations: a review. Mineral. Petrol. 88, 123-148.

Untersweg, T., 1979. Morphologie des Schöcklgebiet. Ph.D. Thesis, Karl-Franzens University of Graz, Austria.

Van der Pluijm, B.A., Hall, C.M., Vrolijk, P.J., Pevear, D.R., Covey, M.C., 2001. The dating of shallow faults in the Earth's crust. Nature 412, 172-175.

Van der Pluijm, B.A., Vrolijk, P.J., Pevear, D.R., Hall, C.M., Solum, J., 2006. Fault dating in the Canadian Rocky Mountains: Evidence for late Cretaceous and early Eocene orogenic pulses. Geology 34, 837-840.

Van Husen, D., 1997. LGM and late-glacial fluctuations in the Eastern Alps. Quaternary International 38/39, 109-118.

Van Husen, D., 1999. Geological Processes during the Quaternary. Mitt. Oesterr. Geol. Ges. 92, 135-156.

Vernon, A.J., van der Beek, P.A., T.Rahn, M.K., Sinclair, H.D., 2006. Quantifying late Cenozoic denudation of the European Alps: Insights from a compilation of fissiontrack ages. Terra Nostra 2, 101.

Vernon, A.J., van der Beek, P.A., Sinclair, H.D., Rahn, M.K., 2008. Increase in late Neogene denudation of the European Alps confirmed by analysis of a fission-track thermochronology database. Earth Planet. Sci. Lett. 270, 316-329.

von Blanckenburg, F., 2005. The control mechanisms of erosion and weathering at basin scale from cosmogenic nuclides in river sediment. Earth Planet. Sci. Lett. 237, 462-479.

von Blanckenburg, F., Wittmann, H., Kruesmann, T., Norton, K.P., Kubik, P.W., 2007. How fast do the Alps erode? A cosmogenic nuclide study on central Alpine river basins. Geochim. Cosmochim. Acta 71, A11073.

Weber, F., 1969. Die refraktionsseismischen Messungen im Murtal zwischen Peggau und Eggenfeld (Mittelsteiermark) und ihre Bedeutung für die hydrogeologische Erforschung der quartären Schotterdecken. Steir. Beitr. z. Hydrogeologie 21, 5-25.

Whipple, K.X., Tucker, G.E., 1999. Dynamics of the stream power river incision model: Implications for height limits of mountain ranges, landscape response time scales and research needs. J. Geophys. Res. 104, 17661-17674.

Whipple, K.X., 2004. Bedrock rivers and the geomorphology of active orogens. Annu. Rev. Earth Planet. Sci. 32, 151-185.

Willett, S.D., Schlunegger, F., Picotti, V.I., 2006. Messinian climate change and erosional destruction of the Central European Alps. Geology 34, 613-616.

Willet, S.D., 2010. Late Neogene Erosion of the Alps: A Climate Driver? Annu. Rev. Earth Planet. Sci. 38, 411-437.

Winkler-Hermaden, A., 1955. Ergebnisse und Probleme der quartären Entwicklungsgeschichte am östlichen Alpensaum außerhalb der Vereisungsgebiete. Denkschr. Akad. Wiss. Math.-naturw. Kl., 110, Wien.

Winkler-Hermaden, A., 1957. Geologisches Kräftespiel und Landformung. – 822 p., Sringer Verlag, Wien.

Wintle, A.G., 1997. Luminescence dating: laboratory procedures and protocols. Radiation Measurements 27, 769-817.

Wittmann, H., von Blanckenburg, F., Kruesmann, T., Norton, K.P., Kubik, P.W., 2007. Relation between rock uplift and denudation from cosmogenic nuclides in river sediment in the Central Alps of Switzerland. J. Geophy. Res. Earth Surf. 112.

Wobus, C., Whipple, K.X., Kirby, E., Snyder, N., Johnson, J., Spyropolou, K., Crosby, B., Sheeha, D., 2006. Tectonics from topography: Procedures, promises, and pitfalls, in: Willet, S.D., Hovius, N., Brandon, M.T., Fisher, D.M., (Eds.), Tectonics, Climate, and Landscape Evolution. Spec. Pap. Geol. Soc. Am. 398, 55-74.

Wölfler, A., Kurz, W., Danišík, M., Rabitsch, R., 2010. Dating of fault zone activity by apatite fission track and apatite (U-Th)/He thermochronometry: a case study from the Lavanttal fault system (Eastern Alps). Terra Nova, doi: 10.1111/j.1365-3121.2010.00943.x.

Yamada, R., Matsuda, T., Omura, K., 2007. Apatite and zircon fission-track dating from the Hirabayashi-NIED borehole, Nojima Fault, Japan: Evidence for anomalous heating in fracture zones. Tectonophysics 443, 153-160.

THANKS TO…

During the years of my PhD many people crossed my path or actually I crossed theirs… I would like to thank all of you for enriching my life in one way or the other. I would like to thank in particular the following persons and at the same time deeply apologize for the ones I forgot in the heat of the moment writing these lines:

Kurt and Harry for initiating this project and supporting me throughout the whole time; all your tolerance and constructive criticism that finally led to the great outcome of this multi-disciplinary research. Kurt in particular for introduce me into the mysteries of manuscript writing and for shared caving adventures. Harry for your quiet manner and spurring me on at the right moments. Stefan for the laws of physics and solving the math. Derek for support concerning final sample preparation and the AMS measurements. And all his family for great accommodation in Glasgow. Philipp for all the chemistry advices, lab support and his cave experience. Markus for giving me the opportunity to join the cosmo group in Vienna. Diana and Bettina for making the lab life a bit more bearable. Petra and Wilfried Körner for the great support in level 4 of the Geozentrum. Helena and Christoph for my stays in Innsbruck and the fantastic support concerning OSL dating. John for the U/Th dating and sorry for all the troubles with the money transfer. Colleague Othmar Nestroy for sharing his knowledge of soils and the local outcrop situations. Walter for discussions during coffee breaks. Steff, Ralf, the two Heinrichs, Luki, Marco, and all the numerous cavers that helped to actually realize this work; the local caving clubs Höhlenbären and Landesverein für Höhlenkunde in der Steiermark. The Karst and Cave Department of the Natural History Museum Vienna for lodging during my lab work in Vienna. My roommates Conny, Deta, Emilie, Vroni, Andi, Flo, Jörg, Nico, and Tamer for discussions, lunch, climbing trips and much more. Especially the coffee breaks towards the end of this thesis are very much appreciated. Wohnzimmer and Beanery for the daily caffeine dose. Roli for the view of a physicist. Steffen, Gerfried, Michi, Cyril and Bernhard for the last months of acceptance and interest for my “burden of the past”. Christoph, for great moments of climbing, skiing and office hours. You left us much too early. All PhD students from KF, TU and MUL for exchange of knowledge and fun during seminars and the field workshop.

And especially my family that supported me financially and with their love all over the time, allowing me to do what I did. And finally to Silke, for tolerating all my peculiarities and sometimes hard to understand actions…

Thanks to all of you!